

# The Constitutive Modeling of Shape Memory Alloys

by

Chen Liang

Dissertation submitted to the Faculty of the

Virginia Polytechnic Institute and State University

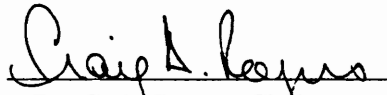
in partial fulfillment of the requirements for the degree of

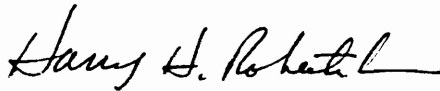
DOCTOR OF PHILOSOPHY

in

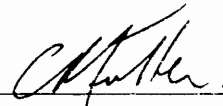
Mechanical Engineering

APPROVED:

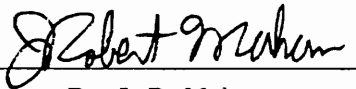
  
Dr. C. A. Rogers, Chairman



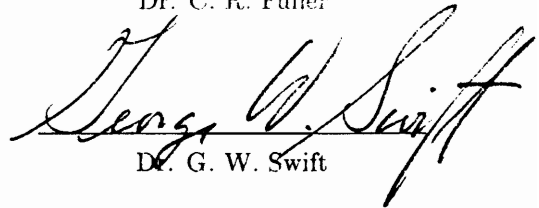
Dr. H. H. Robertshaw



Dr. C. R. Fuller



Dr. J. R. Mahan



Dr. G. W. Swift

August, 1990

Blacksburg, Virginia

LD  
5655  
V856  
1990  
L523  
C.2

# The Constitutive Modeling of Shape Memory Alloys

by

Chen Liang

Committee Chairman: Dr. C. A. Rogers

Mechanical Engineering

## Abstract

This dissertation presents a one-dimensional thermomechanical constitutive model for shape memory alloys based on basic concepts of thermodynamics and phase transformation kinetics. Compared with other developed constitutive relations, this thermomechanical constitutive relation not only reflects the physical essence of shape memory alloys, i.e., the martensitic phase transformation involved, but also provides an easy-to-use design tool for engineers. It can predict and describe the behavior of SMA quantitatively. A multi-dimensional constitutive relation for shape memory alloys is further developed based on the one-dimensional model. It can be used to study the mechanical behavior including shape memory effect of complex SMA structures that have never been analytically studied, and provide quantitative analysis for many diverse applications of shape memory alloys.

A general design method for shape memory alloy actuators has also been developed based on the developed constitutive relation and transient thermal considerations. The design methodology provides a quantitative approach to determine the design parameters of shape memory alloy force actuators, including both bias spring SMA force actuators and differential SMA force actuators.

# Acknowledgements

I would like to express my heartfelt gratitude to my advisor, Dr. Rogers, for his support and encouragement during the past two years. Without his wonderful idea of “smart materials”, I would never have thought about getting my Ph.D in such a short period. I would also like to thank him for his confidence in my research work. I am also thankful to my committee members, Dr. Robertshaw, Dr. Fuller, Dr. Mahan, and Dr. Swift for their kind criticisms. I also would like to thank Ms. Feuerbach for all her effort and time in proofreading my papers and dissertation. I also would like to acknowledge ONR-YIP 4-30264 and Hercules Aerospace Company for their support in my research work.

Thanks also go to the teachers who have given me the unforgettable lessons, especially those in my primary and middle school. I also like to thank the professors in Beijing Institute of Aeronautics and Astronautics for providing the high-quality education. My thanks go especially to Prof. D. G. Chen and Prof. J. X. Nie for recommending that I study in this country.

Finally, I want to thank my wife, Hong Bai, for her great encouragement and love. This dissertation would have been only a dream if my parents had not given me a strict family education and their great love.

# Contents

<b>1</b>	<b>Introduction</b>	<b>1</b>
1.1	Introduction to Shape Memory Alloys . . . . .	5
1.2	Industrial Applications of SMA . . . . .	19
1.2.1	SMA Couplings . . . . .	23
1.2.2	SMA Heat Engines . . . . .	23
1.2.3	SMA Actuators . . . . .	26
1.2.4	SMA Hybrid Composite . . . . .	31
1.3	Review of the Constitutive Modeling of SMA . . . . .	37
1.3.1	Traditional Thermodynamic Modeling . . . . .	38
1.3.2	Müller’s Constitutive Model . . . . .	40
1.3.3	Falk’s Model . . . . .	44
1.3.4	Sprekel and Hoffmann’s Model . . . . .	47
1.3.5	Modeling of SMA with Internal Variables . . . . .	50
1.3.6	Non-Equilibrium Thermostatic Model . . . . .	52
1.3.7	Hysteretic Model . . . . .	57
1.3.8	Plastic Flow Theory Model . . . . .	59
1.3.9	Concluding Remarks . . . . .	62
<b>2</b>	<b>Constitutive Modeling of SMA</b>	<b>64</b>

2.1	Transformation Kinetics . . . . .	64
2.2	Mechanical Behavior of SMA . . . . .	76
2.3	Thermomechanics of SMA . . . . .	81
2.4	Modeling of Shape Memory Alloy . . . . .	85
2.4.1	Stress-Strain Relations . . . . .	87
2.4.2	Constitutive Relations of SME . . . . .	93
2.4.3	Influence of Changing Material Properties . . . . .	102
2.5	Concluding Remarks . . . . .	104
<b>3</b>	<b>Experimental Verifications</b>	<b>106</b>
3.1	Experimental Results . . . . .	106
3.2	Numerical Studies . . . . .	117
3.2.1	Stress-Strain Relations . . . . .	118
3.2.2	Free Recovery Relation . . . . .	120
3.2.3	Recovery Stress and Temperature Relations . . . . .	120
3.2.4	Comparison of the Exp Model and the Cosine Model . . . . .	122
3.3	Concluding Remarks . . . . .	123
<b>4</b>	<b>General Design of Shape Memory Alloy Actuators</b>	<b>125</b>
4.1	Transient Temperature Response of SMA Actuators . . . . .	125
4.2	Bias Spring SMA Actuators . . . . .	126
4.3	Differential SMA Force Actuators . . . . .	133
4.4	Numerical Simulation and Case Studies . . . . .	137
4.4.1	Bias Spring SMA Actuator . . . . .	137
4.4.2	Differential SMA Actuator . . . . .	145
4.5	Concluding Remarks . . . . .	149

<b>5</b>	<b>Multi-Dimensional Constitutive Modeling of SMA</b>	<b>157</b>
5.1	Experimental Background . . . . .	157
5.2	Generalized Multi-Dimensional Constitutive Relations of SMA . . . .	163
5.3	Numerical Example . . . . .	174
5.3.1	Stress-Strain Analysis . . . . .	175
5.3.2	Analysis of the Shape Memory Effect . . . . .	180
5.4	Concluding Remarks . . . . .	182
<b>6</b>	<b>Conclusions</b>	<b>183</b>
	<b>References</b>	<b>186</b>
	<b>Vita</b>	<b>198</b>

# List of Figures

1.1	A Schematic Diagram of the Martensite Fraction vs. Temperature . . .	8
1.2	Stress-Strain Curves of a Nitinol ( $\text{Ti}_{55}\text{Ni}$ ) at Various Temperatures (After Cross et al., 1970) . . . . .	12
1.3	Classification of Stress-Strain Curves (After Funakubo, 1984) . . . . .	13
1.4	One-way and Two-way Shape Memory Effect . . . . .	15
1.5	Young's Modulus of a Nitinol vs. Temperature (After Cross et al., 1970)	16
1.6	Recovery Stress vs. Temperature for Different Initial Strains (After Cross et al., 1970) . . . . .	17
1.7	Electric Resistivity vs. Temperature (After Funakubo, 1984) . . . . .	18
1.8	Internal Friction, $Q^{-1}$ , vs. Temperature (Lin et al., 1989) . . . . .	20
1.9	Schematic of Internal Friction, $Q^{-1}$ , vs. Frequency . . . . .	21
1.10	The Effect of Annealing Temperature on Phase transformation Tem- peratures (After Todorodi and Tamura, 1987) . . . . .	22
1.11	SMA Couplings (After Funakubo, 1984) . . . . .	24
1.12	Bank's Prototype of SMA Heat Engine (After Funakubo, 1984) . . .	25
1.13	Basic Types of SMA Actuators (After Biometal, 1987) . . . . .	28
1.14	Bias Spring SMA Actuator Design Chart 1 (After Hodgson, 1988) . .	29
1.15	Bias Spring SMA Actuator Design Chart 2 (After Funakubo, 1988) .	30



1.16 Schematic Diagram of the Configuration of an SMA Hybrid Composite Plate . . . . .	34
1.17 Change of the First Ten Mode Shape Resulted from ASET (After Liang, Rogers, and Jia, 1989) . . . . .	35
1.18 Transmission Loss of Sound Through a SMA Hybrid Panel vs. Frequency with ASET Technique (After Liang, Rogers, and Fuller, 1990) .	36
1.19 Potential Energy of a Lattice vs. Shear Deformation Length (After Müller, 1986) . . . . .	42
1.20 Influence of External Force and Temperature on $\Phi - \Delta$ Relation (After Müller, 1986) . . . . .	43
1.21 Influence of Temperature on Free Energy and Shear Deformation Relations (After Falk, 1980) . . . . .	46
1.22 Schematic Diagram of Nitinol State Space (After McNichols and Cory, 1987) . . . . .	55
1.23 Schematic Isothermal Cut of Nitinol State Space (After McNichols and Cory, 1987) . . . . .	56
2.1 Schematic Diagram of Martensite Fraction vs. Temperature . . . . .	65
2.2 A Schematic Diagram of Transition Temperatures vs. Applied Stress	73
2.3 Schematics of Stress-Strain-Temperature Relations of SMA . . . . .	78
2.4 Schematic Diagram of Free Strain Recovery Effect . . . . .	80
2.5 Schematic Diagram of Recovery Stress and Temperature Relations . .	82
2.6 Typical Unloading Process . . . . .	91
2.7 Simplified SMA-Spring Force Actuator . . . . .	101
3.1 Elastic Stress Limit, $\sigma_e$ , vs. Temperature . . . . .	111

3.2	The Maximum Recoverable Strain, $\epsilon_L$ , vs. Temperature . . . . .	112
3.3	Stress-Strain Curves at 50 °C and -10 °C . . . . .	113
3.4	Loading and Unloading Young's Modulus vs. Temperature . . . . .	114
3.5	Recovery Stress vs. Temperature for One Percent Initial Strain . . . . .	115
3.6	Comparison of Theoretical Prediction and Experimental Results of Stress-Strain Relations . . . . .	119
3.7	Comparison of Experimental Free Recovery Results with Theoretical Predictions . . . . .	121
4.1	A Schematic of a Bias Spring Hybrid SMA Actuator System . . . . .	129
4.2	A Schematic of a Differential SMA Actuator . . . . .	135
4.3	Comparison Between Coupled Analysis and Decoupled Analysis for a Bias Spring SMA Actuator . . . . .	140
4.4	Stress vs. Temperature of a Bias Spring SMA Actuator for Different Normalized Spring Rate, $kL/s$ . . . . .	141
4.5	Normalized Travel Distance, $S/L$ , vs. Temperature of a Bias Spring SMA Actuator . . . . .	142
4.6	Normalized Travel Distance, $S/L$ , vs. Time of a Bias Spring SMA Ac- tuator . . . . .	143
4.7	Maximum Work Output of a Bias Spring SMA Actuator . . . . .	144
4.8	Temperature History of Element 'A' and 'B' of a Differential SMA Actuator with $\tau = 15$ Seconds and $T_f = 100$ °C . . . . .	147
4.9	Stress of Element 'B' vs. Time of a Differential SMA Actuator . . . . .	148
4.10	Normalized Travel Distance, $S/L_A$ , vs. Time of a Differential SMA Actuator . . . . .	150

4.11	Stress of Element 'B' vs. Normalized Travel Distance of a Differential SMA Actuator . . . . .	151
4.12	Stress of Element 'B' vs. $T^A$ and $T^B$ . . . . .	152
4.13	Normalized Travel Distance, $S/L_A$ , vs. $T^A$ and $T^B$ . . . . .	153
4.14	Martensite Fraction of Element 'A' vs. $T^A$ and $T^B$ . . . . .	154
4.15	Martensite Fraction of Element 'B' vs. $T^A$ and $T^B$ . . . . .	155
5.1	Pressure Dependence of Transformation Temperatures for Single-Crystals (solid line) and Poly-Crystals (dashed line) of two Cu-Al-Ni Shape Memory Alloys (after Kakeshita et al., 1988) . . . . .	160
5.2	Hysteretic Response to $\pm 4.5\%$ Strain of a Nitinol Alloy (After Graesser, 1990) . . . . .	162

# List of Tables

1.1	Materials with Shape Memory Effect . . . . .	6
3.1	Material Properties Used for the Theoretical Verification . . . . .	109
4.1	Material Constants for a Copper Based SMA (after Tanaka, 1984) . .	138

# Nomenclature

A	Austenite phase
$A_0$	Mean average of $A_s$ and $A_f$ , °C
$A_f, A_s$	Austenite finish and start temperatures, °C
$A_f^\sigma, A_s^\sigma$	Mechanical austenite finish and start temperatures, °C
$a_A, a_M$	Material constants associated with temperature induced transformation
$b_A, b_M$	Material constants associated with stress induced transformation
$C_A, C_M$	Stress influence coefficient, $N/m^2 \cdot ^\circ C$
D	Elastic modulus, $N/m^2$
$D_A$	Elastic modulus of austenite, $N/m^2$
$D_M$	Elastic modulus of martensite, $N/m^2$
$\{\mathcal{D}\}$	Material property matrix
$\{\mathcal{E}\}$	Elastic property matrix
$F_s$	Spring force of a bias spring actuator, N
$\mathbf{f}, \mathbf{f}$	Deformation gradient
G	Gibbs free energy (Chapter 2), J/kg

---

<sup>1</sup>Symbols used in Chapter 1 are not listed here, they are specified wherever they appear.

<sup>2</sup>Symbols without specifying chapter are used throughout the dissertation.

<sup>3</sup>Symbols in bold font are their tensor or vector forms.

G	Shear Modulus (Chapter 5), $N/m^2$
I, {I}	Unit tensor and unit matrix
k	Spring constant, N/m
L	Length of the SMA wire of a bias spring SMA actuator, m
$L_A, L_B$	Length of the SMA wires of a differential SMA actuator, m
M	Martensite phase
$M_0$	Mean average of $M_f$ and $M_s$ , °C
$M_f, M_s$	Martensite finish and start temperatures, °C
$M_f^\sigma, M_s^\sigma$	Mechanical martensite finish and start temperatures, °C
n	Transformation coefficient
q	Heat generated by internal heat source, $J/m^2 \cdot s$
$q_{sur}$	Heat transferred from surroundings to SMA, $J/m^2 \cdot s$
R	Universal gas constant (Chapter 2)
R	Electrical resistance of SMA wire (Chapter 4)
S	Travel distance or stroke of an SMA actuator (Chapter 4), m
S	Entropy (Chapter 2), $J/^\circ C \cdot kg$
s	Cross section area of SMA wire, $m^2$
{ $\bar{s}$ }	Deviatoric stress vector
T	Temperature, °C
$T_f$	Stable state temperature of a SMA actuator, °C
$T_M, T_A$	Initial state temperatures of SMA, °C
$T_q$	Quenching temperature of steel, °C
T	Torque, $N \cdot m$
t	Time, s
U	Internal energy, J/kg

$v, \mathbf{v}$	deformation velocity, 1/s
$W$	Weight of the “dead weight body” in the hybrid actuator system, N
$X, \mathbf{X}$	Original Coordinate system
$x, \mathbf{x}$	Current coordinate system
$\alpha$	Thermal expansion coefficient (Chapter 5), 1/°C
$\bar{\gamma}$	Green shear strain
$\epsilon, \boldsymbol{\epsilon}$	Engineering strain
$\epsilon^e$	Elastic strain
$\epsilon_{eq}$	Equivalent strain
$\epsilon^{np}$	None-plastic strain
$\epsilon^p$	Plastic strain
$\epsilon^t$	Transformation strain
$\bar{\epsilon}, \bar{\boldsymbol{\epsilon}}$	Green strain
$\bar{\epsilon}_L$	Max. recoverable strain or recovery strain limit
$\bar{\epsilon}_{res}$	Martensitic residual strain
$\Theta$	Thermoelastic tensor, N/m <sup>2</sup> · °C
$\theta$	Twisting angle per unit length, rad/m
$\{\kappa\}$	Material property Matrix
$\Lambda$	Generalized thermodynamic state variable
$\mu, \nu$	Possion’s ratio
$\xi, \Xi$	Martensite fraction
$\xi_A, \xi_M$	Initial martensite fractions of SMA
$\rho$	Density in current coordinate system, kg/m <sup>3</sup>
$\rho_0$	Density in original coordinate system, kg/m <sup>3</sup>
$\sigma, \boldsymbol{\sigma}$	Engineering stress, N/m <sup>2</sup>

$\bar{\sigma}, \bar{\sigma}$	The second Piola-Kirchhoff stress, $N/m^2$
$\sigma_e$	Elastic stress limit, $N/m^2$
$\sigma_{eq}$	Equivalent stress, $N/m^2$
$\sigma_{As}$	Stress corresponding to $A_s^\sigma$ , $N/m^2$
$\sigma_{Af}$	Stress corresponding to $A_f^\sigma$ , $N/m^2$
$\sigma_{Mf}$	Stress corresponding to $M_f^\sigma$ , $N/m^2$
$\sigma_{Ms}$	Stress corresponding to $M_s^\sigma$ , $N/m^2$
$\sigma_m$	Hydrostatic stress, $N/m^2$
$\sigma_y$	Yield strength, $N/m^2$
$\tau$	Time constant of a piece of SMA wire, s
$\bar{\tau}$	The Second Piola-Kirchhoff shear stress, $N/m^2$
$\Omega$	Transformation tensor, $N/m^2$
$\Phi$	Helmholtz free energy, J/kg

## Superscripts

A	Variables related to the element 'A' of a differential SMA actuator
B	Variables related to the element 'B' of a differential SMA actuator
e	Elastics
p	Plastics
t	Transformation
u	Upper limit
l	Lower limit
'	Modified material properties in a bias spring SMA actuator



## Subscripts

0	Initial condition
A	Austenite
Af	Austenite finish
As	Austenite start
c	Cooling
e	Elastics
eq	Equivalence
M	Martensite
Mf	Martensite finish
Ms	Martensite start
u	Unloading

# Chapter 1

## Introduction

Since the 1970's, there has been a worldwide wave of interest in artificial intelligence. First suggested for computer systems, the idea of intelligence can now be seen everywhere, from intelligent highway systems, intelligent processing methods, to intelligent material systems and structures. The important aspects of these intelligent systems include sensing, control, and activation elements. Shape memory alloys (SMAs), because of their unique characteristics, have been playing an important role in today's intelligent material systems and structures.

Numerous investigations into shape memory alloys have been conducted since the appearance of Nitinol in 1962 (Buehler and Wiley, 1965). Several books have been published devoted to shape memory alloys (Perkins, 1975; Funakubo, 1984). Most of the research has been concentrating on the metallurgical aspects of shape memory alloys. For example, in the Material Research Society Proceedings of 1989, more than three quarters of the papers were about the microscopic aspects of shape memory alloys, i.e., the martensitic phase transformation. A considerable amount of research involving the mechanical characterization of SMAs has also been done over the past twenty years (Cross et al., 1970; Jackson et al., 1972; Perkins, 1975). However, today's

interest in this advanced material has focused on the desperate need for systematic characterization of the shape memory alloys and a complete material data base along with practical design methods.

Shape memory alloys have been used in many fields and applications over the past thirty years. The first major industrial application of a shape memory alloy was a cryogenic pipe fitting device developed by Raychem Corporation in 1969 (Harrison et al., 1975). NASA once tried to use this material to design a deployable antenna for a spacecraft in the 1970's (Funakubo, 1984). Perhaps the most well-known example of this material is the prototype heat engine developed in the middle 70's (Bank, 1975). Because of its biocompatibility and superior resistance to corrosion, nitinol has been used in the medical field as a bone plate (Castleman et al., 1975), artificial joint (Ohnishi et al., 1980) and dental applications (Andreasen et al., 1978). The major industrial application for this material has been as force actuators and robot controls (Funakubo, 1984). Rogers (1988) suggested that SMA fibers could be embedded into composites (known today as SMA hybrid composites) to adaptively control the performance of the composites or composite structures. The theoretical and experimental study of this hybrid composite has demonstrated a far-reaching potential in the areas of dynamic and static structural control as well active structural acoustic control (Rogers, Liang, and Jia, 1989; Rogers and Barker, 1990; Liang, Rogers, and Fuller, 1990).

Considerable research into the microscopic and macroscopic behavior of shape memory alloys has been done in the past and is still being undertaken. Many applications for shape memory alloy have been discovered and many more are yet to be discovered.

However, the design of shape memory alloy products has been very expensive and difficult because the bridge that connects the material studies and the applications have not been completed to date, i.e., the design tools of the shape memory alloys have not matured. Although the behavior of shape memory alloys is very complex, the essence of shape memory effect is the same for all SMAs. Shape memory alloys have certain common features. The primary objective of this dissertation is to identify those common features and establish their relationships in order to create practical design tools.

The tools for designing shape memory alloy devices are rooted in their constitutive relations. Constitutive relations provide the stress-strain relations such as Hook's law, plastic flow rule, and viscoplastic flow relations. The mechanical behavior of shape memory alloys is closely related to the microscopic martensitic phase transformation; the constitutive relations developed for ordinary materials such as Hook's law and plastic flow theory may not be applicable to describe shape memory alloys. Therefore, new constitutive relations, which take into consideration the phase transformation behavior of SMA, must be developed.

Several constitutive relations have been developed for shape memory alloys over the last twenty years (Müller, 1979; Tanaka, 1982; Cory, 1978). While each is unique none of the constitutive relations has a strong experimental justification and each possess distinct limitations. The increasing use of shape memory alloys in the field of intelligent material systems and structures necessitates the development of unified constitutive relations for shape memory alloys, which can be utilized easily in engineering practice and satisfy certain accuracy requirements.

There are two approaches in developing material constitutive relations. One is the macroscopic phenomenological method that requires a significant amount of experimental work; the other is the microscopic or physical method that derives material constitutive relations based upon fundamental physical concepts. For example, the macroscopic phenomenological method measures the stress-strain relations using tensile tests and the slope of the linear elastic section represents the Young's modulus of the material. Microscopic method, however, would predict the Young's modulus based on the information of the micro-structure of the crystal lattice, etc. The macroscopic method is straightforward with accurate results but requires extensive material testing and cannot be used to predict the material response of SMA compositions not tested. The microscopic method, while seeming to be the ideal and logical way of understanding and describing material behavior, so far has not been able to predict and describe material characteristics quantitatively because of the complex nature of materials. From this example, another distinction of these two approaches is observed; the macroscopic method is used to *describe* the material behavior while the microscopic method is used to *predict* and *describe* the material behavior. Combining both approaches will take advantage of each method and yield a more accurate constitutive model capable of predicting and describing material behaviors of SMA. This philosophy is supported throughout this dissertation.

This dissertation has six chapters. The first chapter is the introduction and literature review; the second describes the one-dimensional constitutive modeling of shape memory alloys; the third presents the experimental verification of the newly derived model; the fourth is an application case study of the constitutive model demonstrating

its utility as a design tool for shape memory alloy force actuators; the fifth presents the development of a multi-dimensional constitutive relation of shape memory alloys; and the last chapter is the conclusion and final remarks.

## 1.1 Introduction to Shape Memory Alloys

The first observation of the shape memory effect (SME) was made in 1932 with gold-cadmium (Chang and Read, 1951). The phase transformation associated with the shape memory effect was later discovered in 1938 with brass (Perkins et al., 1975). It was not until 1962 that Buehler et al. (1965) at the Naval Ordnance Laboratory (NOL) discovered a series of Nickel-Titanium alloys that demonstrated this shape memory effect. The shape memory alloy discovered by Buehler et al. was later named Nitinol, and has been made commercially available ever since. Today, more and more materials with shape memory effects have been discovered (Table 1.1) and considerable effort is still be expanded to discover new SMA materials.

A shape memory alloy is able to “memorize” its original configuration after it has been deformed by heating the alloy above characteristic transition temperatures. This unique effect of returning to its original geometry after a large inelastic deformation (more than 1 percent) is known as shape memory effect (SME).

If steel in a high temperature austenitic phase is quenched it will generally harden. After polishing and etching, observation with a microscope will show an extremely fine structure, first named martensite after the German metallurgist Adolf Martens. Later this martensitic phase transformation involving shear deformation was found

Table 1.1: Materials with Shape Memory Effect

Alloy	Composition	Transformation Temperature ( $A_s$ ) Range, °C	Transformation Hysteresis, °C
AgCd	44~49 at % Cd	-190~-50	~15
AuCd	46.5~50 at % Cd	30~100	~15
CuAlNi	14~14.5 wt% Al 3~4.5 wt% Ni	-140~100	~35
CuSn	~15 at % Sn	-120~30	
CuZn	38.5~41.5 wt% Zn	-180~-10	~10
CuZn X (X=Si, Sn, Al)	few wt% X	-180~200	~10
InTl	18~23 at % Tl	60~100	~4
NiAl	36~38 at % Al	-180~100	~10
TiNi	46.2~51 at % Ti	-50~110	~30
TiNi X (X=Pd, Pt)	50 at % Ni+X 5~50 at % X	-200~700	~100
TiNiCu	~15 at % Cu	-150~100	~50
TiNiNb	~15 at % N.b.	-200~50	~125
TiNiAu	50 at % Ni+Au	20~610	
TiPd X (X=Cr, Fe)	50 at% Pd+X ~15 at % X	0~600	~50
MnCu	5~35 at % Cu	-250~180	~25
FeMnSi	32 wt% Mn, 6wt% Si	-200~150	~100
FePt	~25 at % Pt	~-130	~4
FePd	~30 at % Pd	~50	
FeNi X (X=C, Co, Cr)	few wt% X		

to be diffusionless due to the cooperative atomic movement of the crystal lattice. The phase transformation is accompanied by a shape change (or surface relief) (Clark and Wayman, 1970). Different materials have a different amount of surface relief depending upon the crystal orientation of the parental phase during the martensitic phase transformation. Shape memory alloys possess a martensitic transformation similar to steel, but the characteristic transition temperature is much lower than steel. The lower phase transformation temperature and large amount of surface relief during the martensitic transformation of SMAs play an important role in the deformation mechanism operating in the shape memory effect.

The martensitic transformation is the basic characteristic of shape memory alloys that is involved in all the behaviors of SMAs. The martensitic transformation may be simply illustrated by the change of martensite volume fraction with respect to temperature as shown in Fig. 1.1. The four important transition temperatures are martensite finish ( $M_f$ ), martensite start ( $M_s$ ), austenite start ( $A_s$ ), and austenite finish ( $A_f$ ).

Shape memory effects are related to the martensitic phase transformation. From a thermodynamic point of view, internal phase transformations are affected by external conditions, i.e., the phase equilibrium is governed by stress and temperature. The Clausius-Clapeyron equation given below expresses the temperature and stress relation at the state of phase equilibrium.

$$\frac{dT}{d\sigma} = \frac{T\Delta V}{\Delta H} \quad (1.1)$$



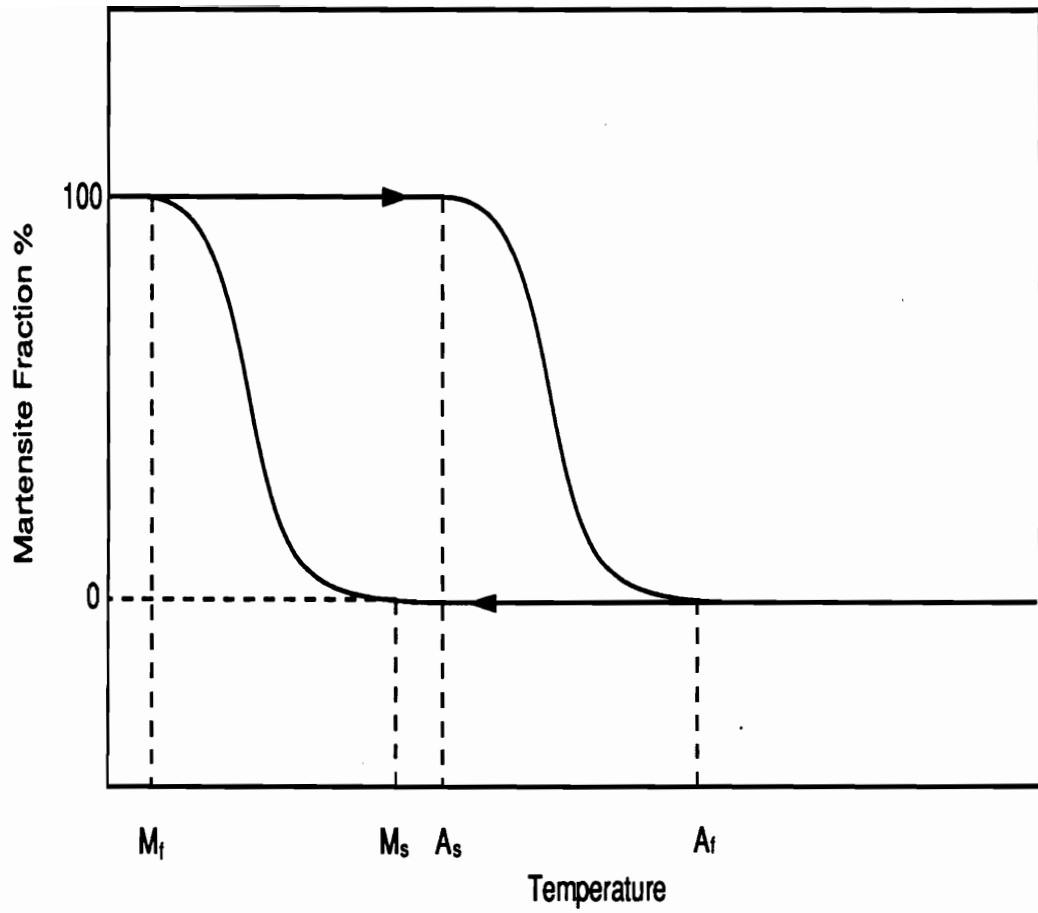


Figure 1.1: A Schematic Diagram of the Martensite Fraction vs. Temperature

where  $\sigma$  is the stress applied on the shape memory alloy,  $T$  is the temperature,  $\Delta V$  is the volume change during the martensitic phase transformation or its reverse transformation, and  $\Delta H$  is the enthalpy difference between the martensite and austenite. The Gibbs chemical free energy,  $G$ , that is the internal driving force of the martensitic phase transformation has a linear relation with temperature (Kaufmann and Cohen, 1958). The enthalpy difference  $\Delta H$  can be expressed linearly in terms of temperature due to the linear relation of Gibbs free energy with temperature. The volume change associated with the phase transformation is a constant for a given shape memory alloy. Therefore, Eq. (1.1) can be expressed as

$$\frac{dT}{d\sigma} = \text{constant} \quad (1.2)$$

Equation (1.2) suggests that the characteristic transition temperatures may have linear relations with applied stress. This is widely referred to as the stress effect on the phase transformation, and it also explains the thermomechanical basis for stress-induced phase transformation. This is to say that because the applied external stress can shift the phase transformation temperatures, the phase transformation involved in the mechanical behavior of shape memory alloys may be postponed or advanced in terms of temperature, or the phase transformation may occur at some temperatures simply due to the applied external stress.

It is necessary to mention that the phase transformation involved in the shape memory alloys is more complex than what has been discussed above. For example, there is another phase transformation, the Rhombohedral-phase transformation associated with the shape memory effect (Wayman, 1989). The R-phase transformation occurs before

the martensitic transformation (also called pre-martensitic transformation) and it is independent of the martensitic transformation. It exhibits a diffusionless structural change and an invariant plane strain shape deformation and shape memory effect. R-phase and martensite are crystallographically reversible, and can be stress induced. The R-phase transformation also exhibits some influence during the cooling process that affects the mechanical behavior as observed by Dye (1990). Usually, the R-phase transformation accounts for less than one-tenth of the total transformation (Wayman, 1989), so it is not considered in this study.

The mechanical behavior of shape memory alloys is unique. Ordinary materials like steel do not involve phase transformations in the working temperature range that affects its mechanical behavior significantly. However, because the associated phase transformation of shape memory alloys is so unique, the mechanical characteristics of SMAs are likewise significantly different from other engineering materials. Figure 1.2 shows the stress-strain curves of a nitinol alloy ( $\text{Ti}_{55}\text{Ni}$ ) at various temperatures (Cross et al., 1970). Schematically, these stress-strain curves fall into four categories as shown in Fig. 1.3. The stress-strain curve shown in Fig. 1.3 (a) shows the shape memory effect where the heating of the SMA following the linear elastic unloading results in full shape recovery. The stress-strain curve shown in Fig. 1.3 (b) is a combination of a pseudoelastic effect and a shape memory effect. The pseudoelastic effect is represented by the nonlinear unloading, which actually can be explained as linear elastic unloading with a superimposed shape memory effect. The stress-strain relation shown in Fig. 1.3 (c) illustrates a complete pseudoelastic effect where unloading of the SMA results in total reversion to its initial position after going through a mechanical hysteresis. The stress-strain curve depicted in Fig. 1.3 (d) indicates

that the shape memory alloy has been loaded to its plastic range, some permanent deformation of crystal lattice has resulted, and therefore, heating of the SMA cannot restore the material back to its original position.

The two kinds of shape recovery for SMA in terms of the recovery path are the ‘one-way effect’ and the ‘two-way effect’. Both of these effects are schematically illustrated in Fig. 1.4. The two-way effect of shape memory alloys can be obtained by ‘training’ SMA which has one-way effect capabilities and is described by (Duerig et al., 1982; Escher et al., 1990).

The change of Young’s modulus of shape memory alloys is very different from conventional metal materials. For most metals, the Young’s modulus decreases as the temperature increases. However, the Young’s modulus of shape memory alloys increases within the phase transformation temperature range for the heating process. The Young’s modulus of nitinol increases by 3 to 4 times from temperatures below  $M_f$  to temperatures above  $A_f$ . This is shown in Fig. 1.5 (Cross et al., 1970).

The shape memory effect does not simply mean that the previous shape will be restored freely upon heating the SMA. Restraining a deformed SMA wire while heating the wire above the transition temperatures will generate a large recovery stress as shown in Fig. 1.6. This unique behavior is one of the fundamental characteristics exploited in many applications of shape memory alloys.

Shape memory alloys are different from other materials in many other aspects. The influence of the phase transformation on the electrical resistance is an example and is

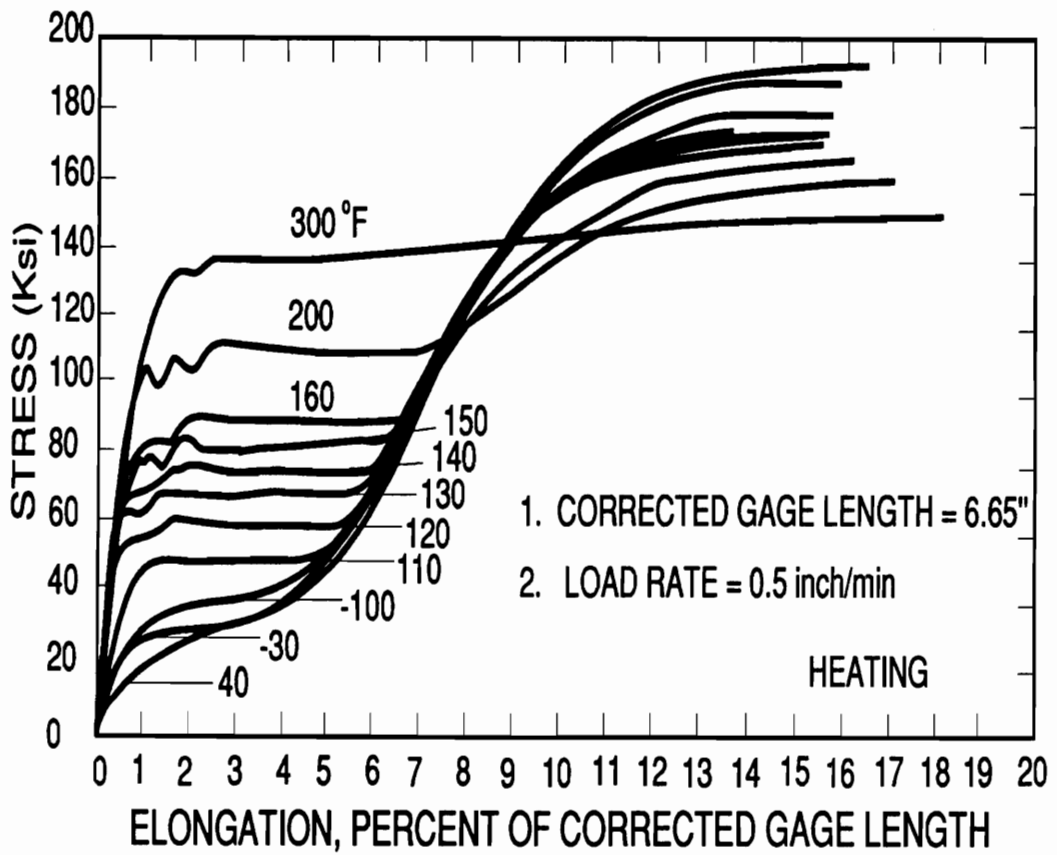


Figure 1.2: Stress-Strain Curves of a Nitinol ( $Ti_{55}Ni$ ) at Various Temperatures (After Cross et al., 1970)

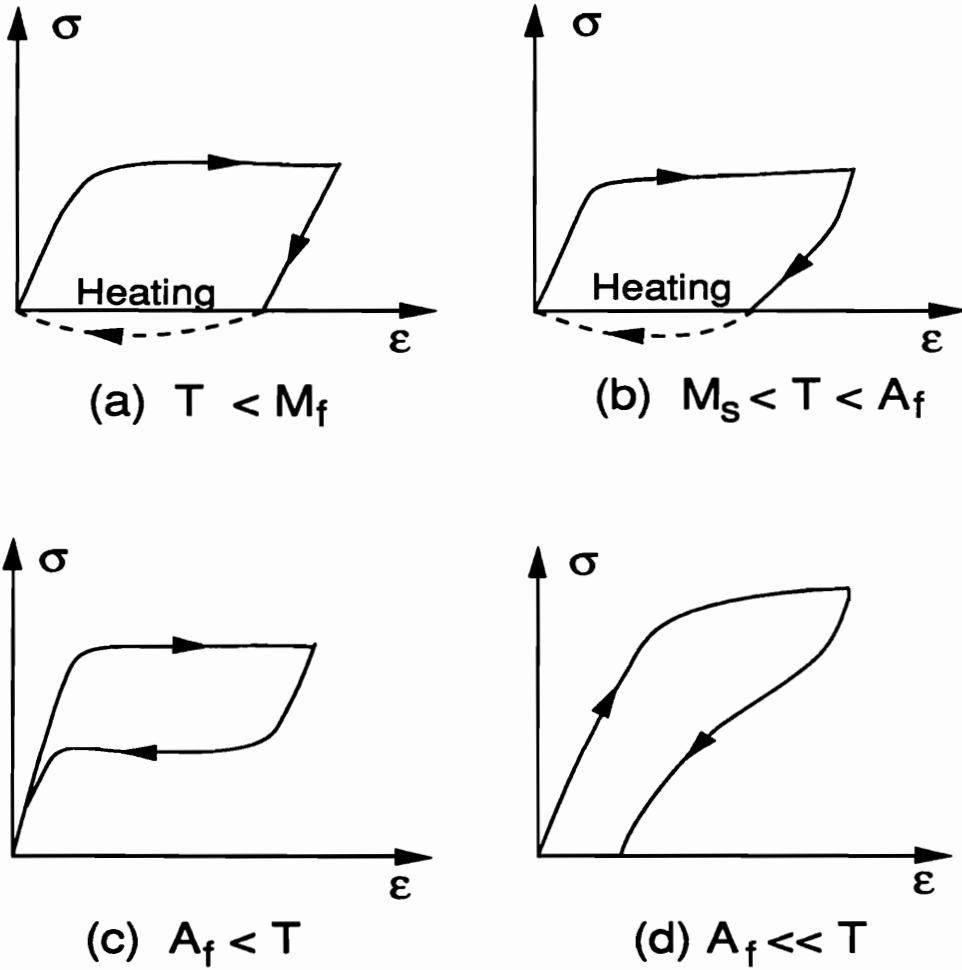


Figure 1.3: Classification of Stress-Strain Curves (After Funakubo, 1984)

shown in Fig. 1.7. The distinction between the heating and cooling process demonstrates the effect of the phase transformation. Measuring the electrical resistance of shape memory alloys is often used to determine the phase transition temperatures as indicated in Fig. 1.7.

Another important property of shape memory alloys that has attracted a great deal of attention is the damping characteristics, i.e. the internal friction characteristics of shape memory alloys. Figure 1.8 shows the change of internal friction of  $\text{Ti}_{50}\text{Ni}_{49}\text{Fe}_1$  with respect to temperature for different frequencies. The damping properties of shape memory alloys may be exploited for passive and adaptive dynamic control applications. The internal friction,  $Q^{-1}$ , shown in Figs. 1.8 and 1.9, represents the vibrational phase difference of an applied dynamic load and resulting deformation, or the strain energy dissipation during the loading and unloading process. As described in Fig. 1.3 (c), the pseudoelastic effect manifests itself in very large stress-strain hysteresis, indicating the potential use of pseudoelastic SMA as high modulus damping materials. However, the structural damping effect is related to the structural vibration frequency as shown in Fig. 1.8. The damping effect and frequency relation is schematically illustrated in Fig. 1.9. The damping effect of shape memory alloy is caused by the resistance to the movement of the martensitic and austenitic interface; 50 percent of martensitic or austenitic phase corresponds to the maximum phase interface, therefore, the maximum damping effect (the maximum  $Q^{-1}$ ) happens approximately in the middle of the phase transformation (Lin et al., 1989). Some of the shape memory alloys such as TiNiPd and FeMnSi listed in Table 1.1 have wider transformation hysteresis and would be the ideal materials to perform passive or passive self-adaptive dynamic control.

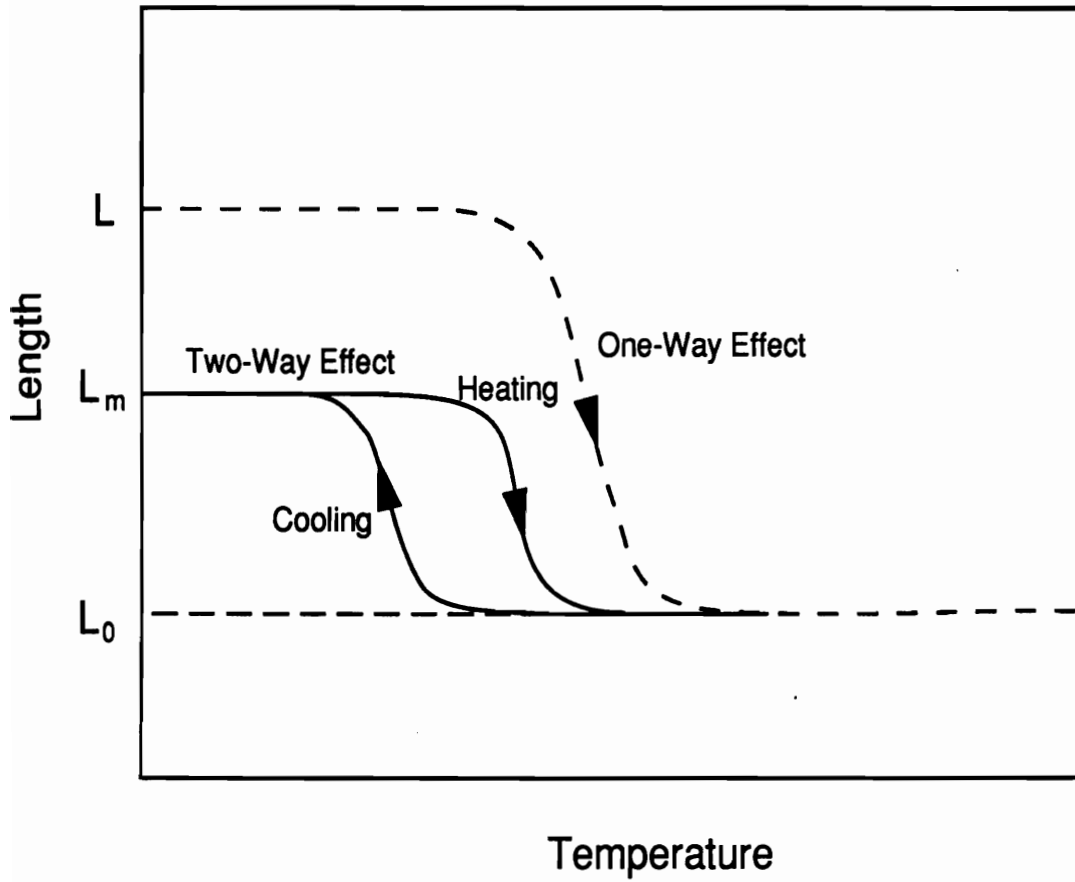


Figure 1.4: One-way and Two-way Shape Memory Effect



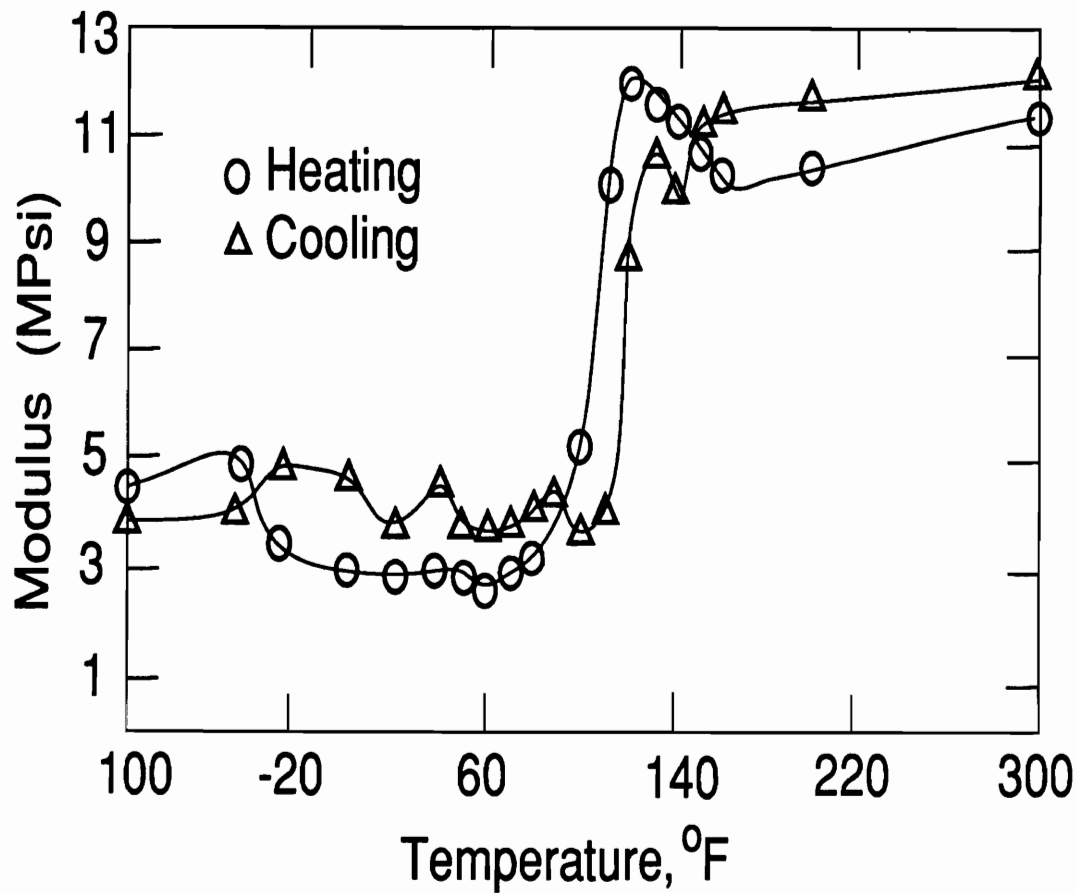


Figure 1.5: Young's Modulus of a Nitinol vs. Temperature (After Cross et al., 1970)

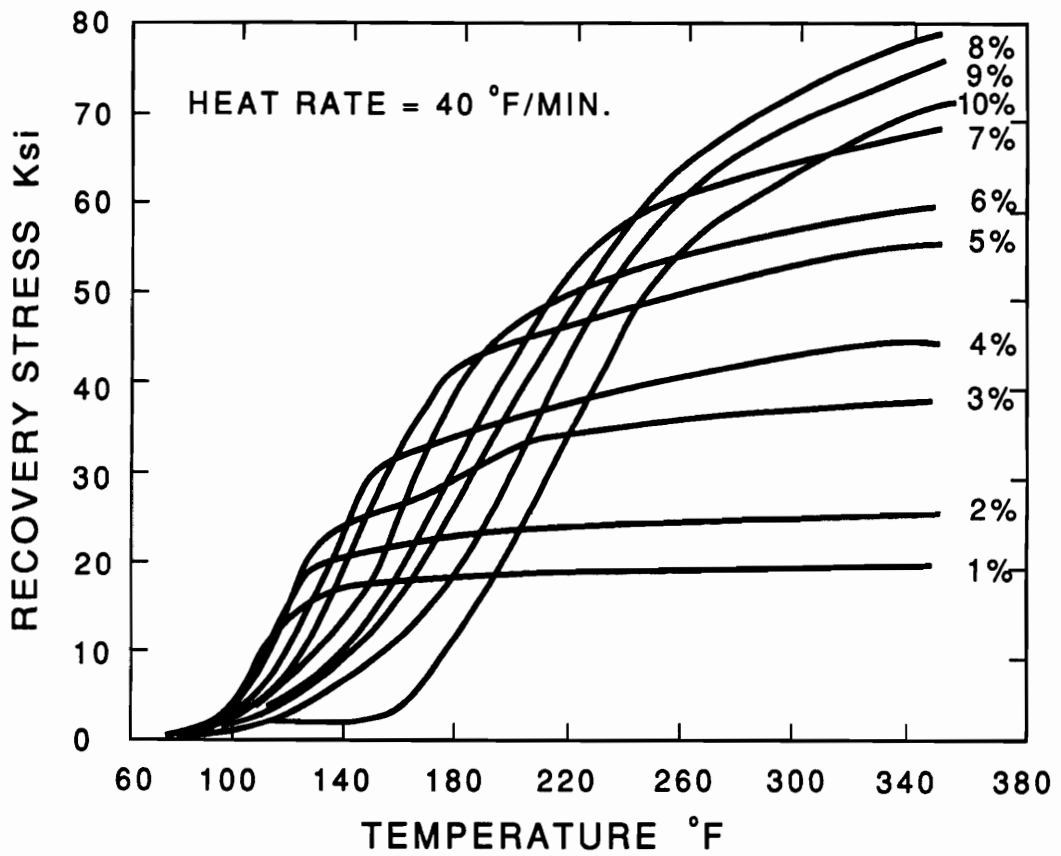


Figure 1.6: Recovery Stress vs. Temperature for Different Initial Strains (After Cross et al., 1970)

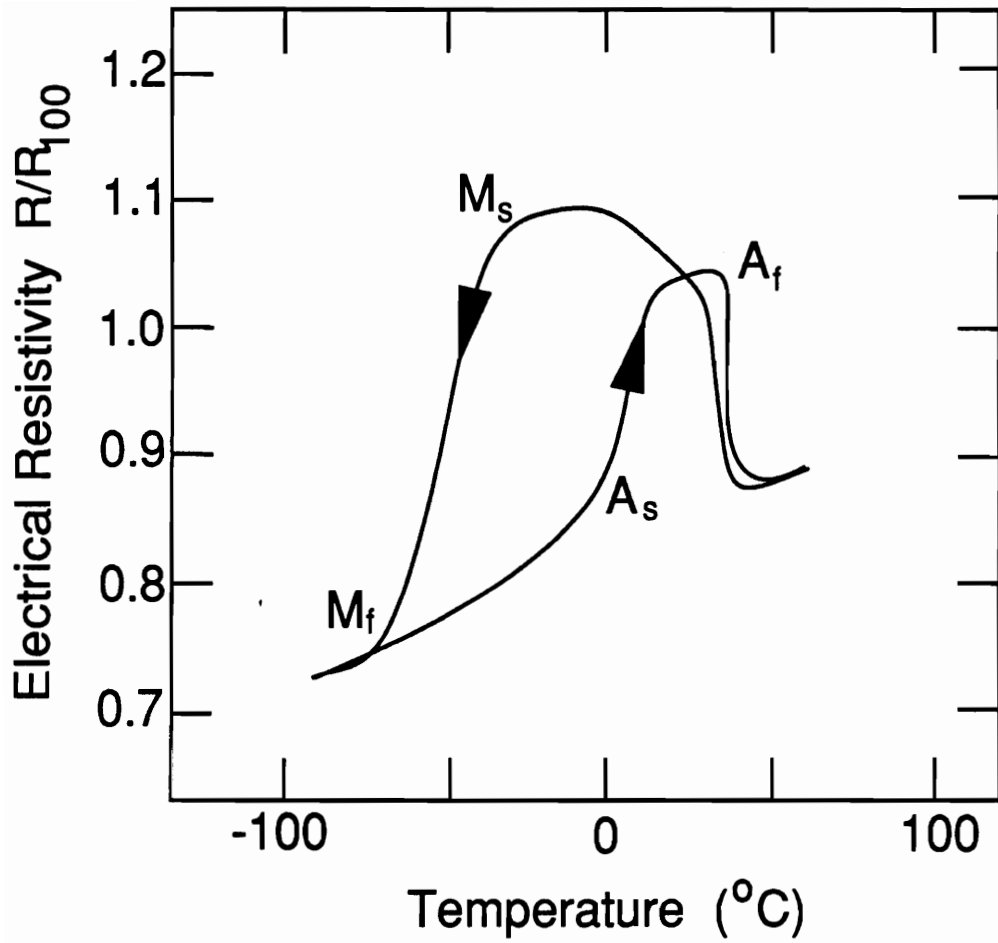


Figure 1.7: Electric Resistivity vs. Temperature (After Funakubo, 1984)

Shape memory alloys are very sensitive to their heat treatment. A great deal of research has been conducted in this field (Tadaki et al., 1987; Todorodi and Tamura, 1987). Figure 1.10 shows the effect of annealing temperatures on phase transformation temperatures. The sensitivity of shape memory alloys to different heat treatment is both a shortcoming and an advantage. This means that a proper heat treatment will provide the material behavior required by a specific application. However, this also means that certain extreme conditions, such as overheating of a SMA actuator, may permanently degrade the material properties or damage the material.

In this section, the general concept of shape memory alloys was introduced and some of the important characteristics of shape memory alloys presented. A detailed discussion of the characteristics associated with the constitutive modeling of shape memory alloys will be presented in Chapter 2.

## **1.2 Industrial Applications of SMA**

Shape memory alloys have been used in a wide variety of applications because of the unique mechanical characteristics discussed above. This section will review some of the industrial applications of shape memory alloys and shape memory alloy hybrid composites.

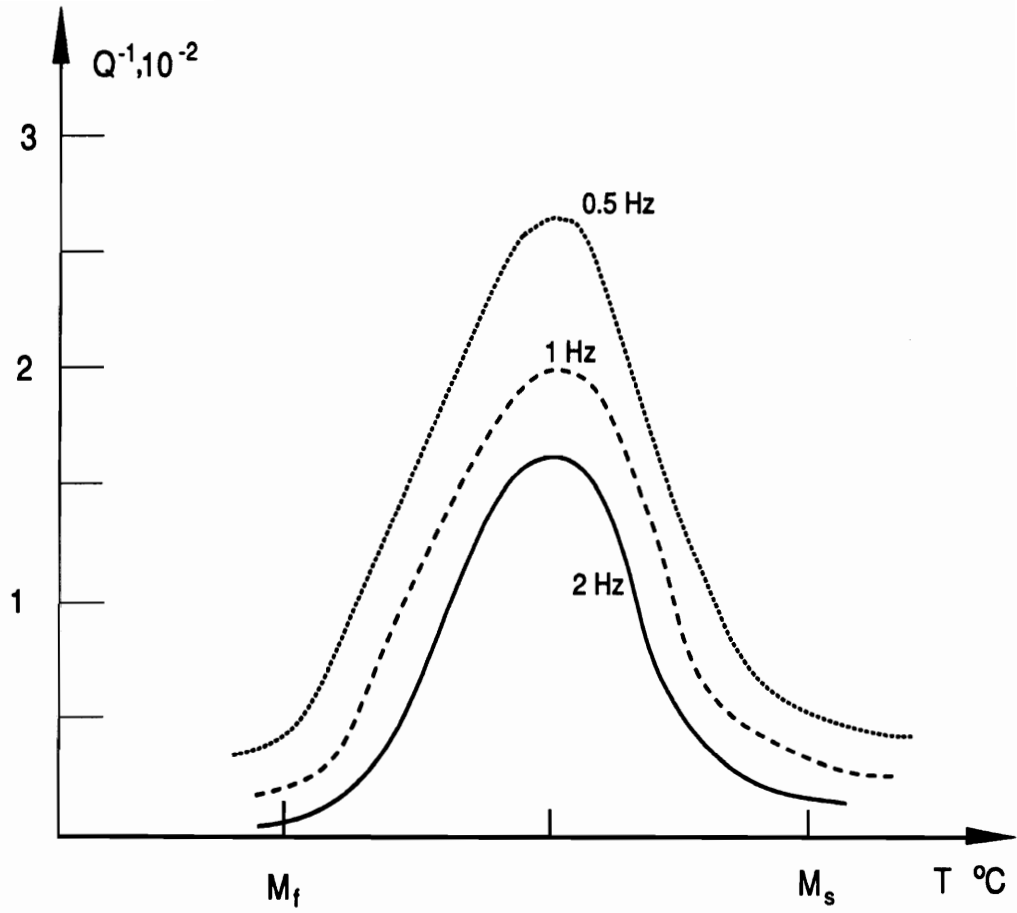


Figure 1.8: Internal Friction,  $Q^{-1}$ , vs. Temperature (Lin et al., 1989)

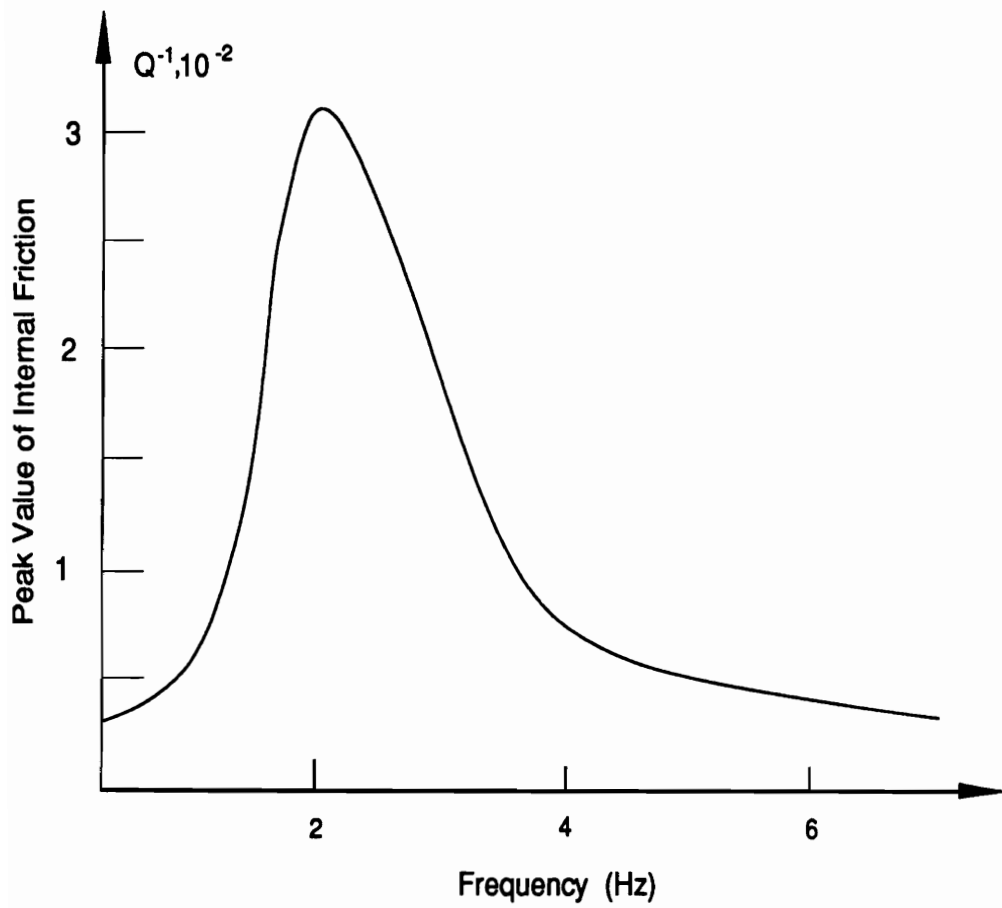


Figure 1.9: Schematic of Internal Friction,  $Q^{-1}$ , vs. Frequency

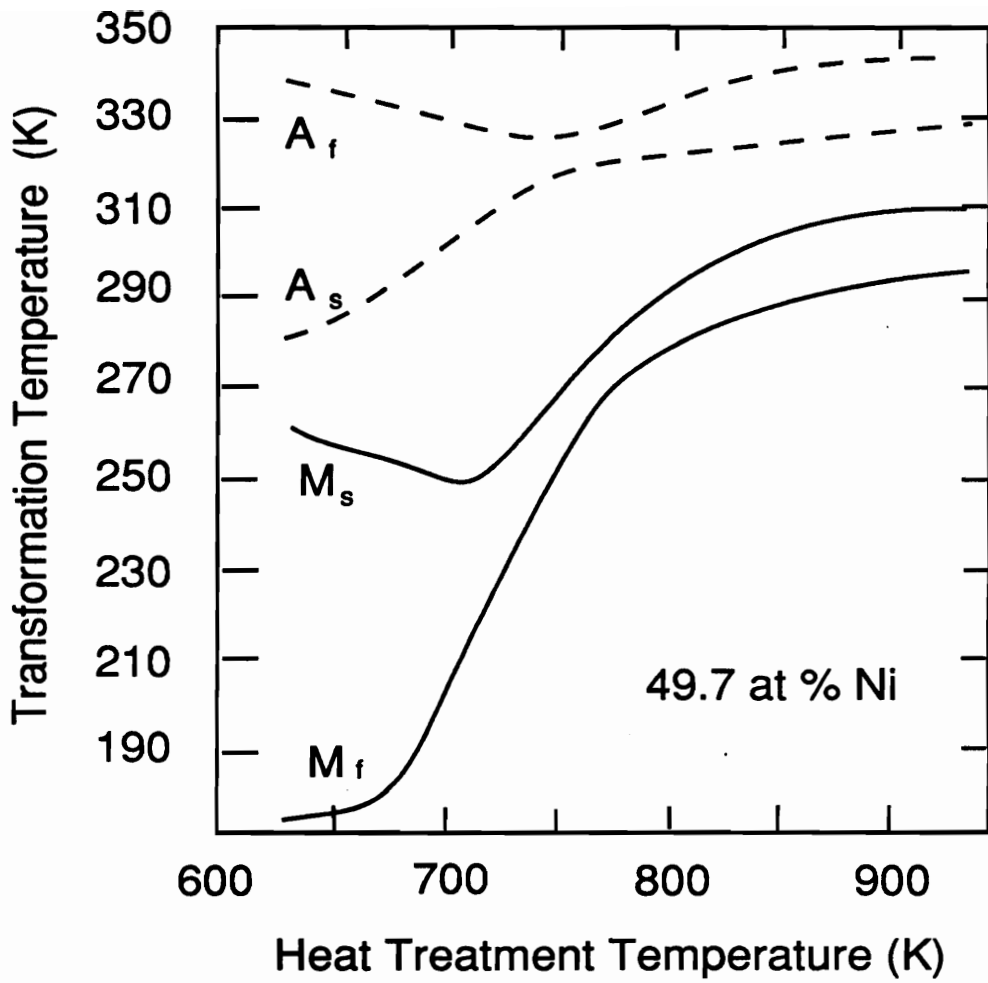


Figure 1.10: The Effect of Annealing Temperature on Phase transformation Temperatures (After Tordorodi and Tamura, 1987)

### **1.2.1 SMA Couplings**

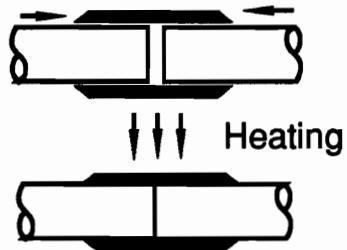
The first large-scale industrial application of shape memory alloys was by Raychem Corporation in 1969 (Harrison et al., 1975) as cryogenic aircraft pipe fitting devices for fuel systems. More than one hundred thousand of these fittings as shown in Fig. 1.11 (a) have been installed in advanced airplanes such as the F-14 and there have been no reported failures. Similar devices include shape memory rivets (Figs. 1.11 (b)) (Buehler et al., 1969), SMA clamps, and SMA seals (Levinsohn et al., US Patent 3,759,552). Note that all the SMA devices illustrated in Fig. 1.11 are designed for one time installation and are generally of two-dimensional or three-dimensional configurations.

### **1.2.2 SMA Heat Engines**

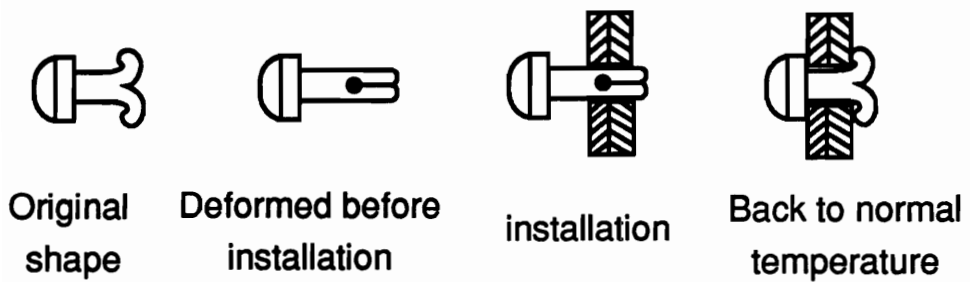
Since shape memory alloys produce large forces when subjected to temperature differences such as hot and cold water, this basic concept has been used to design SMA energy conversion machines, i.e., the heat engines. Banks (1975) designed a prototype of this kind of machine as shown in Fig. 1.12 in 1973. SMA heat engines can be roughly divided into (1) offset crank engines (Banks, 1975; Ginell et al., 1979), (2) turbine (differential pulley) engines (Johnson, 1975; Honma et al., 1978), and (3) field (gravity) engines (Funakubo, 1984). The Carnot efficiency of SMA heat engines has been reported ranging from a very few percent to 20~30 percent. The maximum power output was reported from Trupins' prototype as about 100 watts (Sanders, 1981). However, these machines have only been used for demonstration purposes.



Insert pipes after  
expanding the coupling



(a)



(b)

Figure 1.11: SMA Couplings (After Funakubo, 1984)

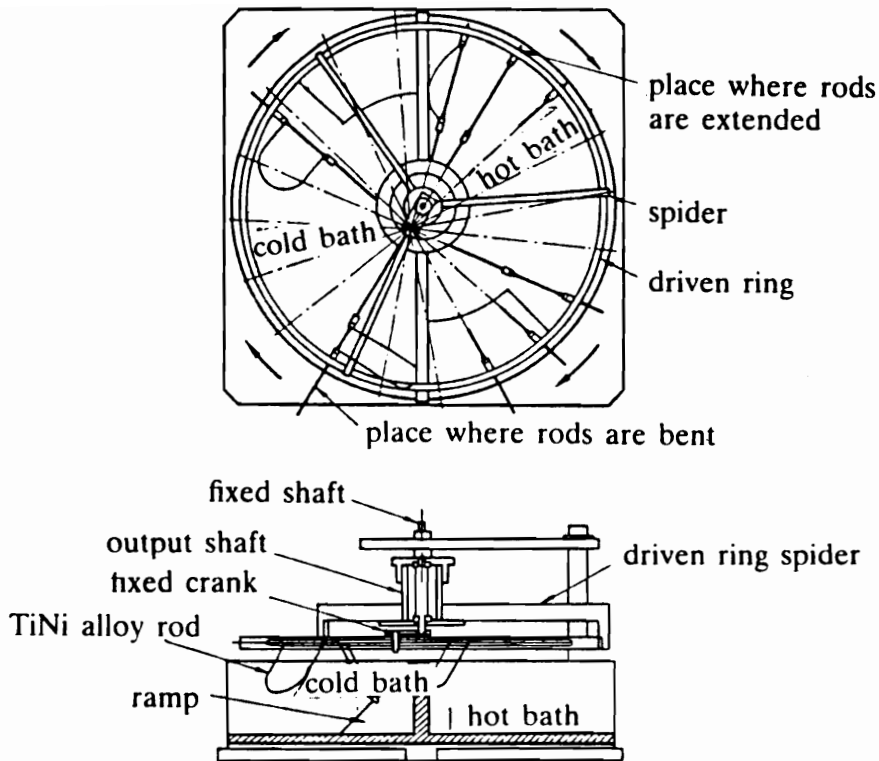


Figure 1.12: Bank's Prototype of SMA Heat Engine (After Funakubo, 1984)

### 1.2.3 SMA Actuators

Shape memory alloys can be used wherever repeated shape, geometry, and positions are required. The concept of shape recovery of SMA has inspired many inventions such as the electric switch and temperature switches (Funakubo, 1984).

There are three basic types of SMA actuator (Biometal, 1987). The actuator shown in Fig. 1.13 (a) is referred to as a one-directional actuator for devices such as SMA cryogenic pipe fittings and other connectors intended for one-time installation. The actuator shown in Fig. 1.13 (b) is called a bias force actuator, which uses a spring to generate the restoring force and thus giving the mechanism a ‘two-way effect’. The SMA spring or wire is first deformed, i.e., elongated at a low temperature before installation. When the SMA spring is heated, the recovery force generated by the shape memory effect pulls the spring to store energy in the spring. When the SMA actuator is cooled, the potential energy stored in the bias spring is released to strain the SMA spring (or wire) back to its initial position, resulting in a deformation-reformation cycle that is accompanied by the martensitic transformation and reverse transformation of SMA elements. The actuator depicted in Fig. 1.13 (c) is called a differential force SMA actuator that includes an opposing SMA element used to create an active bias force and a deformation SMA element with some initially stored energy (characterized by a thermally unstable martensite and represented by initial strain). A specially designed cooling and heating strategy of the two SMA elements can produce a differential motion path. A general design method for the second and third type of SMA actuator depicted in Fig. 1.13 will be developed based upon the newly formulated relations that will be presented. The actuator depicted in Fig. 1.13 (a) generally is a 2-D or 3-D solid element in contrast to the wire or 1-D elements used

in the bias spring and differential force actuators. Based on the multi-dimensional constitutive model that is developed in Chapter 5, the detailed operating mechanism of this type of 2-D SMA actuator (such as a SMA pipe fitting) can be studied.

The operating variables for a SMA actuator are the amount of force output, the maximum travel distance, or stroke, and the work generated by the actuator. The basic design variables include the selection of the SMA material (i.e. alloy composition, cold and hot rolling method, and heat treatment, etc.), the length of the SMA wire(s), cross-sectional area, and the initial state of the SMA (i.e., its initial martensitic residual strain, or initial percentage of martensite). The other important parameter for a bias spring SMA actuator is the bias spring constant. It is assumed in this discussion that both SMA elements of a differential actuator are of the same SMA material so that the design variables of a differential actuator are restricted to its geometric variables and initial states of the SMA elements.

Several methods are used to determine these parameters (Hodgson, 1988; Funakubo, 1984). Figure 1.14 (Hodgson, 1988) shows the stress-strain curves of the high temperature austenitic and low temperature martensitic phase of a shape memory alloy with a bias spring's force superimposed. The slope of the dash line represents the stiffness of the spring. The initial equilibrium position is 'B'. When heated, the SMA wire contracts to 'A'. The lower stress-strain curve corresponds to a temperature lower than the transition temperature (usually the austenite start temperature  $A_s$ ). The upper curve is the stress-strain curve of the same piece of SMA wire at a temperature much higher than  $A_f$ . Since a complete cycle of the SMA elements involves both the martensitic transformation and its reverse transformation, the design method shown

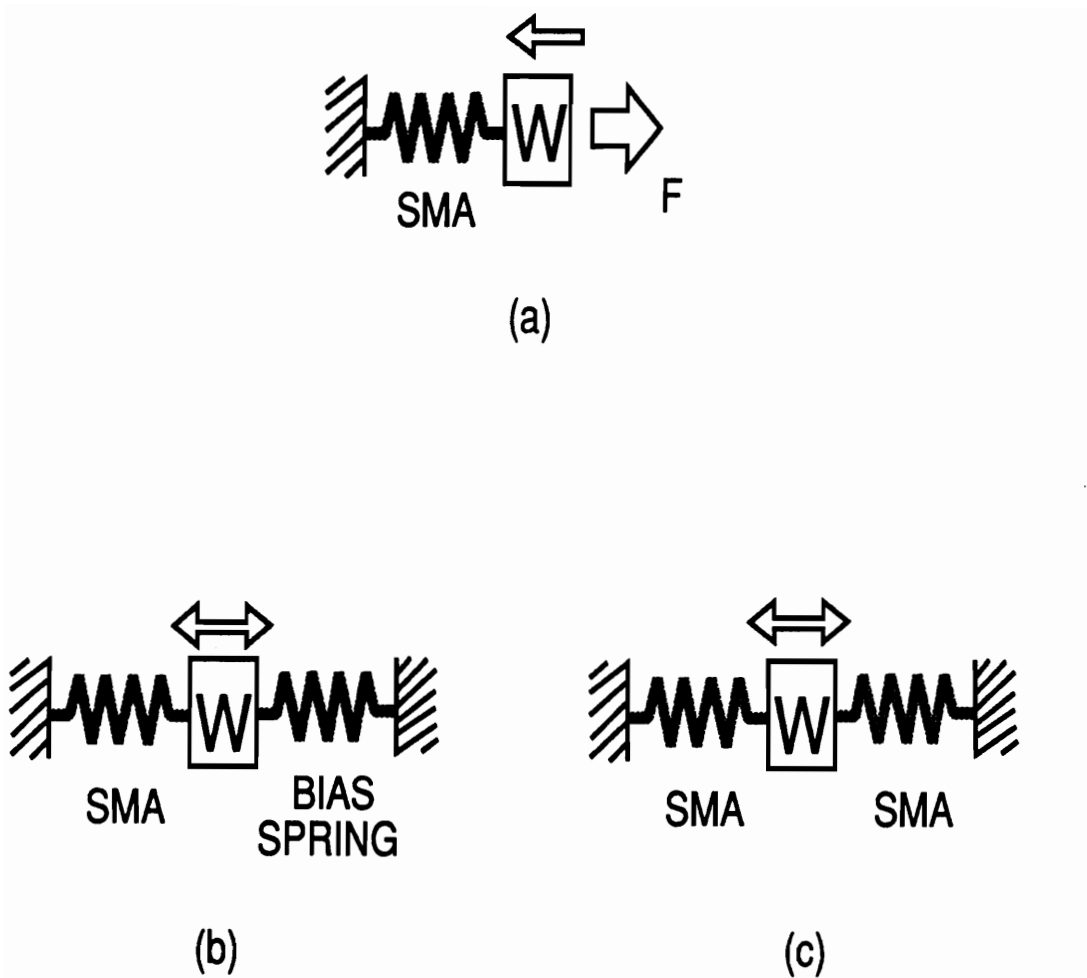


Figure 1.13: Basic Types of SMA Actuators (After Biometal, 1987)

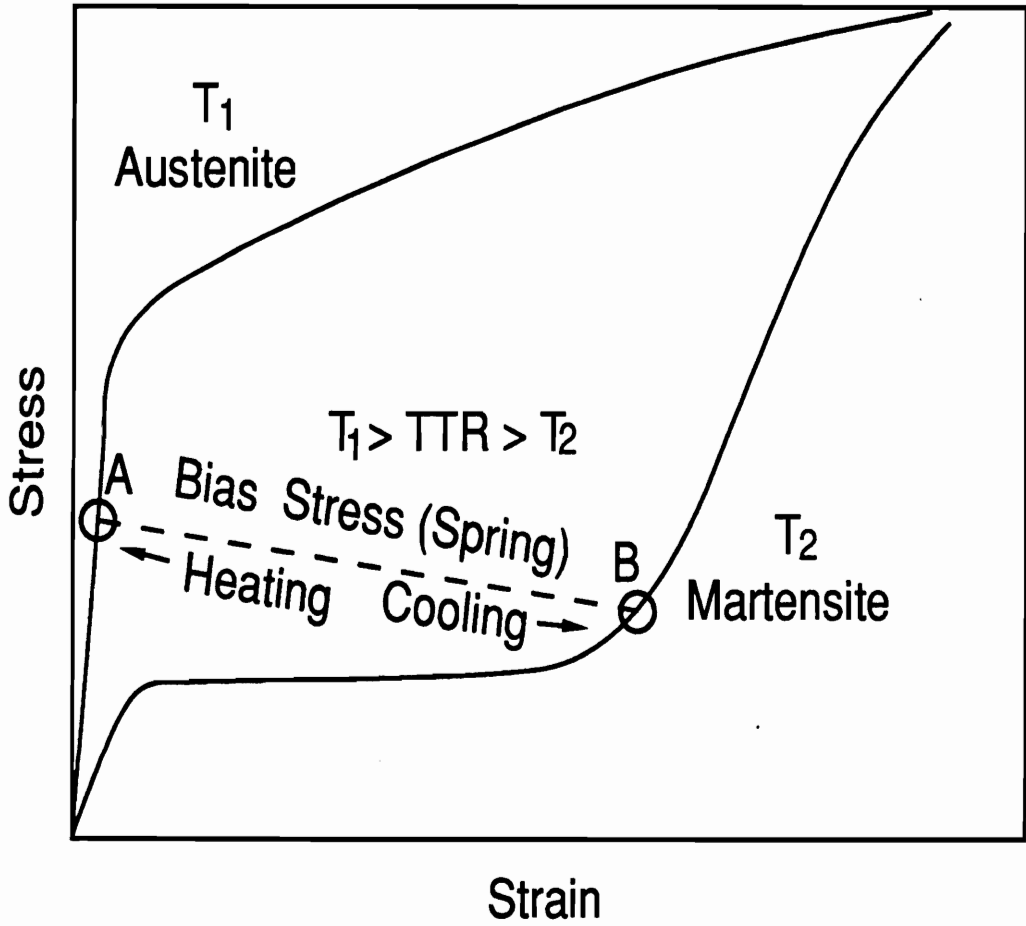


Figure 1.14: Bias Spring SMA Actuator Design Chart 1 (After Hodgson, 1988)

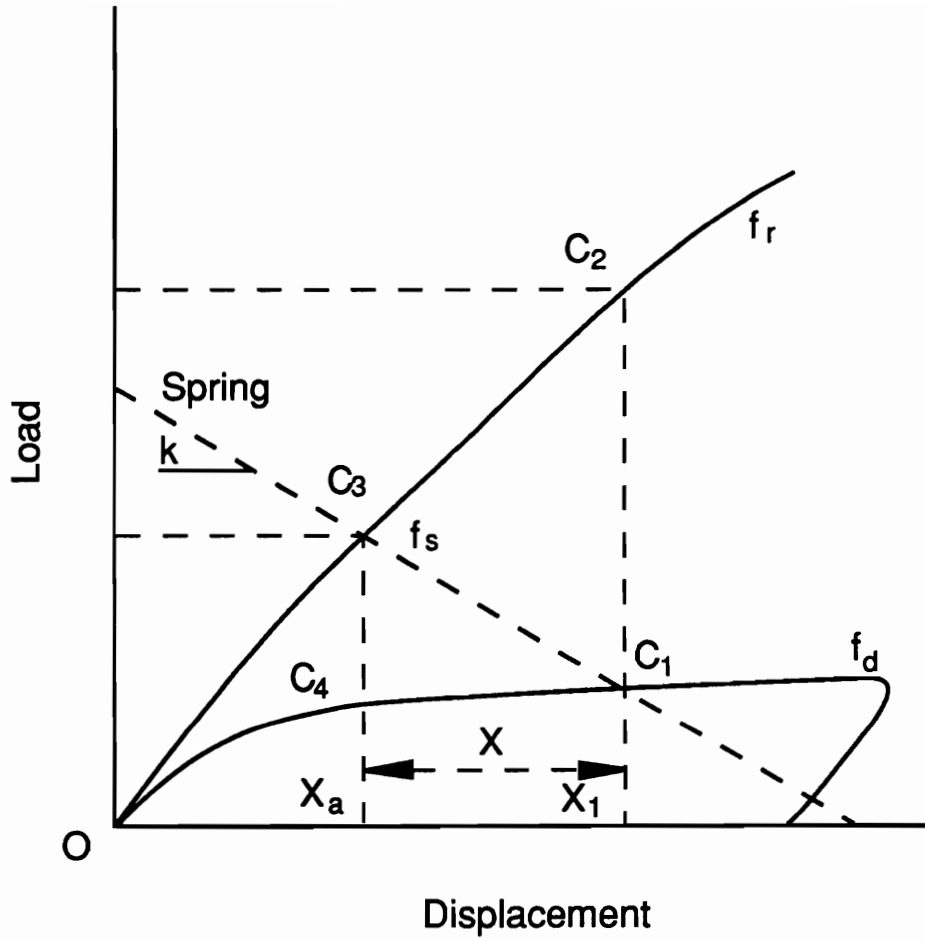


Figure 1.15: Bias Spring SMA Actuator Design Chart 2 (After Funakubo, 1988)

in Fig. 1.14 does not reflect this and can only provide an approximate result. Another design approach for bias spring SMA actuators is shown in Fig. 1.15 (from Funakubo, 1984). Unlike Fig. 1.14, the stress-strain curves (load-displacement curves here) are called deformation and reformation curves. The curve  $OC_1$  is the load-displacement curve at a low-temperature martensitic phase and the curve  $OC_2$  is the recovery stress-strain curve. This method (shown in Fig. 1.15) can provide such information as the amount of force generated (from  $C_1$  to  $C_3$ ), the travel distance of 'X' (from  $X_a$  to  $X_1$ ), and the total available work (area formed by  $C_1C_3C_4$ ). The point  $C_1$  determines the initial state of the SMA wire and 'k' is the spring constant of the bias spring. The primary problem in utilizing this approach is the determination of the reformation curve (or the recovery stress-strain relations) (Liang and Rogers, 1989; Dye, 1990; Duerig et al., 1989).

Although the design approaches mentioned above are not very effective, they can still provide information helpful to the design of bias spring actuators. However, the design of a differential actuator is still very difficult and there has been no published work describing a general design method for differential force SMA actuators.

#### **1.2.4 SMA Hybrid Composite**

Rogers (1988) suggested that shape memory alloy fibers could be embedded into composite materials as active 'reinforcement' and actuators (SMA hybrid composites) to impart adaptive structural modification. The class of the material referred to as SMA hybrid composites is simply a composite material that contains shape memory alloy fibers (or film) in such a way that the material can be stiffened or controlled by the



addition of heat (resistive heating is usually used due to the unusually high electrical resistance of NiTi shape memory alloys). One of the many possible configurations of SMA hybrid composites is one in which the shape memory alloy fibers are embedded in a material off the neutral axis on both sides of the structure in agonist-antagonist pairs as shown in Fig. 1.16. SMA fibers are embedded in a variety matrix materials such as graphite/epoxy, glass/epoxy, thermoplastic materials, and other moldable or formable materials. The SMA hybrid composite materials that are presently under investigation include nitinol/graphite/epoxy (graphite/epoxy as the matrix) and nitinol/glass/epoxy (glass/epoxy as the matrix), silicon/nitinol, APC-2/nitinol, and PLYTRON/nitinol.

Two active structural modification techniques have been developed: one is called active properties tuning (APT), another is active strain energy tuning (ASET) (Rogers, Liang, and Jia, 1989). The first technique (APT) makes use of the characteristics of the change of the Young's modulus (shown in Fig. 1.5) of shape memory alloys as a function of temperatures. Heating the embedded shape memory alloy fibers will increase the overall stiffness of the hybrid composite according to the rule of mixtures. The response of SMA hybrid composites under the same external loading will be modified in a controlled fashion. This can be either a static response or a dynamic response. The static response includes buckling and transverse deformation. Increasing the stiffness of a SMA hybrid composite plate will certainly increase the buckling strength and reduce the transverse deformation of the plate. The active control is achieved by adding heat electrically to the structure rather than altering the structure by putting a control mass.

This technique usually requires a relatively large volume fraction of shape memory

alloy fibers (40 %) in order to have an effective change of the stiffness of the material (Liang, Jia, and Rogers 1989).

The second technique (ASET) requires embedding prestrained shape memory alloy fibers. The restraint of the prestrained SMA fibers will produce a large recovery stress if the SMA wire is heated above its transition temperatures as demonstrated in Fig. 1.6, and thereby creating a large increase in the stored strain energy. The recovery stress of the SMA fibers actually produces a membrane stress and the nature of this membrane stress (compressive or tensile) is highly dependent on the boundary conditions of SMA hybrid composites (Barker, 1989; Rogers and Barker, 1990). Tuning the internal stress field results in the modification of the response of the SMA hybrid composite structures. The name ‘active strain energy tuning’ comes from the concept that the pre-stored strain energy (represented by the initial strain of SMA fibers) can be released or activated by heating the SMA fibers to tune the response much like tuning a guitar string. The objective of tuning the dynamic response of SMA hybrid composites is generally to change the structural dynamic behavior of the structure, i.e., the natural frequency and mode shapes. The activated first natural frequency of a clamped-clamped SMA hybrid composite beam measured experimentally can be as high as six times the inactivated frequency (Barker, 1989). Lower-order mode shapes of an SMA hybrid composite plate also can be varied significantly as shown in Fig. 1.17.

The list of scientific areas that can be influenced by this novel approach made possible with SMA hybrid composites is significant. For example, vibration control can be accomplished by using the distributed force actuator capabilities similar to the common

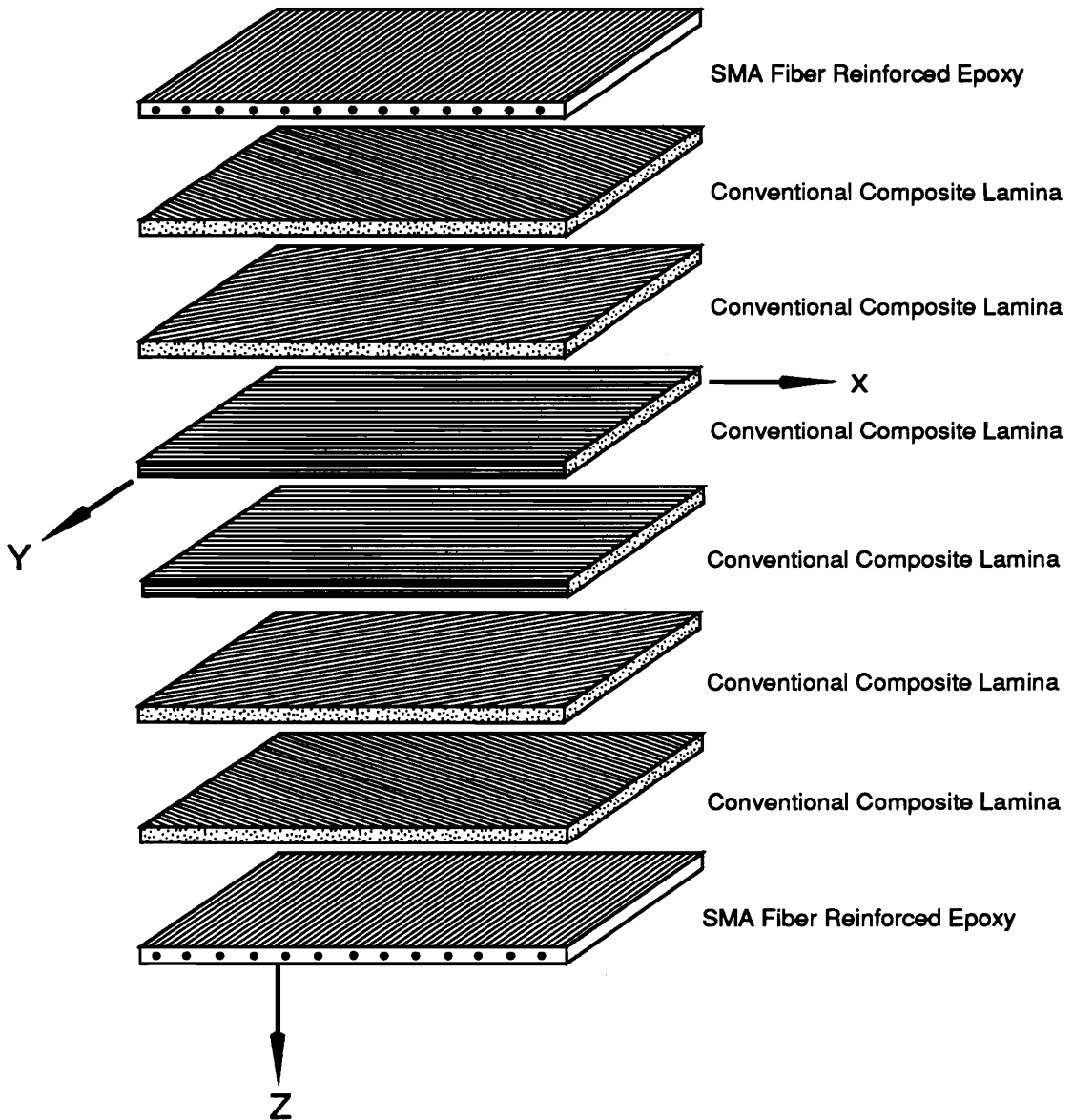


Figure 1.16: Schematic Diagram of the Configuration of an SMA Hybrid Composite Plate

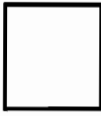


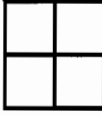




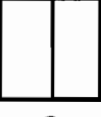

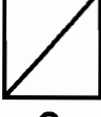
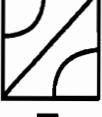
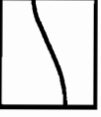



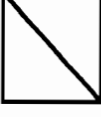

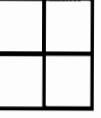
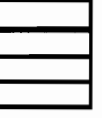

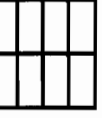
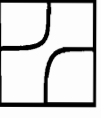

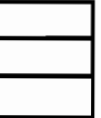
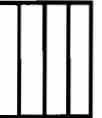




First Ten Mode Shape of a Quasi-isotropic Plate					
All Activated Inactivated		90° Activated		45° Activated	
					
1	6	1	6	1	6
					
2	7	2	7	2	7
					
3	8	3	8	3	8
					
4	9	4	9	4	9
					
5	10	5	10	5	10

Figure 1.17: Change of the First Ten Mode Shape Resulted from ASET (After Liang, Rogers, and Jia, 1989)

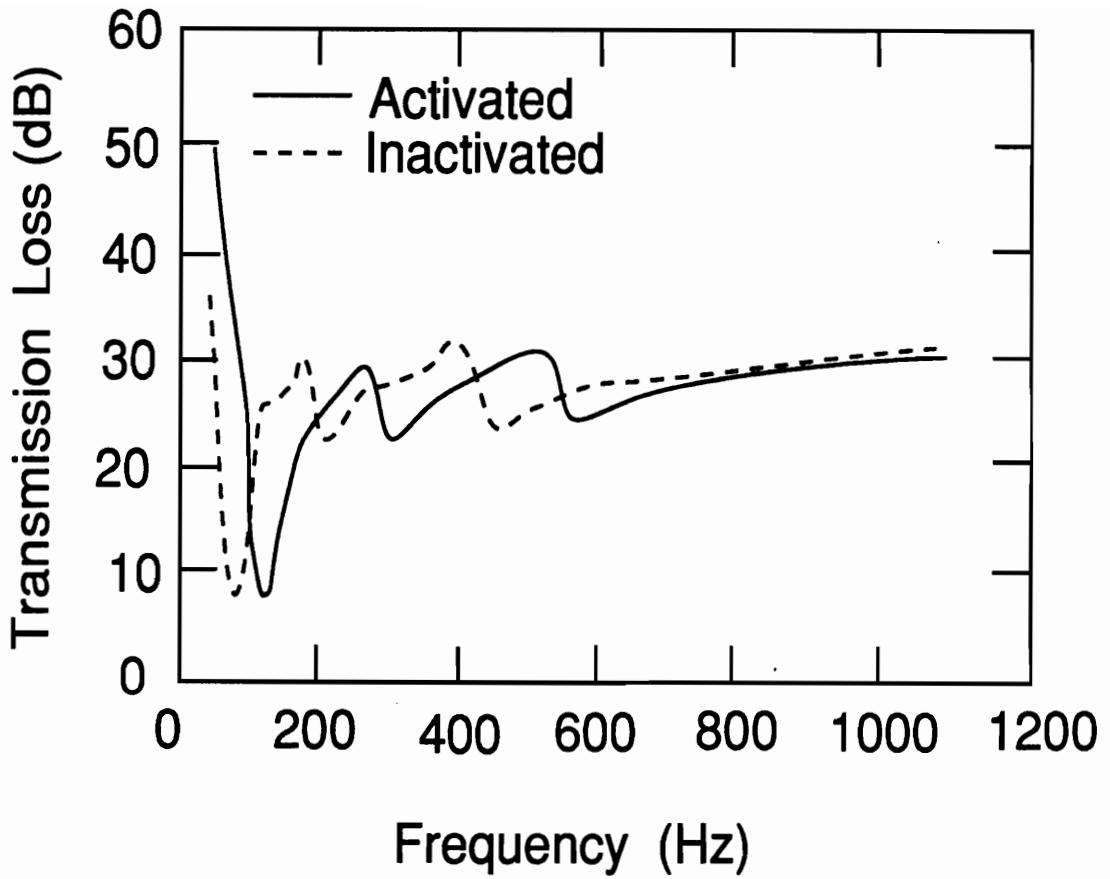


Figure 1.18: Transmission Loss of Sound Through a SMA Hybrid Panel vs. Frequency with ASET Technique (After Liang, Rogers, and Fuller, 1990)

piezoelectric systems. Other active controls such as buckling control can be achieved similarly. One of the main applications of SMA hybrid composites is in active acoustic control. The sound transmission and radiation from a SMA composite structure can be actively controlled by actively modifying the resonance frequency and mode shape of the SMA structure (Liang, Rogers, and Fuller, 1990; Rogers, Fuller, and Liang, 1990). Figure 1.18 shows the profile of transmission loss of sound through a SMA hybrid panel. The experimental study of sound radiation of a SMA hybrid composite beam has been conducted (Saunders, Robertshaw, and Rogers, 1990) which showed the overall sound radiation reduction of 50 dB.

Embedding shape memory alloy into conventional composites makes the new SMA hybrid composites adaptive materials. The SMA hybrid composites have the capability to modify their dynamic response, structural acoustic behavior, and static response. They also have the capability to sense their internal damage possibly due to fatigue or manufacture imperfection as well as perform active damage control. The application of SMA in damage sensing and active damage control will have a tremendous impact on many areas.

### **1.3 Review of the Constitutive Modeling of SMA**

The investigation and formulation of constitutive relations of shape memory alloys has been of considerable interest and intense effort since the 1970's. Many different models have been proposed. A full and detailed review of the constitutive modeling of shape memory alloys will now be presented, starting from a basic introduction to traditional thermodynamic modeling.

### 1.3.1 Traditional Thermodynamic Modeling

The traditional thermodynamic modeling of shape memory effects, i.e., the characteristics of stress-induced martensitic transformations, is based on the Clausius-Clapeyron equation as given in Eq. (1.1). Conventional thermodynamic state variables enthalpy,  $H$ , and Gibbs free energy,  $G$ , are modified by including the potential energy resulting from applied stress.

$$\begin{aligned}H^* &= U + PV - Fl = H - Fl \\G^* &= U + PV - TS - Fl = G - Fl\end{aligned}\tag{1.3}$$

where  $U$  is the internal energy,  $P$  the pressure,  $V$  the volume,  $F$  the force applied to the specimen,  $l$  the length of the specimen and superscript ‘\*’ represents the modification of adding the potential energy. The minimum of free energy corresponds to the state of phase equilibrium. The pressure term, ‘ $PV$ ’, in the above equation can be ignored for solid materials and the Gibbs free energy is, therefore, the same as the Helmholtz free energy. If the free energy of the parental phase and the martensitic phase are denoted as  $G^{*P}$  and  $G^{*M}$ , respectively, when the phase transformation reaches equilibrium, the following relation can be derived from the minimization of the free energy (Reed-Hill, 1973).

$$G^{*P} = G^{*M}\tag{1.4}$$

consequently,

$$\frac{\Delta H^*}{T_0(F)} = \Delta S \quad (1.5)$$

where  $T_0(F)$  is the temperature at which both phases are in equilibrium under a force  $F$ ;  $\Delta H^*$  and  $\Delta S$  are the difference between the  $H^*$  and  $S$  of the two phases at  $T_0$ . The following equation can be obtained by invoking the first and second laws of thermodynamics,

$$dG^* = VdP - SdT - l dF \quad (1.6)$$

Under constant pressure, the first term on the right-hand side of the above equation vanishes. This indicates that the free energy  $G^*$  can be expressed in terms of the two independent variables  $T$  and  $F$ . If the equilibrium boundary of the parental phase and the martensitic phase is altered so that  $T \rightarrow T + dT$  and  $F \rightarrow F + dF$  while the state of equilibrium is maintained, the restriction for the change of equilibrium position can be derived from Eqs. (1.4) and (1.6) as

$$- S^P dT - l^P dF = - S^M dT - l^M dF \quad (1.7)$$

This leads to the relation

$$\frac{dF}{dT} = - \frac{\Delta S^{P \rightarrow M}}{\Delta l^{P \rightarrow M}} = - \frac{\Delta H^{*P \rightarrow M}}{T_0(F) \Delta l^{P \rightarrow M}} \quad (1.8)$$



The stress and strain relation is then expressed as

$$\frac{d\sigma}{dT} = -\frac{\Delta S^{P \rightarrow M}}{\epsilon^{P \rightarrow M}} = -\frac{\Delta H^{*P \rightarrow M}}{T_0(F)\epsilon^{P \rightarrow M}} \quad (1.9)$$

This is another form of the Clausius-Clapeyron equation. Since this equation is based on a strict thermodynamic derivation, it should be able to provide the quantitative description of the stress-strain and temperature relations. However, because this equation requires the quantitative measurement of thermodynamic data such as the free entropy, which is not practical in engineering design, this equation remains as a qualitative description of the thermodynamic nature of the shape memory effects. Detailed discussion of this modeling can be found in Funakubo (1984) and Warlimont (1974).

### 1.3.2 Müller's Constitutive Model

Müller and his colleagues (1979, 1980 and 1986) proposed another model based on shape memory effect phenomenology, thermodynamics, and statistical physics. For a small lattice, the potential energy at a certain temperature is schematically shown in Fig. 1.19. There are two stable minima corresponding to the martensitic twins and a metastable center for the austenitic state as shown in Fig. 1.19. The shear length of each layer of the martensitic lattice is denoted by  $\Delta$ , and the stable martensitic phases are denoted by  $M+$  and  $M-$ . If an external force  $P$  is applied, the total potential energy is given by  $\Phi - P\Delta$  as shown in Fig. 1.20. At a lower temperature, the material particles lie still in their potential well. The yielding from  $M-$  to  $M+$  will occur when the applied external load is so large that the potential barrier on the

left is eliminated as shown on the top of Fig. 1.20. The bottom of Fig. 1.20 refers to higher temperatures at which particles are fluctuating about their minima with a mean kinetic energy that is proportional to the temperature. The height of the pools of the potential wells of Fig. 1.19 indicates the strength of the fluctuation. The figure indicates that at higher temperatures the yielding from  $M-$  to  $M+$  will occur at a lower load than that at lower temperatures. If there is such a fluctuation, it may be described using statistical mechanics. Assuming the distribution function of phase 'k' is  $N_k$  in a single lattice, the total deformation  $D - D_0$  may be written as

$$D - D_0 = \frac{1}{\sqrt{2}}(N_{M-}\Delta_{M-} + N_{M+}\Delta_{M+} + N_A\Delta_A) \quad (1.10)$$

The thermodynamics behind the phase transformation can be described as: "the energy  $E$  tries to minimize by pulling all particles into the depths of the potential wells and the entropy  $S$  attempts to maximize by distributing the particles evenly over the available range of shear lengths. In this competition, it is the free energy,

$$\Phi = E - TS \quad (1.11)$$

that achieves a minimum" (Müller, 1986). The free energy and the distribution function  $N_k$  can be related using statistical mechanics. Minimization of the free energy will yield the explicit expression of  $D - D_0$  and martensitic volume fraction,  $\xi$ , in terms of the applied load and temperature. The expression for  $D - D_0$  is given as

$$D - D_0 = \frac{N}{\sqrt{2}} \frac{e^{\left(\frac{2\epsilon x_A}{kT}\right)} \sum \left[ \Delta e^{\left(\frac{P\Delta - \phi(\Delta)}{kT}\right)} \right] + e^{\left(-\frac{2\epsilon x_M}{kT}\right)} \sum \left[ \Delta e^{\left(\frac{P\Delta - \phi(\Delta)}{kT}\right)} \right]}{e^{\left(\frac{2\epsilon x_A}{kT}\right)} \sum e^{\left(\frac{P\Delta - \phi(\Delta)}{kT}\right)} + e^{\left(-\frac{2\epsilon x_M}{kT}\right)} \sum e^{\left(\frac{P\Delta - \phi(\Delta)}{kT}\right)}} \quad (1.12)$$

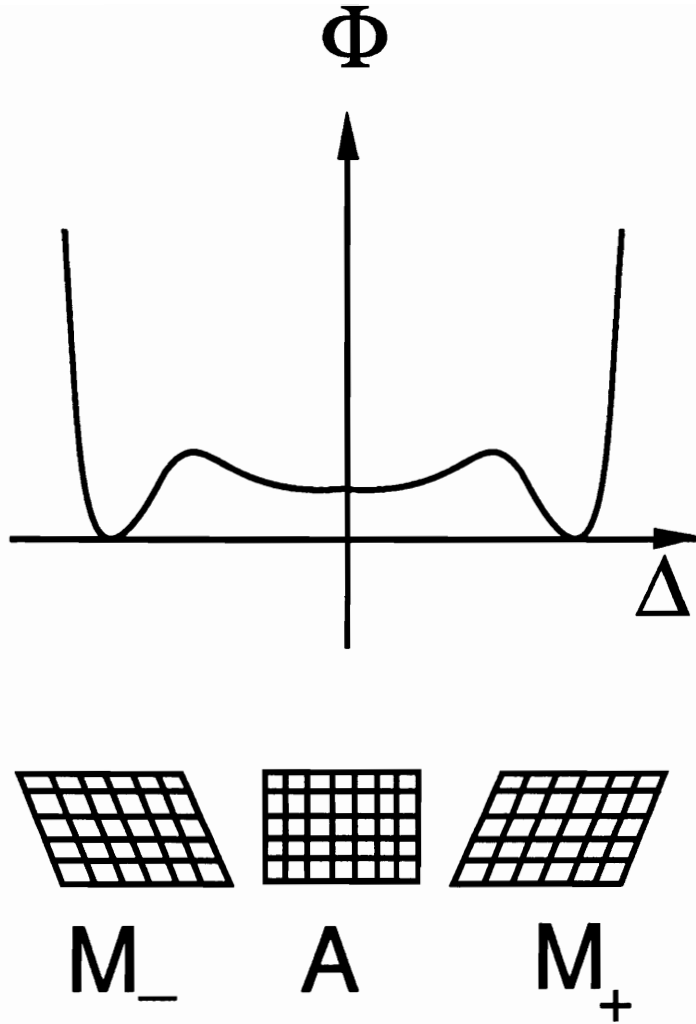


Figure 1.19: Potential Energy of a Lattice vs. Shear Deformation Length (After Müller, 1986)

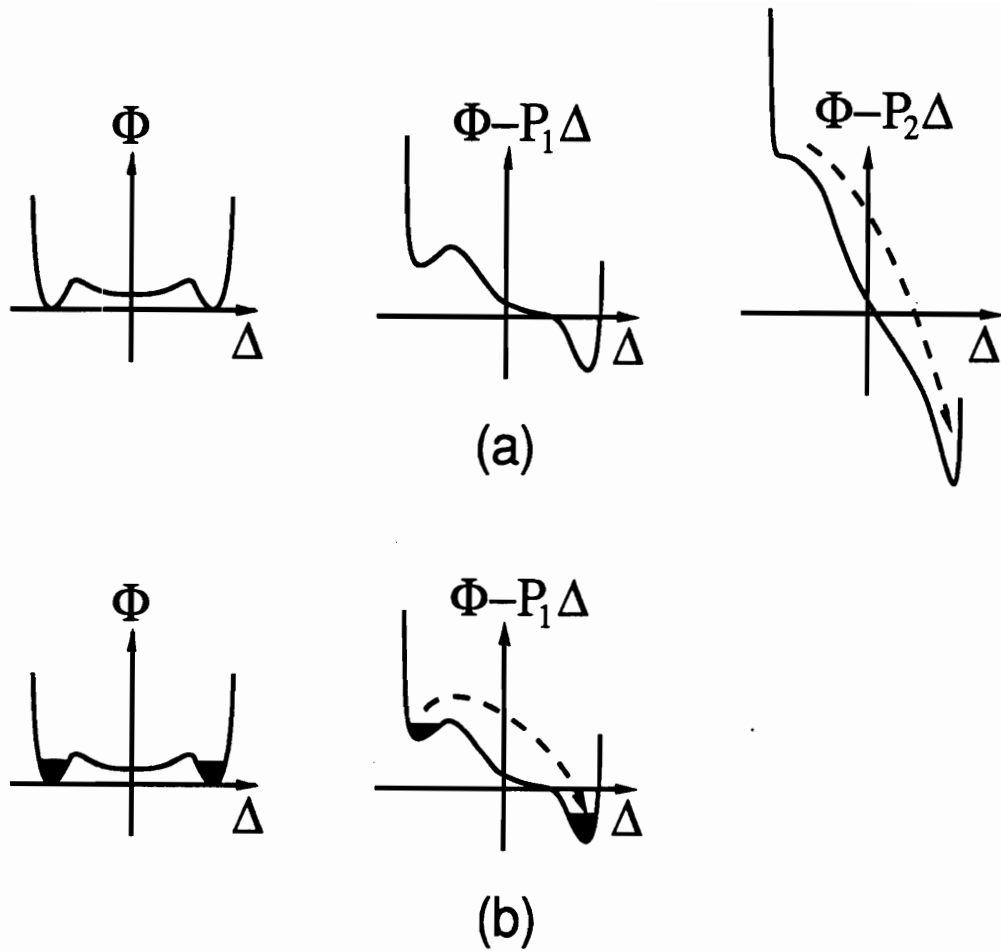


Figure 1.20: Influence of External Force and Temperature on  $\Phi - \Delta$  Relation (After Müller, 1986)

This model gives an excellent physical explanation of the phase transformation and its related material behavior. However, this model presents only a qualitative picture of SMA and is too complex to be used for engineering design other than to evaluate the microstructures associated with different processing schemes.

### 1.3.3 Falk's Model

In Müller's model, the influence of temperature is described as the fluctuation of energy of the particles in the potential well which is represented by the depth of the potential wells. With increasing temperature, the height of the potential well will increase. This indicates that a small applied force may cause the transformation from  $M_-$  to  $M_+$  at high temperatures as depicted in Fig. 1.20. The potential energy from an applied force is superimposed on the chemical Helmholtz free energy resulting in the distortion of the free energy-shear length curves. It is difficult for Müller's model to explain why larger forces are needed to induce martensitic transformation at higher temperatures. Falk (1980) modified the free energy-force-temperature relation and obtained much simpler results.

In Falk's model, the relative position of  $M_-$  and  $M_+$  stable and metastable position  $A$  varies as a function of applied force and temperature. Figure 1.21 shows the normalized Helmholtz free energy,  $\phi$ , over shear strain,  $\epsilon$ , ( $\Delta$  in Müller's model) with normalized temperature,  $t$ , as a parameter. The curve with a higher  $t$  has only one stable phase (austenite) and a very low temperature such as the one corresponding to  $t = -5/16$  has two stable phases ( $M_-$  and  $M_+$ ). At some medium temperatures like  $t = 1/24$  or 0, there are three stable phases. The metastable (center minimum)

corresponding to the austenite phase may vanish as a result of the phase transformation if force is applied. Falk proposed an expression for the Helmholtz free energy per volume,  $\Phi$ , as

$$\Phi(E, T) = \alpha E^6 - \beta E^4 + (\delta T - \gamma) E^2 + \Phi_0(T) \quad (1.13)$$

where  $\alpha$ ,  $\beta$ ,  $\gamma$  and  $\delta$  are positive material constants.  $E$  is the strain and  $T$  is temperature. The above expression can be normalized to

$$\phi = e^6 - e^4 + (t + 1/4)e^2 + \phi_0(t) \quad (1.14)$$

From thermoelasticity, the shear stress  $\Sigma$  can be derived as

$$\Sigma = \frac{\partial \Phi(E, T)}{\partial E} \quad (1.15)$$

Normalization of the shear stress yields

$$\sigma(e, t) = \frac{\partial \phi}{\partial e} = 6e^5 - 4e^3 + 2(t + 1/4)e \quad (1.16)$$

This normalized shear stress,  $\sigma$ , gives a qualitative assessment of the stress-strain relations of shape memory alloys at different temperatures.

With this assumed free energy expression, the model can be used to study the change of elastic modulus ( $\frac{\partial \sigma}{\partial e}$ ), shape memory effect, temperature and stress-induced phase transition, latent heat of the phase transition, internal energy, Gibbs free energy, and

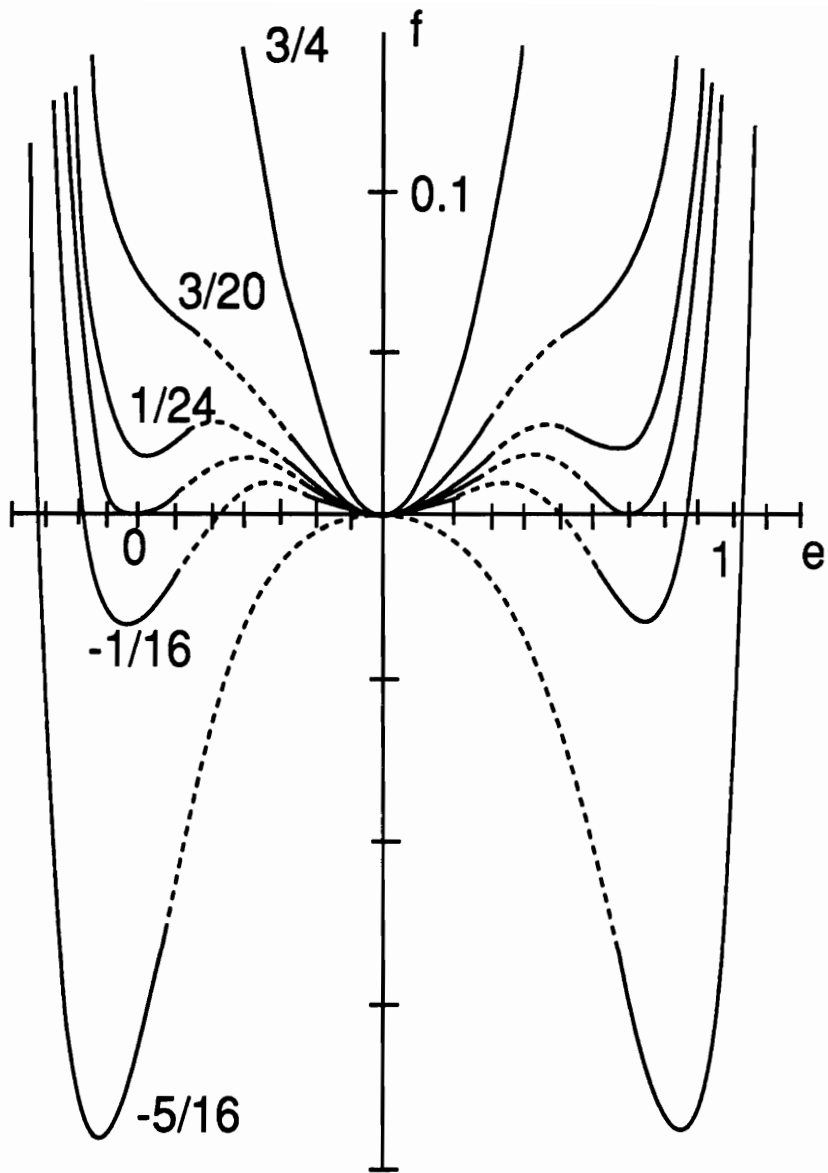


Figure 1.21: Influence of Temperature on Free Energy and Shear Deformation Relations (After Falk, 1980)

entropy (the entropy can be expressed as  $-\partial\Phi/\partial T$ ). Since the free energy here can be scaled to fit any material, a specific material can be characterized as long as the four scaling parameters  $\alpha$ ,  $\beta$ ,  $\delta$ , and  $\gamma$  are known. These parameters can be determined by comparison with thermodynamic and mechanical experiments. For instance,  $\gamma$  is the Young's modulus of the material and  $\delta$  somehow represents the influence of temperature on the Young's modulus. The reason that this theory has not been widely used is that it is adapted to a single crystal and the measurement of the scaling parameters for a general shape memory alloy is very difficult.

### 1.3.4 Sprekel and Hoffmann's Model

Sprekel and Hoffmann (1985, 1986 and 1987) have developed a thermodynamic model similar to Falk's model. Unlike Falk, instead of assuming an explicit expression for the free energy, Hoffmann et al. used a generalized free energy expression.

$$\Phi(\epsilon, \theta) = \Phi_0(\theta) + \Phi_1(\theta)\epsilon^2 + \Phi_2(\epsilon) \quad (1.17)$$

where  $\theta$  is the absolute temperature and  $\epsilon$  the linearized strain. Considering a one-dimensional SMA specimen undergoing a transient temperature and mechanical loading, the general one-dimensional constitutive relations are

$$\begin{aligned} s &= -\Phi_\theta \\ e &= \Phi + s\theta \\ \epsilon &= u_x \\ q &= -k_1\theta_x - k_2\theta_{xt} \end{aligned} \quad (1.18)$$



$$\sigma = \Phi_\epsilon + \mu \epsilon_t$$

where  $q$  is the heat flow,  $s$  the specific entropy,  $e$  the specific internal energy,  $u$  the displacement,  $\sigma$  the stress, and  $t$  the time;  $\mu$  is the viscosity coefficient and  $k_1$  and  $k_2$  are positive coefficients. Notation  $Y_x$  represents the differential of  $Y$  with respect to  $x$ .

The governing equations (first law of thermodynamics and momentum balance) are

$$\begin{aligned} \dot{e} &= \sigma \dot{\epsilon} - q_x + \lambda \\ f &= u_{tt} - \sigma_x \end{aligned} \quad (1.19)$$

where  $\lambda$  is the heat source and  $f$  is the external load. The system equations in the spatial and time domain can be derived from the above equations as

$$\begin{aligned} f &= u_{tt} - (\Phi_\epsilon)_x - \mu u_{txx} \\ \lambda &= \theta s_t - \mu u_{tx}^2 - k_1 \theta_{xx} - k_2 \theta_{xxt} \end{aligned} \quad (1.20)$$

The boundary conditions are specified in this case as

$$\begin{aligned} u(x, 0) &= u_0(x) \\ u_t(x, 0) &= u_1(x) \\ \theta(x, 0) &= \theta_0(x) \end{aligned} \quad (1.21)$$

and the initial conditions are

$$\begin{aligned} u(0, t) &= u(1, t) = 0 \\ k_1 \theta_\Omega(t) &= \alpha(\theta_\Gamma(t) - \theta(t)) \end{aligned} \quad (1.22)$$

where  $\Omega$  represents the spatial domain and  $\Gamma$  the boundary of the spatial domain;  $\alpha$  is the heat convection coefficient. The above system equations and boundary conditions satisfy the following variational equations.

$$\begin{aligned} \int_0^T \int_\Omega [\theta s_t \xi + \mu u_t (\epsilon_{xt} \xi + \epsilon_t \xi_t) + k_1 \theta_x \xi_x + k_2 \theta_{xt} \xi_x + \lambda \xi] dx dt + \\ \int_0^T \int_\Gamma \alpha [(\theta - \theta_\Gamma) + \frac{k_1}{k_2} (\theta_t - \theta_{\Gamma,t})] \xi dx dt = 0 \end{aligned} \quad (1.23)$$

and

$$\int_0^T \int_\Omega [u_{tt} \eta - (\Phi_\epsilon)_x \eta - \mu \epsilon_{xt} \eta - f \eta] dx dt = 0 \quad (1.24)$$

For a set of given  $f$ ,  $\lambda$ ,  $\theta_\Gamma$ ,  $u_0$ ,  $u_1$ , and  $\theta_0$ , solving the above variational equation may yield the unknown functions in Eq. (1.17). However, getting a closed-form solution is very difficult and a numerical technique has been used to solve the above variational equations. One method is to assume the free energy as a summation of some known functions weighted by unknown coefficients, those coefficients can be determined by solving the above variational equations. Spatial domain finite elements and time domain finite differences also can be used to solve the displacement, strain and stress (Tiihonen, 1988).

This model is based on strict mathematical derivations, its numerical simulations reflect the physics of the martensitic transformation of shape memory alloy and its related material behavior. However, the complex formulation requires sophisticated programs and its validity still needs experimental verification.

### 1.3.5 Modeling of SMA with Internal Variables

Tanaka and Sato et al. (1982, 1985, 1986, and 1988 ) developed a model based on the concept of the free energy driving force. Tanaka's model considers a one-dimensional metallic material of length  $L$  that is undergoing either martensitic transformation or its reverse transformation. The state variables for the material are strain, temperature, and extent of phase transformation,  $\xi$ , which is defined as the martensite fraction. The general state variable is defined as

$$\Lambda \equiv (\bar{\epsilon}, T, \xi) \quad (1.25)$$

The Helmholtz free energy defined in Eq. (1.11) is a function of the state variable  $\Lambda$ . Like Müller, Hoffmann, and Falk, the same general constitutive relations can be derived from the first and second laws of thermodynamics as<sup>1</sup>

$$\bar{\sigma} = \rho_0 \frac{\partial \Phi}{\partial \bar{\epsilon}} = \sigma(\bar{\epsilon}, T, \xi) \quad (1.26)$$

---

<sup>1</sup>A detailed derivation will be given in Chapter 2

The stress is a function of the martensite fraction, an internal variable. From the above equation, the rate form of the mechanical constitutive equation is obtained as

$$\dot{\sigma} = \frac{\partial \sigma}{\partial \bar{\epsilon}} \dot{\bar{\epsilon}} + \frac{\partial \sigma}{\partial T} \dot{T} + \frac{\partial \sigma}{\partial \xi} \dot{\xi} = D \dot{\bar{\epsilon}} + \Theta \dot{T} + \Omega \dot{\xi} \quad (1.27)$$

where  $D$  is the Young's modulus,  $\Theta$  the thermoelastic tensor, and  $\Omega$  the transformation tensor, a metallurgical quantity which represents the change of strain during phase transformation. The material properties derived from thermomechanics are given as

$$\begin{aligned} D &= \rho_0 \frac{\partial^2 \Phi}{\partial \bar{\epsilon}^2} \\ \Theta &= \rho_0 \frac{\partial^2 \Phi}{\partial \bar{\epsilon} \partial T} \\ \Omega &= \rho_0 \frac{\partial^2 \Phi}{\partial \bar{\epsilon} \partial \xi} \end{aligned} \quad (1.28)$$

If the expression of free energy is known, the minimization of the free energy may determine the equilibrium states of phases, i.e., the relation of the martensite fraction with the applied stress and temperature can be determined. However, instead of making the effort to find the free energy expression, the martensite fraction,  $\xi$ , is assumed to be an exponential function of stress and temperature based on the study of transformation kinetics in Tanaka's model. These functions are

$$\begin{aligned} \xi_{M \rightarrow A} &= \exp[A_a(T - A_s) + B_a \sigma] \\ \xi_{A \rightarrow M} &= 1 - \exp(A_m(T - M_s) + B_m \sigma) \end{aligned} \quad (1.29)$$

where  $A_a$ ,  $A_m$ ,  $B_a$ , and  $B_m$  are material constants in terms of the transition temperatures,  $A_s$ ,  $A_f$ ,  $M_s$ , and  $M_f$ , etc.

Tanaka's model is simple and yet reflects the thermomechanics of shape memory alloy. It has been used to predict and describe the stress-strain relations, pseudoelastic effects and the energy dissipation of pseudoelastic effects qualitatively. Based on Tanaka's work, Liang and Rogers (1990) further modified and extended this model in order to predict and describe quantitatively the behavior of shape memory alloys including the shape memory effects and develop multi-dimensional constitutive model (Liang and Rogers, 1990a; 1990b).

### **1.3.6 Non-Equilibrium Thermostatic Model**

Cory and McNichols (1978, 1985, and 1987) have developed a thermomechanical model based on what they have termed non-equilibrium thermostatics (NET) systems. If a thermodynamic system undergoes an equilibrium path, which means that every position of the path must correspond to an equilibrium state, the process is required to take place very slowly (i.e., quasi-static). Such processes are likewise reversible. Since shape memory alloys involve an irreversible phase transformation and have macroscopic hysteric characteristics, their thermodynamic paths are described by a non-equilibrium thermostatic process. For NET systems, instead of using the inequality form of the second law of thermodynamics, a path-dependent heat generation term is introduced and the newly modified second law of thermodynamics is

given as

$$TdS = dQ + Td\bar{S} \quad (1.30)$$

where  $dQ$  is the path-dependent heat into the system, while the newly introduced term  $\bar{S}$  is the internally generated entropy change for a differential path element relating directly to the energy dissipation of the hysteresis. Cory and McNichol summarized their model with the following points (McNichols and Cory, 1987).

1. All thermodynamic paths of force, length of SMA wire, and temperature (FLT) in its state space are limited within a bounded volume.
2. The surface of the bounded volume is the asymptotic boundary of the paths.
3. All observed paths are one of two types, each type having a characteristic ‘direction’ in state space. The two types are defined as AM (austenite to martensite) and MA (martensite to austenite). Therefore, as shown in Fig. 1.22, the surfaces of the bounded volume are distinguished as AM and MA surfaces.
4. The direction of the path is related to the increase or decrease of a new state variable  $Z$  defined especially for the NET system. The ‘history’ dependence of SMA state variables (FLT) is completely determined by the FLT location (called  $F_0$ ,  $L_0$ , and  $T_0$ ) of the last change in the sign of the differential  $dZ$ , and is independent of the history of the system prior to that time.
5. The initial slope of each single controlled state variable paths is nearly the same and is tangent to a set of  $Z$  surfaces in FLT space.

6. There exist reversible paths in the FLT space which are characterized by the surface of constant  $Z$  value.

Figure 1.23 gives a schematic isothermal cut of the SMA state space from which the phenomenological equations of the stress-strain curves can be determined. First, the AM surface is given by

$$F_{BAM}(L, T) = (a - f)L + (b + g)T - N \quad (1.31)$$

where 'BAM' represents the 'boundary surface of the martensitic phase transformation.' The MA surface is given by

$$F_{BMA}(L, T) = F_{BAM}(L, T) - h \quad (1.32)$$

where 'BMA' represents 'boundary surface of the MA transformation.' The  $Z$  surface that is tangent to the initial slope is described by

$$Z = aL + bT - F \quad (1.33)$$

The stress-strain AM path is phenomenologically described by

$$F_{BAM} - F = (F_{BAMx} - F_x) \exp \left| \frac{g(T - T_x) - f(L - L_x)}{F_{BAMx} - F_x} \right| \quad (1.34)$$

where the history variables,  $(L_x, T_x, F_x)$ , correspond to the minimum  $Z$  at  $Z_x = Z(L_x, T_x, F_x)$ , and the subscript 'x' of ' $F_{BAM}$ ' and 'F' indicate their corresponding values at  $(L_x, T_x)$ . For the stress-strain curve of the MA path, the equation is ex-

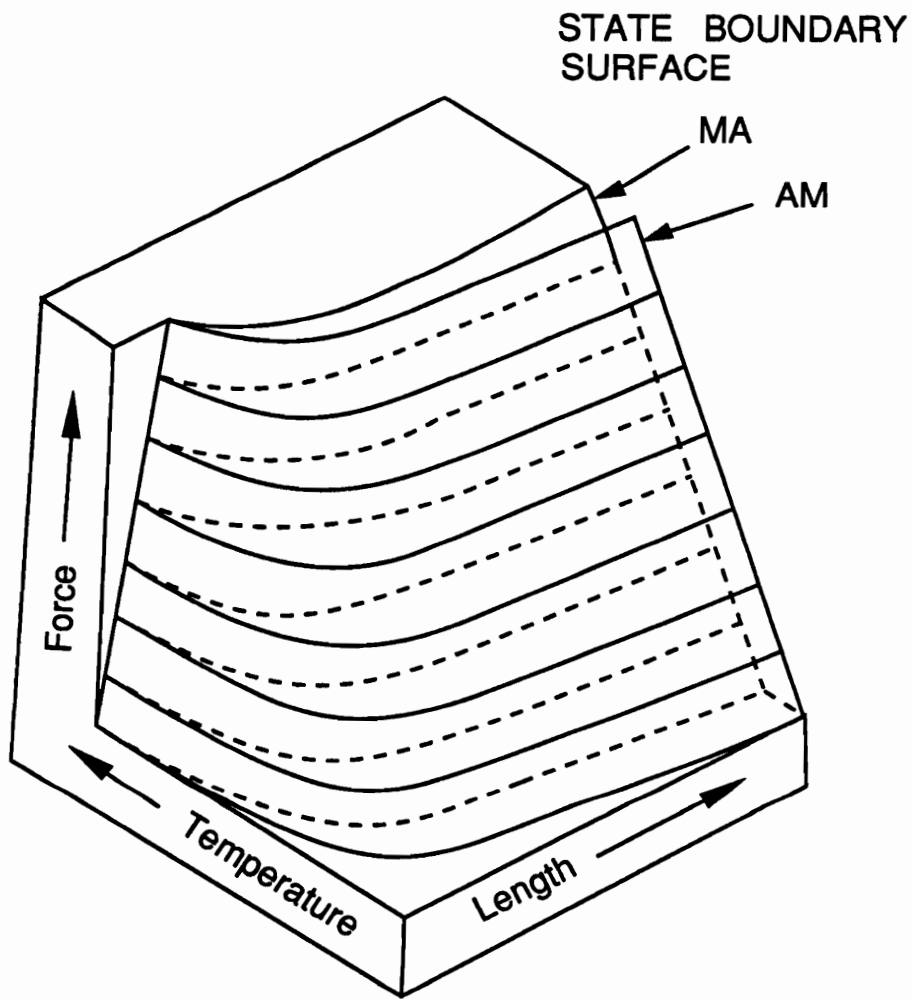


Figure 1.22: Schematic Diagram of Nitinol State Space (After McNichols and Cory, 1987)



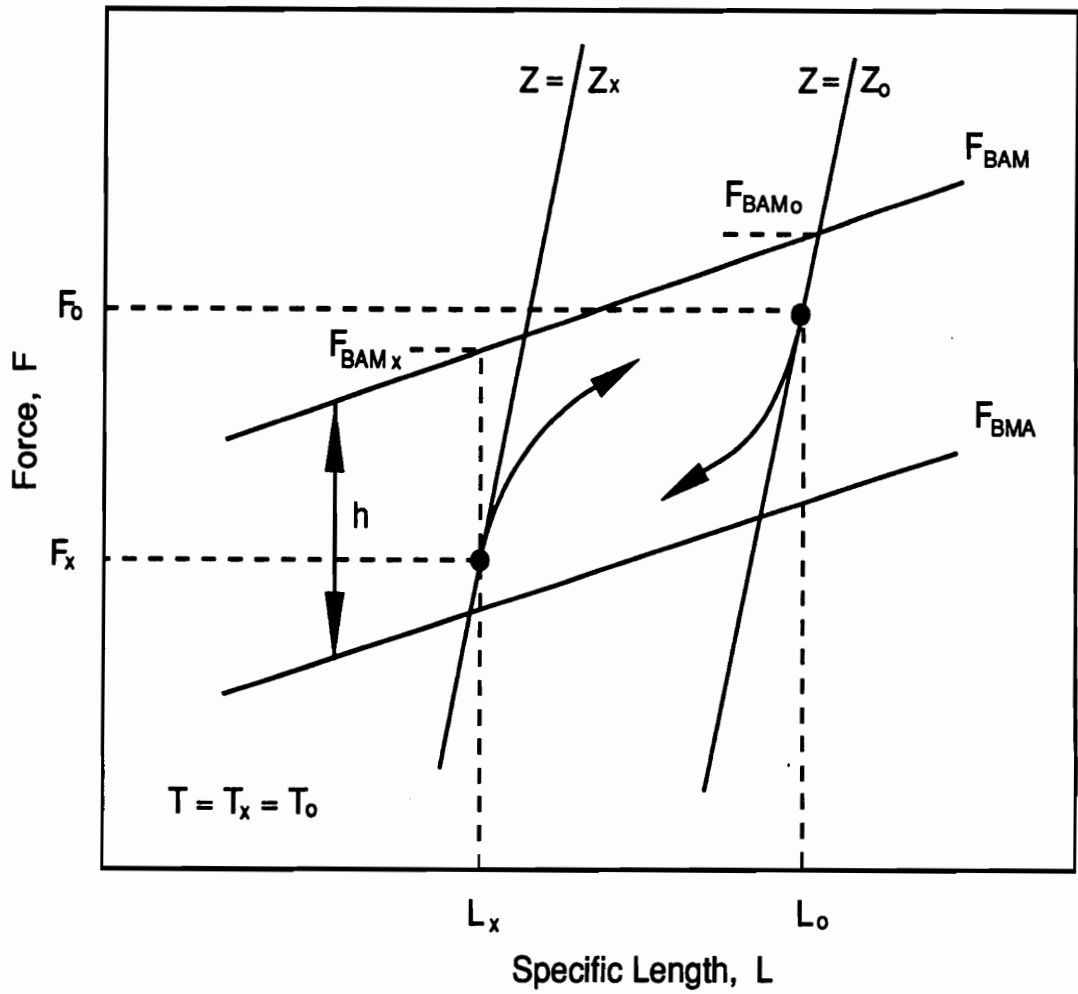


Figure 1.23: Schematic Isothermal Cut of Nitinol State Space (After McNichols and Cory, 1987)

pressed as:

$$F - F_{BMA} = (F_{BMA0} - F_0) \exp \left| \frac{g(T_0 - T) - f(L_0 - L)}{F_0 - F_{BMA0}} \right| \quad (1.35)$$

where  $(L_0, T_0, F_0)$ , correspond to the maximum  $Z$  at  $Z_0 = Z(L_0, T_0, F_0)$ , and the subscript '0' of ' $F_{BMA}$ ' and 'F' indicate their corresponding values at  $(L_0, T_0)$ .

In the above equations, 'a', 'b', 'g', 'f', 'h', and 'N' must be measured from from experiments. Besides the stress-strain relations, this model has been used to predict the thermodynamic path behavior, heat dissipation and other thermodynamic parameters. However, the SME behavior is directly related to the martensitic phase transformation. Cory's model does not consider the phase transformation as the internal driving force which results in the hysteresis. The state variable,  $Z$ , also lacks a physical explanation (probably related to the martensite/austenite fraction). Cory's model describes only the one-dimensional stress-strain relation of SMA. The other phase transition characteristics, such as the recovery effects, have not been modeled.

### 1.3.7 Hysteretic Model

Shape memory alloys present large hysteresis during loading and unloading. Although this hysteresis is a result of the irreversible aspects of the material phase transformation, the large hysteretic phenomena of shape memory alloys indicates great energy dissipation. This characteristic falls into the category of viscoplastic material and the constitutive relations for hysteretic material may, therefore, be capable of describing shape memory alloys. This method is developed and presented in detail in Graesser's

dissertation (1990) and is briefly described below.

The rate form of stress and strain relation for a hysteretic material is expressed as

$$\begin{aligned}\dot{\epsilon} &= \dot{\epsilon}^e + \dot{\epsilon}^{in} \\ &= \frac{\dot{\sigma}}{E} + |\dot{\epsilon}| \left( \frac{\sigma - \beta}{Y} \right)\end{aligned}\quad (1.36)$$

where

$$\dot{\beta} = \alpha E |\dot{\epsilon}| \frac{\sigma - \beta}{Y} \quad (1.37)$$

$\beta$  is the one-dimensional backstress,  $E$  the elastic modulus,  $Y$  the yield stress,  $n$  the constant describing the sharpness of transition from elastic to plastic states, and  $\alpha$  is a constant controlling the slope of the  $\sigma - \epsilon$  curve (given approximately by  $\alpha = E_Y / (E - E_Y)$  where  $E_Y$  is the slope of the  $\sigma - \epsilon$  curve after yielding). Superscript ‘e’ means ‘elastic’ and ‘in’ means ‘inelastic’. This expression is very similar in form to the rate sensitive flow rule of the nonlinear Kelvin-St. Venant (K-V) viscoplastic model.

Some modifications for the above equations have been made to describe the cyclic SMA hysteretic and/or pseudoelastic behavior, and a tensor form analogous to plastic flow theory was derived to extend this model to multi-dimension. However, the initial assumption of non-change uniform temperature field marks the limitation of this model. It is only capable of modeling the stress-strain behavior of shape memory alloys. The shape memory effect which is inseparable from temperatures cannot be

described.

### 1.3.8 Plastic Flow Theory Model

Bondaryev and Wayman (1988) suggested a model based on the plastic flow theory and thermoelastic martensitic phase transformation. Their work can be basically described as follows.

The strain tensor is decomposed into elastic strain,  $\epsilon_{ij}^e$ , and inelastic strain,  $\epsilon_{ij}^u$ , as

$$\epsilon_{ij} = \epsilon_{ij}^e + \epsilon_{ij}^u \quad (1.38)$$

The elastic strain in both martensite and austenite obeys Hook's law for an isotropic material.

$$e_{ij}^e = \frac{1}{2\mu_x} s_{ij} + \frac{1}{9k_x} \sigma_{ss} \delta_{ij} \quad (1.39)$$

where  $e_{ij}^e$  is the strain deviator;  $\delta_{ij}$  is Kroneker's delta;  $\mu_\rho$  and  $k_\rho$  are shear and bulk modulus,  $x = M$  or  $A$  denotes martensitic or austenitic state, respectively;  $s_{ij}$  is the deviatoric stress.  $\sigma_{ss}$  implies a summation over the repeated indices 'ss'.

The inelastic strain is assumed to be governed by the normality rule as accepted in plastic flow theory as

$$d\epsilon_{ij}^u = d\lambda \frac{\partial f}{\partial s_{ij}} \quad (1.40)$$

where  $d\lambda$  is a finite multiplier related to the martensite fraction. Proper construction of this parameter leads to the solution to different problems for shape memory alloys (stress-strain mechanism and shape memory effects). The term  $f$  is generally referred to as the yielding function.  $f = 0$  indicates the beginning of the martensitic phase transformation and an accumulation of inelastic strain. The yielding function can be derived from the energy relations involved in the phase transformation.

The beginning of the martensitic phase transformation can be represented by

$$\Delta G^{A \rightarrow M} = \Delta G_C^{A \rightarrow M} + \Delta G_{NC}^{A \rightarrow M} = R > 0 \quad (1.41)$$

where  $\Delta G_C^{A \rightarrow M}$  and  $\Delta G_{NC}^{A \rightarrow M}$  are the chemical and nonchemical Gibbs free energy, respectively.  $R$  reflects ‘frictional’ resistance.  $A \rightarrow M$  denotes the martensitic transformation (from Austenite to Martensite). The Gibbs free energy for austenite and martensite is written respectively as

$$G_A = -\frac{1}{4\mu_A} s_{ij} s_{ij} - \frac{1}{18k_A} \sigma_s^2 s + G_C^A(T) \quad (1.42)$$

and

$$G_M = -\frac{1}{4\mu_M} s_{ij} s_{ij} - \frac{1}{18k_M} \sigma_s^2 s - \alpha_{ij} \sigma_{ij} + G_C^M(T) \quad (1.43)$$

where  $\alpha_{ij}$  is the maximum inelastic recoverable strain tensor.

Substituting Eqs. (1.43) and (1.42) into (1.41) yields

$$\frac{1}{4}\left(\frac{1}{\mu_M} - \frac{1}{\mu_A}\right)s_{ij}s_{ij} + \frac{1}{18}\left(\frac{1}{k_M} - \frac{1}{k_A}\right)\sigma_{ss}^2 + \alpha_{ij}\sigma_{ij} + \Delta G_C^{A \rightarrow M} = R \quad (1.44)$$

The nature of the martensitic transformation is primarily shear as there is no significant change of volumetric properties and volume itself. Therefore, the second term ( $\sigma_{ss}$  term) of Eq. (1.44) vanishes. Experiments show that the stress field causes the appearance of crystal variants that provide maximum work with respect to the inelastic strain. This means that the unit vector  $n_{ij}$  of the maximum recovery strain tensor,  $\alpha_{ij}$ , and the unit stress vector  $s_{ij}^0 = s_{ij}/s = s_{ij}/\sqrt{s_{mn}s_{mn}}$  are parallel. Therefore,  $\alpha_{ij}\sigma_{ij}$  can be written as  $\alpha\sqrt{s_{ij}s_{ij}}$  which is much larger than the first term of Eq. (1.44). A linear approximation is used for the chemical Gibbs free energy. All these considerations finally yield the following simplified yielding function.

$$f = \alpha\sqrt{s_{ij}s_{ij}} - W(T - M_S) \quad (1.45)$$

A similar yielding function which can be used to describe the inelastic unloading caused by the pseudoelastic effect was derived based on the same discussion as

$$f_2 = \alpha_{ij}^*s_{ij} - W(T - A_S) = 0 \quad (1.46)$$

where  $\alpha_{ij}^*$  is the maximum inelastic recoverable strain tensor caused by the martensitic phase transformation. It is assumed that the maximum inelastic strain tensor is proportional to the inelastic strain,  $\epsilon_{ij}^u$ , at any moment. Proper modification to these yielding functions (Eqs. (1.45) and (1.46)) makes this model capable of modeling the

low temperature and high temperature states.

This model is based on the plastic flow theory with some modification to capture the essence of the special characteristics of shape memory alloys, i.e., the phase transformation. The question one may ask is whether we can still use the flow rule to describe the inelastic strain caused by transformation. The inelastic strain caused by plastic deformation is different in nature from the one caused by phase transformations. The second question is the validity of this model in describing the shape memory effect. For example, the stress generated in a SMA specimen under restrained conditions can be derived from the discussion assuming a constant total strain, that yields

$$s_{ij} = \frac{W}{(\alpha^*)^2} \alpha_{ij}^* (T - A_S) \quad (1.47)$$

where  $(\alpha^*)^2 = \alpha_{ij}^* \alpha_{ij}^*$  can be viewed as the residual strain prior to the heating. Considering a special case of one dimension, the stress from this equation is proportional to the temperature and inversely proportional to the initial strain  $\alpha^*$ , which is contrary to the experimental result shown in Fig. 1.6.

### 1.3.9 Concluding Remarks

Eight constitutive models of shape memory alloys have been reviewed. These models can be roughly divided into two categories. One is the thermomechanical model represented by Müller's and Tanaka's model; another is based on a well-developed mechanical theory such as plastic flow theory, for instance, the one developed by Bondaryev and Wayman. Some of these models can only provide qualitative under-

standing of the characteristics of shape memory alloys. Other models appear to be able to describe the behavior of a shape memory alloy quantitatively, but require material constants which are difficult to measure. Almost all these models lack experimental verification. Among them, Tanaka's model which was developed to study SMA qualitatively is found to be modified to predict and describe shape memory alloys quantitatively. The constitutive relation of SMA presented in this dissertation is, therefore, based on Tanaka's early work.



# Chapter 2

## Constitutive Modeling of SMA

In this chapter, a one-dimensional thermomechanical constitutive model based on Tanaka's early work (Tanaka, 1982 and 1985) is presented. This model is based on thermomechanics and phase transformation phenomenology. We begin with an introduction of the transformation kinetics and some important features of the mechanical behavior of SMA.

### 2.1 Transformation Kinetics

The stress-induced martensitic phase transformation is the most important characteristics of SMA materials; therefore, it is necessary to begin the development of the model with phase transformation relations and effects of stress on the phase transformations. In this model, an internal variable,  $\xi$ , is introduced to represent the extent of a martensitic transformation. This variable is characterized as a martensite fraction (the ratio of the volume of martensite to the total volume of the material). Transformation kinetics is the study of the relations of the martensite fraction with other state variables such as temperature and strain.

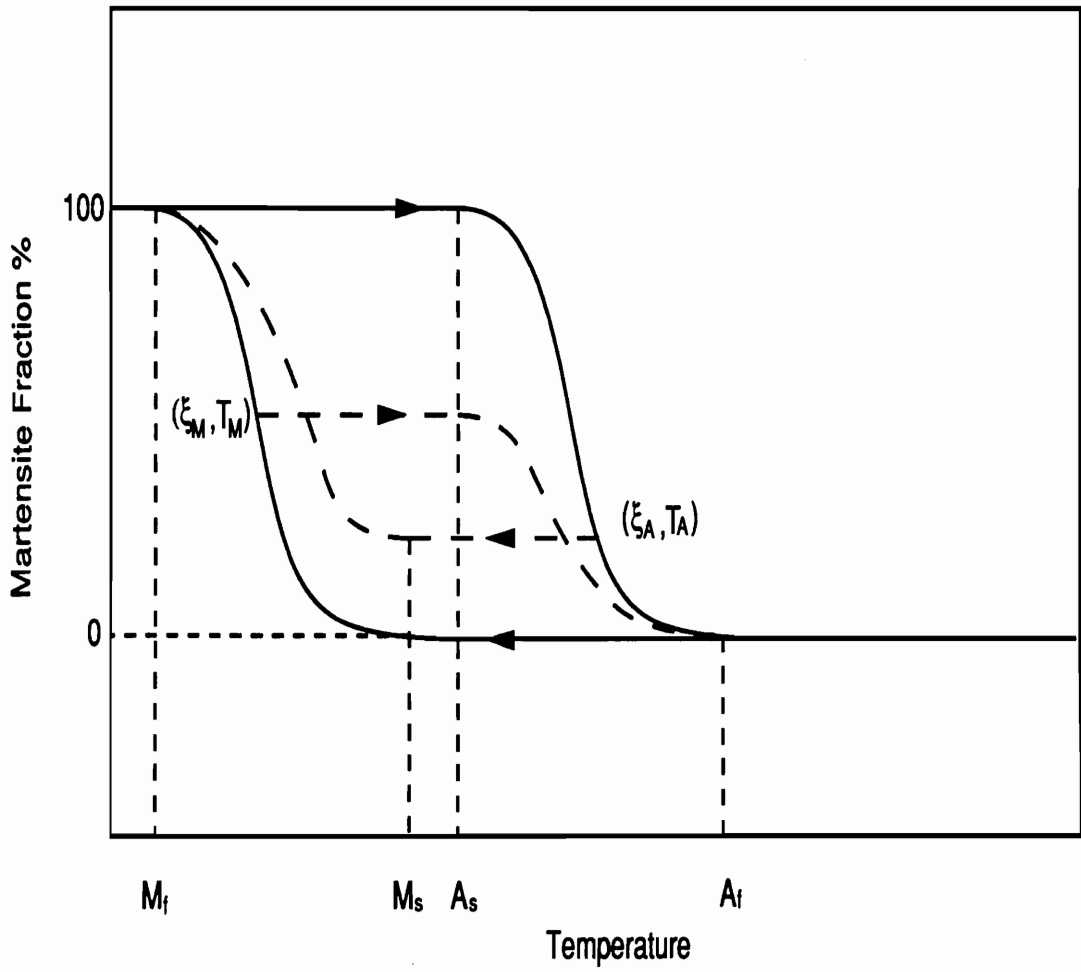


Figure 2.1: Schematic Diagram of Martensite Fraction vs. Temperature

As illustrated in Fig. 2.1, the martensite fraction changes as a function of temperature for all the materials that can undergo martensitic phase transformation. The four important temperature parameters in Fig. 2.1 are the martensite finish temperature ( $M_f$ ), martensite start temperature ( $M_s$ ), austenite start temperature ( $A_s$ ), and austenite finish temperature ( $A_f$ ).

There is no direct approach to measure the relations of the martensite fraction with temperature for shape memory alloys because of the very fine microscopic structures of SMA, in particular nitinol alloys. However, it is possible to obtain the four transition temperatures and the relations between the martensite fraction and temperature indirectly. The four transition temperatures can be measured accurately by using a differential scanning calorimeter (DSC), by measuring the change of resistivity, or by measuring the change of the volume in the material during the phase transformation (Funakubo, 1984). They can also be estimated by examining the mechanical behaviors such as the stress-strain relations of shape memory alloys.

Theoretical studies show that the relations between martensite fraction and other state variables can be obtained by calculating the phase equilibrium (Hillert, 1968) and transformation kinetics (Magee, 1968).

Considering the calculation of the phase equilibrium of a two-phase alloy where the two phases are denoted as  $\alpha$  and  $\beta$ , the volume fraction ratio,  $K^{\alpha/\beta}$ , can be expressed by (Hillert, 1968)

$$K^{\alpha/\beta} = \frac{\xi_\alpha}{\xi_\beta} = \exp\left[\frac{1}{RT}(G_0^\beta - G_0^\alpha + G_E^\beta - G_E^\alpha)\right] \quad (2.1)$$

where  $R$  is the universal gas constant,  $T$  the temperature, and  $G$  the chemical potential or Gibbs free energy.  $G_0^\alpha$  is the molar free energy of the  $\alpha$  phase at the standard state chosen, as is  $G_0^\beta$ . Subscript 'E' means 'excess'. This equation offers a very convenient way to calculate the phase equilibrium of two-phase alloys. However, the material data required to perform this calculation is very difficult to measure and, thus, limits the use of this equation in engineering design.

The calculation of transformation kinetics is based on the concept of the free energy driving force. Numerous studies on transformation kinetics, particularly in dynamically stabilized steels, have resulted in knowledge concerning the relationship between the volume fraction,  $\xi$ , and the quenching temperature,  $T_q$ , under standard quenching procedures. More transformation occurs at lower temperatures, because the driving free energy favors the formation of martensite,  $\Delta G^{A \rightarrow M}$ , and increases at lower temperatures. Moreover, the nature of the nucleation centers is such that more nucleation events occur at higher driving forces. An expression of the martensite fraction,  $\xi$ , and the quenching temperature,  $T_q$ , can be derived based on the fact that the generation of new martensitic plates per unit volume of austenite,  $dN$ , is the result of the increase of the driving force,  $d(\Delta G^{A \rightarrow M})$ . The simplest relation is

$$dN = -\kappa d(\Delta G^{A \rightarrow M}) = -\kappa \frac{d\Delta G^{A \rightarrow M}}{dT} dT \quad (2.2)$$

where  $\kappa$  is a proportionality constant. The change of the martensite fraction,  $d\xi$ , is simply related with  $dN$  by

$$d\xi = \bar{V}(1 - \xi)dN \quad (2.3)$$

where  $\bar{V}$  is the average volume of the newly formed martensitic plates. Finally, the relationship between the martensite fraction,  $\xi$ , and other state variables is derived from the above equations as

$$d\xi = -\bar{V}(1 - \xi)\kappa \frac{d\Delta G^{A \rightarrow M}}{dT} dT \quad (2.4)$$

Integrating from  $M_s$ , where  $\xi = 0$  to  $T_q$  assuming  $\bar{V}$ ,  $\kappa$ , and  $\frac{d\Delta G^{A \rightarrow M}}{dT}$  constant yields

$$\ln(1 - \xi) = \bar{V}\kappa \frac{d\Delta G^{A \rightarrow M}}{dT} (M_s - T_q) \quad (2.5)$$

or

$$1 - \xi = \exp[\bar{V}\kappa \frac{d\Delta G^{A \rightarrow M}}{dT} (M_s - T_q)] \quad (2.6)$$

The empirical equation from Koistinen and Marburger (1959) is

$$1 - \xi = \exp[\alpha(M_s - T_q)] \quad (2.7)$$

For ferrous materials, the coefficient  $\alpha$  is -0.011 (Koistinen and Marburger, 1959). The above empirical equation agrees with experimental results for higher quenching temperatures. However, the equation does not fit with experimental results well when the quenching temperature approaches the martensite finish temperature ( $M_f$ ). Equation (2.7) provides a smooth transition around the martensite start temperature ( $M_s$ ) because the integration of Eq. (2.4) begins from  $M_s$ . Similarly, getting a smooth transition around the martensite finish temperature requires integration from

$M_f$ . Equation (2.4) can also be expressed in another form as

$$\frac{d\xi}{\xi} = V' \kappa' \frac{d\Delta G^{A \rightarrow M}}{dT} dT \quad (2.8)$$

Integrating from  $M_f$ , where  $\xi = 1$ , to any quenching temperature  $T_q$  yields

$$\xi = \exp[\beta(T_q - M_f)] \quad (2.9)$$

The martensitic transformation of ferrous materials occurs in a wider temperature range, usually several hundred degrees, while the phase transformation of shape memory alloys, especially nitinol, takes place in a very narrow temperature range (tens of degrees). It is important to give an accurate expression of  $\xi$  vs.  $T$  at the beginning and the end of the phase transformation in shape memory alloys. The middle portion of the phase transformation can use different approximations such as linear relations.

Tanaka (1985 and 1986) used the expression of Eq. (2.7) to describe the relation between the martensite fraction,  $\xi$ , and temperature for martensitic transformation (austenite  $\rightarrow$  martensite) and Eq. (2.9) for the reverse transformation (martensite  $\rightarrow$  austenite). As discussed above, Eq. (2.7) provides a good approximation around  $M_s$  but a poor description around  $M_f$ .

It is suggested herein that both Eqs. (2.7) and (2.9) may be used to describe the relationship of the martensite fraction,  $\xi$ , and temperature piecewisely. It is assumed

that both equations yield a  $\xi$  of 0.5 at  $M_0$  and  $A_0$  where  $M_0$  and  $A_0$  are defined as

$$M_0 = \frac{M_f + M_s}{2} \quad (2.10)$$

and

$$A_0 = \frac{A_s + A_f}{2} \quad (2.11)$$

This assumption leads to  $\alpha = \beta$ . For the convenience of our calculation, the relations of the martensite fraction,  $\xi$ , and temperature for the martensitic transformation and the reverse transformation are rewritten as follows based on Eqs. (2.7) and (2.9). Considering that  $\bar{V}\kappa\frac{d\Delta G^{A \rightarrow M}}{dT}$  cannot be constant in most cases, some modifications as shown below are made. The relations between  $\xi$  and  $T$  for the martensitic transformation are assumed to be

$$\xi = 1 - \frac{1}{2} \exp[a_M(M_0 - T)^n] \quad M_0 \geq T \geq M_f \quad (2.12)$$

and

$$\xi = \frac{1}{2} \exp[a_M(T - M_0)^n] \quad M_s \geq T \geq M_0 \quad (2.13)$$

where  $n$  is a newly introduced parameter referred to as the phase transformation coefficient in this dissertation. This parameter,  $n$ , is found to be between  $0.75 \sim 1$ , as determined from the free recovery experimental data discussed later.

If  $M_f$  and  $M_s$  are assumed to correspond to the transformation of 99 percent and 1 percent of austenite, respectively,  $a_M$  may be solved for as

$$a_M = \frac{2^n \ln(2 \times 0.01)}{(M_s - M_f)^n} \quad (2.14)$$

Similarly, the relations of the martensite fraction,  $\xi$ , and temperature for the reverse transformation are assumed to be

$$\xi = 1 - \frac{1}{2} \exp[a_A(A_0 - T)^n] \quad A_0 \geq T \geq A_s \quad (2.15)$$

and

$$\xi = \frac{1}{2} \exp[a_A(T - A_0)^n] \quad A_f \geq T \geq A_0 \quad (2.16)$$

where  $a_A$  can be derived in a similar manner to  $a_M$  as

$$a_A = \frac{2^n \ln(2 \times 0.01)}{(A_f - A_s)^n} \quad (2.17)$$

If the reverse transformation ( $M \rightarrow A$ ) begins from a state which has mixed austenite and martensite phases, denoted by  $(\xi_M, T_M)$  as shown in Fig. 2.1, it is assumed that there will not be new austenite generated during the heating process until the temperature is higher than  $A_s$ . The reverse transformation at a temperature higher than  $A_s$  is described by

$$\xi = \xi_M - \frac{\xi_M}{2} \exp[a_A(A_0 - T)^n] \quad A_0 \geq T \geq A_s \quad (2.18)$$



and

$$\xi = \frac{\xi_M}{2} \exp[a_A(T - A_0)^n] \quad A_f \geq T \geq A_0 \quad (2.19)$$

Similarly, if the martensitic transformation begins from a mixed phase state denoted by  $(\xi_A, T_A)$  as shown in Fig. 2.1, there will be no new martensite until the temperature is cooled down below  $M_s$ . The martensitic transformation is then described by

$$\xi = 1 - \frac{1 - \xi_A}{2} \exp[a_M(M_0 - T)^n] \quad M_0 \geq T \geq M_f \quad (2.20)$$

and

$$\xi = \frac{1 - \xi_A}{2} \exp[a_M(T - M_0)^n] \quad M_s \geq T \geq M_0 \quad (2.21)$$

The phase transformation is affected by stress. The influence of stress on the phase transformation is approximately linear as indicated by Eq. (1.1). This agrees with the experimental evidence (Goldstein et al., 1987). The two transition temperatures,  $M_s$  and  $A_s$ , are usually linearly related to the applied stress as shown in Fig. 2.2. However, the change of  $M_f$  and  $A_f$  are more complicated. To simplify the model, it is assumed that the  $M_f$  and  $A_f$  lines are straight and parallel to the  $M_s$  and  $A_s$  lines, respectively, as shown in Fig. 2.2. Two other material constants indicating the influence of stress on the transition temperatures are given by

$$\begin{cases} C_M = \tan(\alpha) \\ C_A = \tan(\beta) \end{cases} \quad (2.22)$$

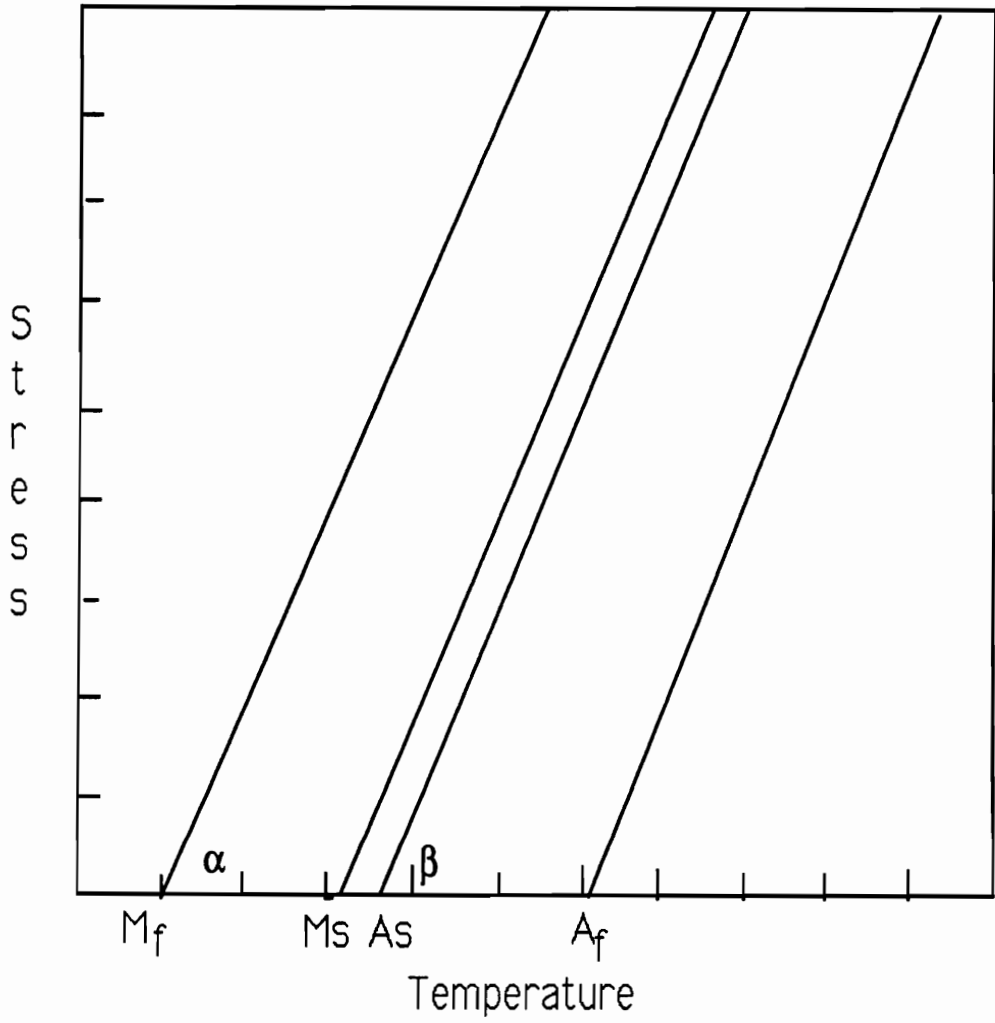


Figure 2.2: A Schematic Diagram of Transition Temperatures vs. Applied Stress

where  $\alpha$  and  $\beta$  are shown in Fig. 2.2. Combining both Figs. 2.1 and 2.2, it can be seen that the martensite-temperature hysteresis loop will move to the right if external stresses are applied. This is reflected in Eqs. (2.18) to (2.21) by adding a stress induced phase transition term. From Fig. 2.2, the transition temperatures under the influence of stress can be expressed as

$$\begin{cases} M_f^\sigma = M_f + \frac{\sigma}{C_M} \\ M_s^\sigma = M_s + \frac{\sigma}{C_M} \\ M_0^\sigma = M_0 + \frac{\sigma}{C_M} \end{cases} \quad (2.23)$$

and

$$\begin{cases} A_s^\sigma = A_s + \frac{\sigma}{C_A} \\ A_f^\sigma = A_f + \frac{\sigma}{C_A} \\ A_0^\sigma = A_0 + \frac{\sigma}{C_A} \end{cases} \quad (2.24)$$

where the superscript ‘ $\sigma$ ’ means ‘under the influence of stress’. Replacing the transition temperatures in Eqs. (2.20) and (2.21) with the above stress-affected transition temperatures yields the kinetic expression for the martensitic transformation as

$$\begin{cases} \xi = 1 - \frac{1-\xi_A}{2} \exp[a_M(M_0 + \frac{\sigma}{C_M} - T)^n] & M_0^\sigma \geq T \geq M_f^\sigma \\ \xi = \frac{1-\xi_A}{2} \exp[a_M(T - \frac{\sigma}{C_M} - M_0)^n] & M_s^\sigma \geq T \geq M_0^\sigma \end{cases} \quad (2.25)$$

and for the reverse transformation

$$\begin{cases} \xi = \xi_M - \frac{\xi_M}{2} \exp[a_A(A_0 + \frac{\sigma}{C_A} - T)^n] & A_0^\sigma \geq T \geq A_s^\sigma \\ \xi = \frac{\xi_M}{2} \exp[a_A(T - A_0 - \frac{\sigma}{C_A})^n] & A_f^\sigma \geq T \geq A_0^\sigma \end{cases} \quad (2.26)$$

The above model for the phase transformation of SMA is referred to as an ‘exp model’ in this dissertation. Since this model describes phase transformations in a

piecewise fashion, the calculation may sometimes be very complex; another simpler model called the cosine model is proposed. In the cosine model, a complete cosine curve fits the whole martensitic transformation or reverse transformation process. For a free transformation (no stress influence), the reverse transformation is described as

$$\xi = \frac{1}{2} \{ \cos[a_A(T - A_s)] + 1 \} \quad (2.27)$$

and the martensitic transformation is given by

$$\xi = \frac{1}{2} \{ \cos[a_M(T - M_f)] + 1 \} \quad (2.28)$$

where the two material constants,  $a_A$  and  $a_M$ , are determined from

$$\begin{cases} a_A = \pi/(A_f - A_s) \\ a_M = \pi/(M_s - M_f) \end{cases} \quad (2.29)$$

Similarly, if the starting state of the phase transformation is a mixed phase and some stress is applied, the transformation kinetics for the reverse transformation is given by

$$\xi = \frac{\xi_M}{2} \{ \cos[a_A(T - A_s) + b_A\sigma] + 1 \} \quad (2.30)$$

and for the martensitic transformation

$$\xi = \frac{1 - \xi_A}{2} \cos[a_M(T - M_f) + b_M\sigma] + \frac{1 + \xi_A}{2} \quad (2.31)$$

where the two new material constants are defined as

$$\begin{cases} b_A = -a_A/C_A \\ b_M = -a_M/C_M \end{cases} \quad (2.32)$$

The transformation stress range can be obtained directly from Fig. 2.2. For a specified ambient temperature,  $T$ , the stress range in which the martensitic transformation can be stress-induced may be given as

$$C_M(T - M_f) \geq \sigma \geq C_M(T - M_s) \quad (2.33)$$

while the stress range for the reverse transformation may be derived as

$$C_A(T - A_s) \geq \sigma \geq C_A(T - A_f) \quad (2.34)$$

There are two types of SMA materials; one has the typical  $\xi$ -T relation as shown in Fig. 2.1 in which  $A_s \geq M_s$ , while the other type is characterized by  $A_s \leq M_s$ . Since most commercially available SMA materials belong to the first category, only the first type of SMA materials is considered in this dissertation.

## 2.2 Mechanical Behavior of SMA

The typical stress-strain relations of SMAs are shown in Fig. 2.3. The stress-strain curve can be roughly divided into three sections. The first section is an elastic section;  $\sigma_e$  is the elastic stress limit. The second section corresponds to the martensitic transformation; the transformation occurs between  $\sigma_e$  and the yield stress,  $\sigma_y$ . The

third section after  $\sigma_y$  is a plastic section. This model primarily focus on the first and the second sections. Unlike the conventional definition which defines the yield stress at the beginning of the stress-strain plateau, the yield stress is defined here according to the micromechanics which describes the plastic deformation as the movement of dislocations. The large deformation between  $\sigma_e$  and  $\sigma_y$  is caused by re-orientation of martensitic plates and is different from the plastic deformation which can be viewed as the slip deformation of crystal lattices. Therefore, the yield stress,  $\sigma_y$ , is defined at the end of the martensitic transformation where plastic slip begins to occur. The unloading is an elastic process at a temperature below  $A_s$ . The large residual strain obtained by unloading before  $\sigma_y$  (dash line in Fig. 2.3) is recoverable by heating the material above  $A_f$  (shape memory effect). The maximum recoverable strain corresponds to the yield stress,  $\sigma_y$ . The deformation after the yield stress,  $\sigma_y$ , is basically described as plastic deformation and is assumed to obey the plastic flow rule. The superposition rule of strain for shape memory alloys is

$$\epsilon = \epsilon^e + \epsilon^t + \epsilon^p \quad (2.35)$$

where  $\epsilon^t$  is the transformation strain caused by the formation of martensitic detwinning and  $\epsilon^e$  the elastic strain. The non-plastic strain  $\epsilon^{np} = \epsilon^e + \epsilon^t$  is considered in this model while the plastic strain is assumed to be simply governed by the plastic flow rule.

The upper curve in Fig. 2.3 corresponds to a higher temperature ( $T \gg A_f$ ). The stress-strain curve looks much like the one of a conventional material, but it still can be divided into three sections. The first section for stress under  $\sigma_e$  is elastic. The

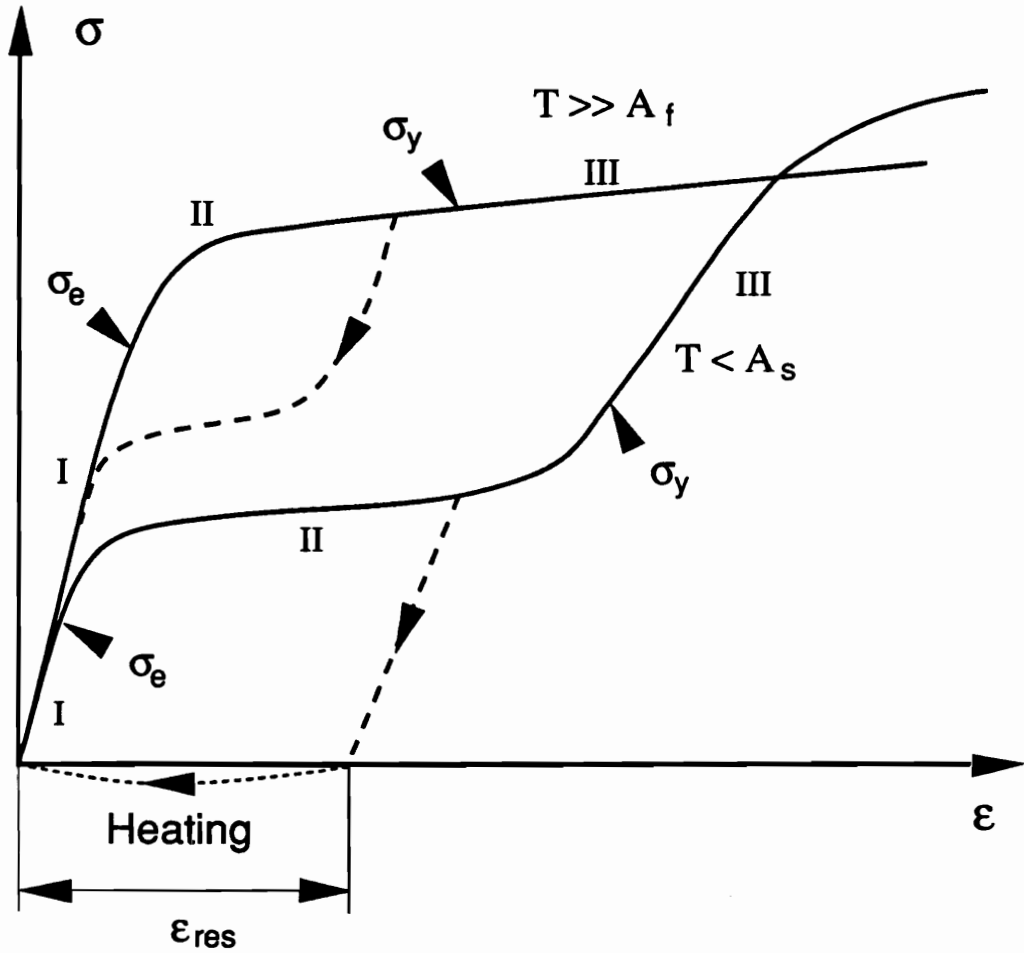


Figure 2.3: Schematics of Stress-Strain-Temperature Relations of SMA

phase transformation occurs between  $\sigma_e$  and  $\sigma_y$ . Plastic deformation starts from  $\sigma_y$ . This classification is based on the experimental evidence that an unloading before a certain stress level ( $\sigma_y$  here) can produce complete recovery due to the pseudoelastic effect, as illustrated in Fig. 2.3. If the unloading occurs after  $\sigma_y$ , complete recovery is impossible and the unrecovered portion of the strain is characterized as plastic strain. The maximum recoverable strain of a nitinol alloy is about 6 ~ 8%, the strain limit for a complete pseudoelastic effect is usually half of the above strain (3 ~ 4%). This indicates a nonlinear  $M_f$  and stress relation. Nevertheless, the linear relations of transition temperatures and applied stress are assumed in this dissertation. However, modeling of this nonlinear effect can be easily realized by including some nonlinear terms in Eqs. (2.23) and (2.24).

The shape memory effect usually means a free strain recovery effect or a recovery stress effect. When an elongated SMA sample is heated above its austenite start temperature, the residual strain of the SMA sample (with no applied load) will be restored when the temperature reaches the austenite finish temperature. This effect is called free strain recovery, or simply free recovery, and is illustrated in Fig. 2.4. The free recovery effect is simply the result of the internal phase transformation, so it appears that this free recovery curve may very well represent the martensite fraction and temperature relation. The unknown transformation coefficient,  $n$ , introduced in Eq. (2.12) may be determined from the free recovery experimental results.

Another of the shape memory effect characteristics is the recovery stress effect. When an elongated SMA sample is restrained while being heated, a large stress can be generated to prevent the SMA sample from recovering to its original shape or geometry.



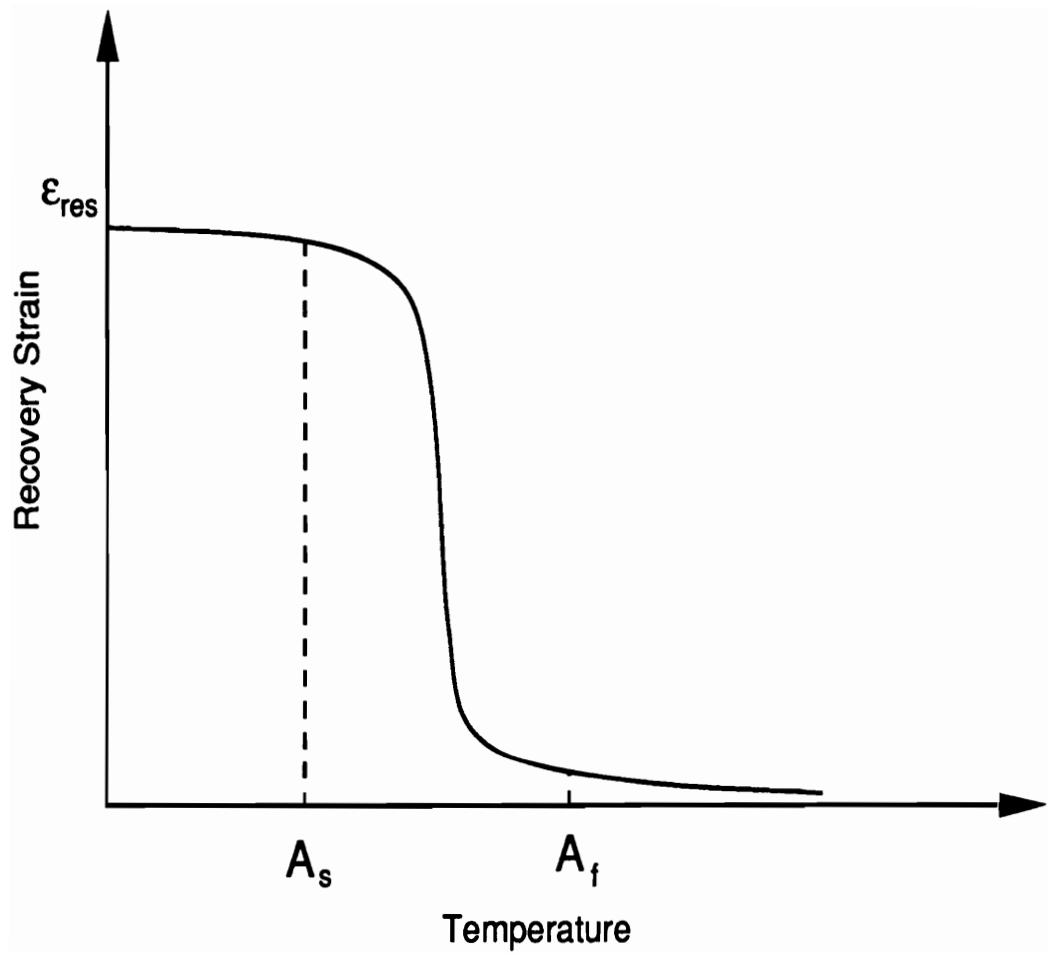


Figure 2.4: Schematic Diagram of Free Strain Recovery Effect

This recovery stress is much higher than the elastic limit,  $\sigma_e$ , and yield stress,  $\sigma_y$ . This effect is schematically depicted in Fig. 2.5. The elongated SMA sample is characterized by some deformed martensite which is not thermally stable at higher temperatures (above  $A_s$ ). The heating process corresponds to the reverse transformation. This transformation starts at about  $A_s$  ( $A_s^\sigma$  is a little higher than  $A_s$ ) and ends at  $A_f^\sigma$ . The cooling process corresponds to a martensitic transformation as shown in Fig. 2.5. The hysteresis of this recovery stress and temperature relation is caused by the irreversible aspects of phase transformations. If the SMA sample is allowed to have some recovery strain, the recovery stress-temperature relation depicted in Fig. 2.5 will be different. The new relationship is called the recovery stress-strain-temperature relation.

## 2.3 Thermomechanics of SMA

Considering a one-dimensional metallic material of length  $L$  which is undergoing either a martensitic transformation or its reverse transformation, the original reference state is denoted as  $X$ , the current configuration is  $x$ , the deformation gradient  $f$  is defined as

$$f = \frac{\partial x}{\partial X} \quad (2.36)$$

The deformation velocity  $v$  is expressed in terms of the deformation gradient:

$$v = \frac{\dot{f}}{f} \quad (2.37)$$

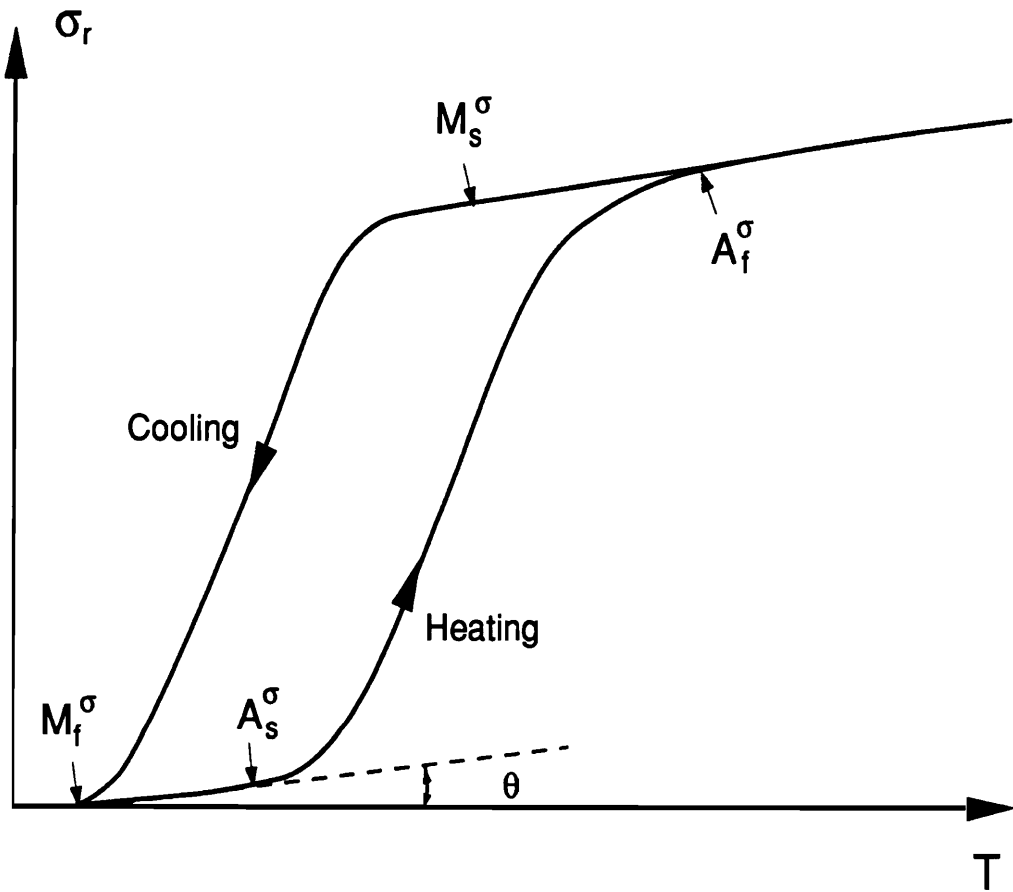


Figure 2.5: Schematic Diagram of Recovery Stress and Temperature Relations

The general governing equations are the first and the second laws of thermodynamics. Written in the current configuration, the two laws are

$$\begin{cases} \rho \dot{U} - \sigma v + \frac{\partial q_{sur}}{\partial x} - \rho q = 0 \\ \rho \dot{S} - \rho \frac{q}{T} + \frac{\partial}{\partial x} \left( \frac{q_{sur}}{T} \right) \geq 0 \end{cases} \quad (2.38)$$

where  $\rho$  is the density,  $\sigma$  the Cauchy stress,  $q_{sur}$  the heat flux from the surroundings,  $q$  the internal heat source,  $T$  the temperature,  $U$  the internal energy,  $S$  the entropy and  $(\dot{\phantom{x}})$  denotes a time derivative. Rewriting the above energy balance equation in the original configuration yields

$$\begin{cases} \rho_0 \dot{U} - \bar{\sigma} \dot{\bar{\epsilon}} + f^{-1} \frac{\rho_0}{\rho} \frac{\partial q_{sur}}{\partial X} - \rho_0 q = 0 \\ \rho_0 \dot{S} - \rho_0 \frac{q}{T} + f^{-1} \frac{\rho_0}{T \rho} \frac{\partial q_{sur}}{\partial X} - f^{-1} \frac{\rho_0 q_{sur}}{T^2 \rho} \frac{\partial T}{\partial X} \geq 0 \end{cases} \quad (2.39)$$

where variables with subscript '0' are measured with reference to the original configuration. The Green strain,  $\bar{\epsilon}$ , and the second Piola-Kirchhoff stress,  $\bar{\sigma}$ , are defined as

$$\begin{cases} \bar{\sigma} = \frac{\rho_0}{\rho} \frac{\sigma}{f^2} \\ \bar{\epsilon} = \frac{f^2 - 1}{2} \end{cases} \quad (2.40)$$

The state variables for SMA are strain, temperature, and the martensite fraction,  $\xi$ . The general state variable is simply written as

$$\Lambda \equiv (\bar{\epsilon}, T, \xi) \quad (2.41)$$

The Helmholtz free energy, which is the driving force of phase transformations, is a

function of the above state variables and is given by

$$\Phi = \Phi(\Lambda) = U - TS \quad (2.42)$$

Taking a time derivative of  $\Phi$  yields

$$\dot{\Phi} = \frac{\partial \Phi}{\partial \bar{\epsilon}} \dot{\bar{\epsilon}} + \frac{\partial \Phi}{\partial T} \dot{T} + \frac{\partial \Phi}{\partial \xi} \dot{\xi} = \dot{U} - \dot{T}S - \dot{S}T \quad (2.43)$$

Substituting Eq. (2.43) and the first law of thermodynamics (Eq. (2.39)) into the Clausius-Duhem inequality (the second law of thermodynamics) and expressing every term in the original configuration yields

$$\left(\frac{\bar{\sigma}}{\rho_0} - \frac{\partial \Phi}{\partial \bar{\epsilon}}\right) \dot{\bar{\epsilon}} - \left(S + \frac{\partial \Phi}{\partial T}\right) \dot{T} - \frac{\partial \Phi}{\partial \xi} \dot{\xi} - \frac{1}{\rho_0 T} f^{-1} q_{sur} \frac{\rho_0}{\rho} \frac{\partial T}{\partial X} \geq 0 \quad (2.44)$$

The Clausius-Duhem inequality represents the change of entropy of two thermodynamic states. The change of entropy of two states is independent of time, it only depends on its path. Therefore, the coefficients of  $\dot{\bar{\epsilon}}$  and  $\dot{T}$  should vanish, which yields the general constitutive equations as

$$\bar{\sigma} = \rho_0 \frac{\partial \Phi}{\partial \bar{\epsilon}} \quad (2.45)$$

and

$$S = -\frac{\partial \Phi}{\partial T} \quad (2.46)$$

Assuming an adiabatic process or uniform temperature distribution, the Clausius-Duhem inequality can be written as

$$\frac{\partial \Phi}{\partial \xi} \dot{\xi} \leq 0 \quad (2.47)$$

The equal sign is adopted if the process is reversible such as elastic loading or unloading. From Müller's and Falk's study of free energy relations, it is impossible to have  $\frac{\partial \Phi}{\partial \xi} = 0$  when  $\dot{\xi}$  is not zero. This indicates that the martensite volume fraction will remain the same during an elastic loading or unloading.

The maximum recoverable strain of a piece of SMA wire is about 6–8 percent for nitinol, the strain corresponding to the elastic stress limit is generally 0.1 percent to 0.6 percent. The constitutive model of SMA, therefore, must be formulated to deal with large deformation problems. Since the Green strain and its corresponding stress, the second Piola-Kirchhoff stress, are used in the derivation, and the governing equations are written in the original configuration, the constitutive equations are able to capture the physics of the shape memory effect with large deformation.

## 2.4 Modeling of Shape Memory Alloy

The stress in Eq. (2.45) is a function of several internal variables. Therefore, the time derivative of stress can be written as

$$\dot{\sigma} = \frac{\partial \sigma}{\partial \bar{\epsilon}} \dot{\bar{\epsilon}} + \frac{\partial \sigma}{\partial T} \dot{T} + \frac{\partial \sigma}{\partial \xi} \dot{\xi} = D\dot{\bar{\epsilon}} + \Theta\dot{T} + \Omega\dot{\xi} \quad (2.48)$$

where  $D$  is the Young's modulus,  $\Theta$  the thermoelastic tensor (it is different from the stress caused by a temperature gradient), and  $\Omega$  the transformation tensor, a metallurgical quantity which represents the volume change during the phase transformation. These material properties derived from thermomechanics are given by

$$\begin{cases} D = \rho_0 \frac{\partial^2 \Phi}{\partial \bar{\epsilon}^2} \\ \Theta = \rho_0 \frac{\partial^2 \Phi}{\partial \bar{\epsilon} \partial T} \\ \Omega = \rho_0 \frac{\partial^2 \Phi}{\partial \bar{\epsilon} \partial \xi} \end{cases} \quad (2.49)$$

The material variables given above are still functions of the state variables. For example, Young's modulus varies as shown in Fig. 1.5. To simplify the expression of the constitutive relations, assuming constant material properties, integration of Eq. (2.48) with respect to time results in the following time-independent constitutive relation.

$$\bar{\sigma} - \bar{\sigma}_0 = D(\bar{\epsilon} - \bar{\epsilon}_0) + \Omega(\xi - \xi_0) + \Theta(T - T_0) \quad (2.50)$$

where variables with subscript '0' may be obtained from initial conditions. Higher strain rates can affect the mechanical behavior significantly. The above equation can only be applied for small strain rate problems, i.e., quasi-static problems.

The stress from Eq. (2.48) is a function of strain, martensite fraction, and temperature; the martensite fraction,  $\xi$ , is provided by Eqs. (2.25) and (2.26) or (2.30) and (2.31). Therefore, an iterating technique must be used to solve for the stress. The independent variables are now stress, strain, and temperature, giving any two of them leads to the third. The derivation of this equation allows it to be used in the marten-

sitic transformation or the reverse transformation. The selection of the martensite fraction expression from Eqs. (2.25) and (2.26) is based on whether it is a martensitic transformation or a reverse transformation. The cosine model or exp model can be selected depending on the accuracy required and the material data available.

Shape memory alloys may be used in several geometric forms and utilize various transduction principles for active control applications. One approach is to use SMA wire or fiber as distributed force actuators. SMA force actuators are first elongated at a low temperature and then unloaded to generate some martensitic residual strain; upon heating the wire, the martensitic residual strain will be restored. The shape memory recovery generally falls into one of the following categories. The first is free recovery in which there is no external load on the wire, and therefore, no work. The second category includes fully restrained 'recovery'. In this case, the martensitic residual strain of the SMA wire is restrained from being restored to its original length. This restraining causes large internal 'recovery' stress. The third category is called controlled recovery. In this case, some residual martensitic strain is restored (the restored part is called the recovery strain), but the wire is still under some tension which is required to prevent full recovery of the residual strain. The following models may be applied to any of these three categories.

### **2.4.1 Stress-Strain Relations**

The constitutive model presented in this chapter considers only one-dimensional systems; therefore, the material will often be referred to as wire or fiber. To give the constitutive relations for the SME, we must first consider the stress-strain relations



which provide the initial conditions for the recovery process. The ‘cosine model’ is used in order to simplify our derivation, but the ‘exp model’ may be used similarly.

Consider a piece of SMA wire undergoing an isothermal mechanical loading and unloading process. It is assumed that the surrounding temperature is below  $A_s$ , so no pseudoelastic effect during the unloading can be presented. The initial state of a piece of SMA wire can range from all martensite to all austenite, depending on the heat treatment process and the ambient temperature. Here, we consider only the case which has loading and unloading temperatures between  $M_s$  and  $A_s$  and 100 percent austenite before loading. To achieve the stress induced martensite, the applied stress must be in the stress range given by Eq. (2.33). In Eq. (2.48), there is no T term for the isothermal process, and  $\xi$  is zero if the stress is less than  $\sigma_e = C_M(T - M_s)$ , as given in Eq. (2.33). After applying the initial conditions which are zero stress, zero strain, and full austenite, Eq. (2.50) changes into the following form.

$$\bar{\sigma} = D\bar{\epsilon} \quad (2.51)$$

The linear elastic stress limit,  $\bar{\sigma}_e$ , and its corresponding strain,  $\bar{\epsilon}_e$ , are defined as

$$\begin{cases} \bar{\sigma}_e = C_M(T - M_s) \\ \bar{\epsilon}_e = \bar{\sigma}_e/D \end{cases} \quad (2.52)$$

When the applied stress becomes greater than  $\bar{\sigma}_e$ , there will be stress-induced martensite, and Eq. (2.50) now becomes

$$\bar{\sigma} - \bar{\sigma}_0 = D(\bar{\epsilon} - \bar{\epsilon}_0) + \Omega(\xi - \xi_0) \quad (2.53)$$

with the initial conditions,  $\bar{\sigma}_0 = \bar{\sigma}_e$ ,  $\bar{\epsilon}_0 = \bar{\epsilon}_e$ , and  $\xi_0 = 0$ . Equation (2.53) then simply becomes

$$\bar{\sigma} = D\bar{\epsilon} + \Omega\xi \quad (2.54)$$

The loading is a martensitic transformation process, so Eq. (2.31) is used for the martensite fraction (cosine model). Together Eqs. (2.51), (2.54), and (2.31) yield the stress-strain curve up to the yield strength,  $\sigma_y$ . To determine the value of  $\Omega$  from a mechanical engineering point of view, which is concerned with the crystallographic volume change due to the phase transformation, it is necessary to consider the unloading process at  $\xi = 1$ . From the discussion of Eq. (2.47), the elastic loading and unloading does not change the martensite fraction. Since the ambient temperature is below  $A_s$ , there is no pseudoelasticity; it is an elastic unloading. After unloading at  $\xi = 1$ , the martensitic residual strain (the unloaded phase is completely deformed martensite),  $\bar{\epsilon}_{res}$ , or the transformation strain,  $\bar{\epsilon}_t$ , can be derived as

$$\bar{\epsilon}_{res} = -\frac{\Omega}{D} \quad (2.55)$$

This residual strain is the maximum recoverable strain. Experimental results have shown that this maximum recoverable martensitic strain, or recovery strain limit, is almost a constant between  $M_f$  and  $A_s$ . The recovery strain limit,  $\bar{\epsilon}_L$ , is therefore, considered a temperature-independent material constant and it has the following relation with  $\Omega$  and  $D$ .

$$\bar{\epsilon}_L = -\frac{\Omega}{D} \quad (2.56)$$

The maximum recoverable strain is a material property for a shape memory alloy and it should be specified by manufacturers. The above equation provides an indirect approach to determine the phase transformation tensor,  $\Omega$ .

If unloading occurs before  $\xi = 1$ , the SMA material is composed of both the deformed martensite and austenite. The residual strain resulting from the martensitic transformation can be stated as

$$\bar{\epsilon}_{res} = -\xi \frac{\Omega}{D} \quad (2.57)$$

The martensite fraction,  $\xi$ , which is the initial condition for the recovery process, can likewise be expressed as

$$\xi = \frac{\bar{\epsilon}_{res}}{\bar{\epsilon}_L} \quad (2.58)$$

A pseudoelastic effect occurs when unloading at a temperature above  $A_s$ . Equation (2.34) specifies the stress range in which the reverse transformation occurs. The upper and lower stress limits for the reverse transformation are

$$\begin{cases} \bar{\sigma}_r^u = C_A(T - A_s) \\ \bar{\sigma}_r^l = C_A(T - A_f) \end{cases} \quad (2.59)$$

where ‘u’ and ‘l’ denote ‘upper’ and ‘lower’. As shown in Fig. 2.6, if the unloading starts from a state  $(\bar{\epsilon}_u, \bar{\sigma}_u, \xi_u)$  (subscript ‘u’ represents ‘unloading’), it is a linear elastic process before the stress is unloaded to  $\bar{\sigma}_r^u$ . The reverse phase transformation starts at  $\bar{\sigma}_r^u$ . The nonlinear unloading is known as the pseudoelastic effect. The

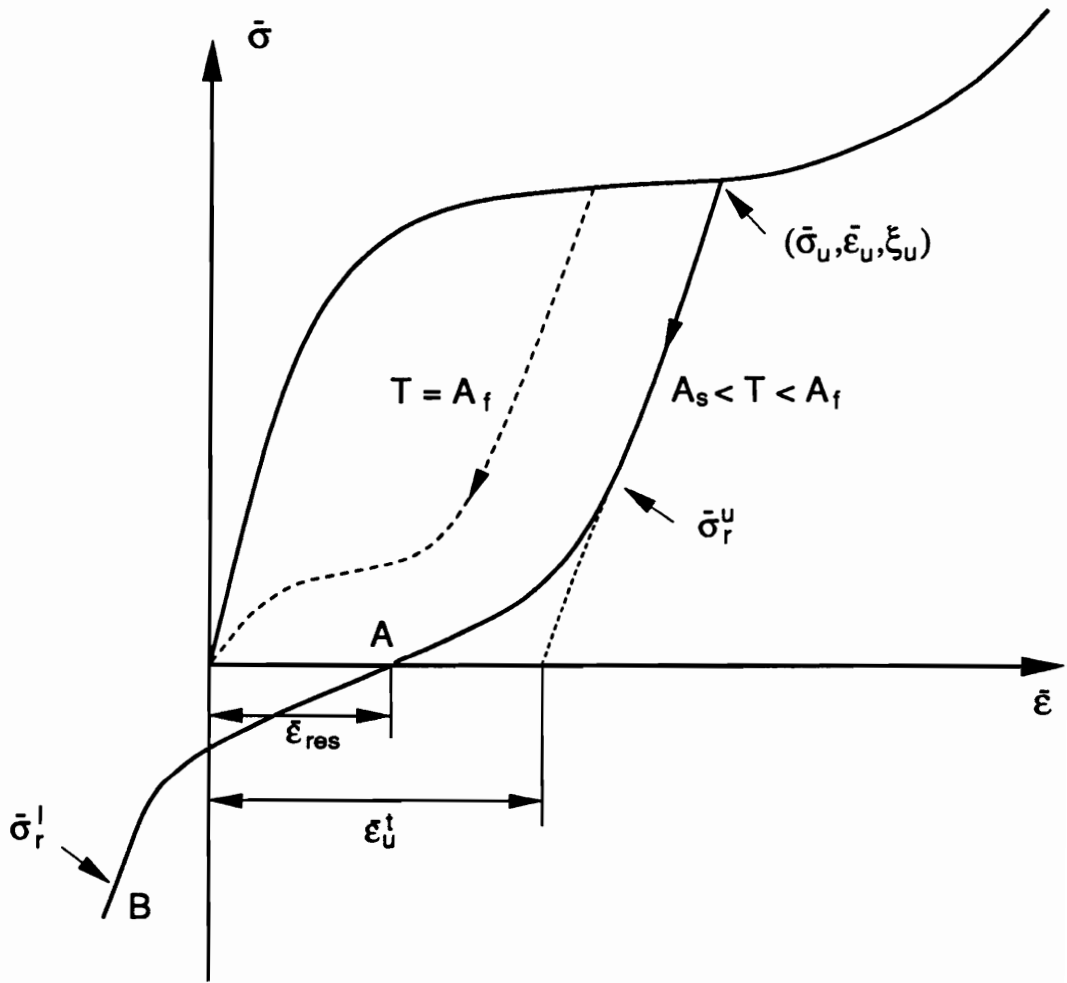


Figure 2.6: Typical Unloading Process

nonlinear stress-strain relation for the pseudoelastic effect may be derived from Eq. (2.50) with the following initial conditions.

$$\begin{cases} \bar{\epsilon}_0 = \bar{\epsilon}_u - \frac{\bar{\sigma}_u - \bar{\sigma}_r^u}{D} \\ \bar{\sigma}_0 = \bar{\sigma}_r^u \\ \xi_0 = \xi_u \end{cases} \quad (2.60)$$

which yields

$$\bar{\sigma} - \bar{\sigma}_u = D(\bar{\epsilon} - \bar{\epsilon}_u) + \Omega(\xi - \xi_u) \quad (2.61)$$

where  $\xi$  is given by Eq. (2.30). Note that  $\xi$  does not change until the stress is unloaded to  $\bar{\sigma}_r^u$ . It is obvious that the stress-strain relations rely on the history of loading and unloading, just like plastic deformation.

After the stress is unloaded to zero, the residual strain is denoted as  $\bar{\epsilon}_{res}$ . The total strain consists of three components: elastic strain, plastic strain, and transformation strain. The plastic strain is negligible if the unloading occurs at stresses lower than  $\sigma_y$ . Therefore, the residual strain illustrated in Fig. 2.6 is the strain resulting from the phase transformation,  $\bar{\epsilon}^t$ . The transformation strain,  $\bar{\epsilon}^t$ , can be obtained from

$$\bar{\epsilon}^t = \bar{\epsilon} - \bar{\epsilon}^e = \bar{\epsilon} - \frac{\bar{\sigma}}{D} \quad (2.62)$$

This equation leads to the general expression of the martensite fraction as

$$\xi = \frac{\bar{\epsilon}^t}{\bar{\epsilon}_L} \quad (2.63)$$

The residual martensite fraction for a pseudoelastic unloading (Fig. 2.6) may be derived from the above equations as

$$\xi = \xi_u - \frac{\bar{\epsilon}_u^t - \bar{\epsilon}_{res}}{\bar{\epsilon}_L} \quad (2.64)$$

where  $\bar{\epsilon}_u^t$  is the transformation strain component corresponding to  $\bar{\epsilon}_u$ . If a compressive force is applied after a complete unloading, the stress-strain relation still follows Eq. (2.61) and the reverse transformation begins at  $\bar{\sigma}_r^u$ . If the test temperature is  $A_f$ , a complete unloading is accompanied by a complete strain recovery theoretically as demonstrated by the dash line in Fig. 2.6. If the ambient temperature is lower than  $A_f$ , the compressive stress required to get a complete strain recovery can also be derived from Eq. (2.61).

The assumption of homogeneity of SMA in tension and compression is only correct during a one-time operation. The cyclic behavior of SMA is very complex and is left for future research. The current model is restricted for complete tensile or compression only.

## 2.4.2 Constitutive Relations of SME

The martensitic residual strain or the residual martensite fraction, which is the primary parameter in the determination of the shape memory effect, appears in the constitutive relations only as an initial condition. This is to say that in spite of what happens in the loading and unloading process, the shape memory effect depends only on the final state of the material, namely, the deformed martensite fraction or the

martensitic residual strain.

### Free Strain Recovery

The external mechanical stress is zero for a free recovery process. Equation (2.50), therefore, is rewritten as

$$D(\bar{\epsilon}^r - \bar{\epsilon}_0) + \Theta(T - T_0) + \Omega(\xi - \xi_0) = 0 \quad (2.65)$$

where the superscript 'r' represents 'recovery'. Assuming no pseudoelastic effect involved in the unloading, the following initial conditions result.

$$\begin{cases} \bar{\epsilon}_0 = \bar{\epsilon}_{res} \\ T_0 = A_s \\ \xi_0 = \xi_M = \frac{\bar{\epsilon}_{res}}{\bar{\epsilon}_L} \end{cases} \quad (2.66)$$

Equation (2.66) ignores the thermal expansion effects which are negligible in comparison to the recovery effects. Since free recovery must occur above  $A_s$ , the austenite start temperature is set as the initial condition for the temperature. In Eq. (2.65), the martensite fraction is governed by Eq. (2.30) in which  $\sigma$  is zero. Note that the recovery strain is still measured in reference to the original coordinate 'X.' Equations (2.30), (2.65), and the above initial conditions give the constitutive equation for the free recovery as

$$\bar{\epsilon}^r = \bar{\epsilon}_{res} - \frac{1}{D} \left\{ \Theta(T - A_s) + \frac{\Omega}{2} \frac{\bar{\epsilon}_{res}}{\bar{\epsilon}_L} [\cos a_A(T - A_s) - 1] \right\} \quad (2.67)$$

## Restrained Recovery

In the scenario, the strain is restrained during the recovery process. Therefore, the constitutive equation from Eq. (2.50), then becomes

$$\bar{\sigma}^r - \bar{\sigma}_0^r = \Theta(T - T_0) + \Omega(\xi - \xi_0) \quad (2.68)$$

The initial state in Fig. 2.1 is  $(\xi_M, T_M)$ , where  $\xi_M$  is  $\xi_0$ .  $T_M$  can be found from Eq. (2.28) as

$$T_M = M_f + \frac{\cos^{-1}[2(\xi_M - 0.5)]}{a_M} \quad (2.69)$$

From  $T_M$  to  $A_s$ , there is no new austenite; the recovery stress-temperature relation is linear and is given by

$$\bar{\sigma}^r - \bar{\sigma}_0^r = \Theta(T - T_M) \quad (2.70)$$

The initial stress,  $\bar{\sigma}_0^r$ , is assumed to be zero at  $T_M$ . If there is some stress, the austenite start temperature will be increased as shown in Fig. 2.2. Defining the new austenite start temperature as  $A_s^\sigma$ , and combining Eqs. (2.70) and (2.30) at the transition point where  $C_A(A_s^\sigma - A_s) = \bar{\sigma}^r$  gives the new transition temperature:

$$A_s^\sigma = \frac{C_A A_s - \Theta T_M}{C_A - \Theta} \quad (2.71)$$



Substituting this temperature into Eq. (2.70) gives the corresponding stress  $\bar{\sigma}_{A_s}^r$  as

$$\bar{\sigma}_{A_s}^r = \Theta(A_s^\sigma - T_M) \quad (2.72)$$

If the ambient temperature is higher than  $A_s^\sigma$ , then there is new austenite and the constitutive relation has the complete form of Eq. (2.68). The initial conditions are

$$\begin{cases} \bar{\sigma}_0^r = \bar{\sigma}_{A_s}^r \\ T_0 = A_s^\sigma \\ \xi_0 = \xi_M = \bar{\epsilon}_{res}/\bar{\epsilon}_L \end{cases} \quad (2.73)$$

Replacing  $\sigma$  with  $\bar{\sigma}^r$  in Eq. (2.30), and substituting it and the above initial conditions into Eq. (2.68), yields the final constitutive equation for the restrained recovery as

$$\bar{\sigma}^r - \bar{\sigma}_{A_s}^r = \Theta(T - A_s^\sigma) + \frac{\Omega \bar{\epsilon}_{res}}{2 \bar{\epsilon}_L} \{ \cos[a_A(T - A_s) + b_A \bar{\sigma}^r] - 1 \} \quad (2.74)$$

The above stress-temperature relation is not explicit. For a given temperature, iteration is needed to converge. When the test temperature reaches a certain level, there will no longer be any stress-induced martensite for the  $M \rightarrow A$  transformation. This temperature is denoted as  $A_f^\sigma$ . In this case, the recovery stress-temperature relation will be linear again, giving

$$\bar{\sigma}^r - \bar{\sigma}_0^r = \Theta(T - T_0) \quad (2.75)$$

where  $T_0$  is  $A_f^\sigma$  and  $\bar{\sigma}_0^r$  is the recovery stress at  $T = A_f^\sigma$ , resulting in

$$\bar{\sigma}^r = \bar{\sigma}_{A_f}^r = \Theta(A_f^\sigma - A_s^\sigma) + \Omega\left(0 - \frac{\bar{\epsilon}_{res}}{\bar{\epsilon}_L}\right) + \bar{\sigma}_{A_s}^r \quad (2.76)$$

$A_f^\sigma$  can be solved for by substituting Eq. (2.76) into Eq. (2.30) as

$$A_f^\sigma = \frac{a_A A_s - b_A \bar{\sigma}_{A_s}^r + b_A \Omega \xi_M + b_A \Theta A_s^\sigma + \pi}{a_A + b_A \Theta} \quad (2.77)$$

Equation (2.75) indicates that the recovery stress has a linear relation with temperature after  $T$  is higher than  $A_f^\sigma$ . This point is observed in the experiment by Cross et al. (1970).

The recovery stress-temperature relations are different in cooling than for heating processes. The preceding discussion was devoted to the heating process. Experiments reveal hysteric behavior for heating and cooling cycles as shown in Fig. 2.5. However, using the above approach, the mathematical simulation will in fact describe and predict the complete recovery stress-temperature hysteresis.

Let us assume cooling begins when the restrained SMA wire is heated to some temperature,  $T_c$ . Before the cooling begins, the recovery stress-temperature relations are given by Eqs. (2.70), (2.74), and (2.75). After cooling starts, the  $A \rightarrow M$  process is initiated, and Eq. (2.31) must be used with Eq. (2.68) to describe the process. In

this case, the initial conditions are

$$\begin{cases} \bar{\sigma}_0^r = \bar{\sigma}_c^r \\ T_0 = T_c \\ \xi_0 = \xi_c \end{cases} \quad (2.78)$$

where the subscript 'c' indicates the initial cooling state. Considering the effect of stress on  $M_s$ , the reverse phase transformation will occur at the temperature,  $M_s^\sigma$ , which is higher than  $M_s$ . Before the temperature reaches this transition point, there is no new martensite. As in solving  $A_s^\sigma$  for the heating process, the transition temperature,  $M_s^\sigma$  and its corresponding stress,  $\bar{\sigma}_{M_s}^r$ , can be determined from

$$M_s^\sigma = \frac{a_M M_f - b_M \bar{\sigma}_c^r + b_M \Theta T_c + \pi}{a_M + b_M \Theta} \quad (2.79)$$

and

$$\bar{\sigma}_{M_s}^r = \bar{\sigma}_c^r + \Theta(M_s^\sigma - T_c) \quad (2.80)$$

The phase transformation occurs for temperatures below  $M_s^\sigma$ . Equations (2.31) and (2.68) yield the governing equation:

$$\bar{\sigma}^r - \bar{\sigma}_{M_s}^r = \Theta(T - M_s^\sigma) + \Omega \frac{1 - \xi_c}{2} \{\cos[a_M(T - M_f) + b_M \bar{\sigma}^r] + 1\} \quad (2.81)$$

Similarly, if the SMA wire is cooled to  $M_f^\sigma$ , which is higher than  $M_f$  because of the stress effect, the  $M \leftarrow A$  transformation finishes, and the recovery stress and temperature is again a linear relation.  $M_f^\sigma$  and its corresponding stress,  $\bar{\sigma}_{M_f}^r$ , are

calculated from

$$\bar{\sigma}_{M_f}^r = \Theta(M_f^\sigma - M_f) + \Omega(1 - \xi_c) + \bar{\sigma}_{M_s}^r \quad (2.82)$$

and

$$M_f^\sigma = \frac{a_M M_f - b_M \bar{\sigma}_{M_s}^r - b_M \Omega(1 - \xi_c) + b_M \Theta M_s^\sigma}{a_M + b_M \Theta} \quad (2.83)$$

The linear recovery stress-temperature relation after the temperature drops below  $M_f^\sigma$  is given by

$$\bar{\sigma}^r - \bar{\sigma}_{M_f}^r = \Theta(T - M_f^\sigma) + \Omega(1 - \xi_c) \quad (2.84)$$

### Controlled Recovery

Controlled recovery is defined as the shape memory recovery process in which some recovery strain is allowed during the heating and cooling cycle. Since the martensite fraction-temperature relation has been described in a piecewise continuous fashion, the recovery stress-strain-temperature should also be studied in a similar manner. For the controlled recovery, Eq. (2.50) can be expressed as

$$\bar{\sigma}^r - \bar{\sigma}_0^r = D(\bar{\epsilon}^r - \bar{\epsilon}_0^r) + \Theta(T - T_0) + \Omega(\xi - \xi_0) \quad (2.85)$$

The controlled recovery process can be subdivided into two regions defined by the loading mechanism. The first region assumes that a constant load is applied, e.g., a piece of elongated SMA wire is loaded by a dead weight. In this case, Eq. (2.85) is

expressed as

$$D(\bar{\epsilon}^r - \bar{\epsilon}_0^r) + \Theta(T - T_0) + \Omega(\xi - \xi_0) = 0 \quad (2.86)$$

where the stress caused by the dead weight appears in the martensite fraction term. Transition points can be determined following the reasoning described in the last section.

The second loading scenario assumes that the loading is proportional to the recovery strain and may be modeled as SMA-spring structures. Most SMA force actuators can also be simplified to this physical model <sup>1</sup>. Consider a spring-SMA system as shown in Fig. 2.7, if the spring constant is 'k', the length of SMA wire 'L', and the cross section area of the SMA wire 's', then the stress-strain relation for the spring is described by

$$\bar{\sigma}^r - \bar{\sigma}_0^r = \frac{kL}{s}(\bar{\epsilon}_{res} - \bar{\epsilon}^r) \quad (2.87)$$

Substituting this equation into Eq. (2.85) yields

$$(1 + \frac{s}{kL}D)(\bar{\sigma}^r - \bar{\sigma}_0^r) = \Theta(T - T_0) + \Omega(\xi - \xi_0) \quad (2.88)$$

This equation can be handled in the same way as the restrained recovery.

---

<sup>1</sup>Detailed discussion is presented in Chapter 4

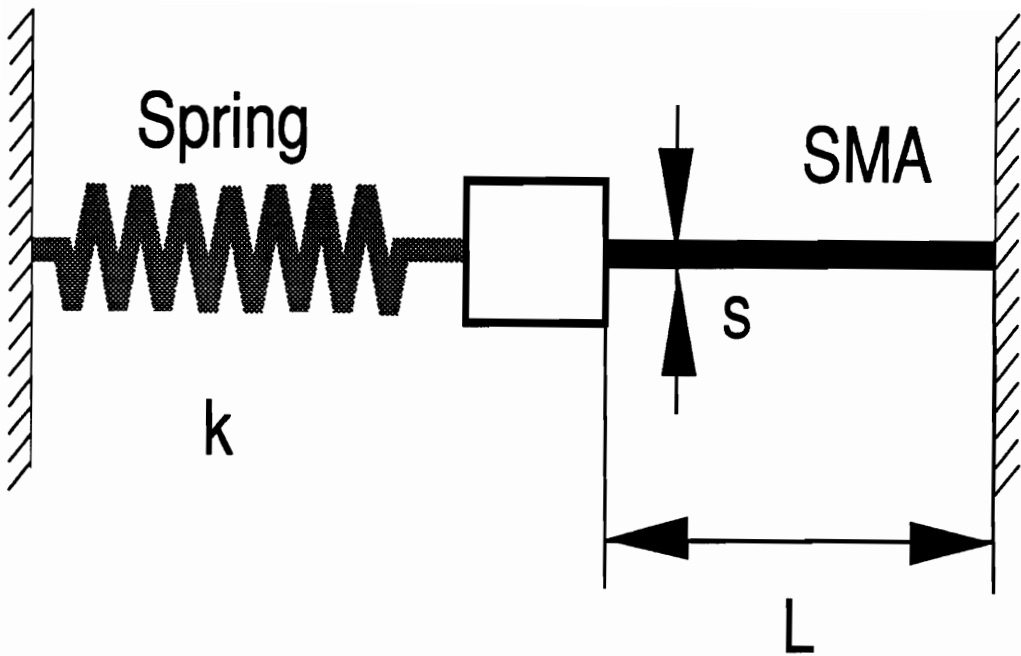


Figure 2.7: Simplified SMA-Spring Force Actuator

### 2.4.3 Influence of Changing Material Properties

The Young's modulus,  $D$ , and the thermoelastic tensor,  $\Theta$ , can be measured directly from experiment; the phase transformation tensor,  $\Omega$ , can be obtained indirectly. The phase transformation tensor governs the transformation behavior. This material constant is, therefore, assumed to be independent of martensite fraction and is a constant for a specified material. In most cases, an assumption of constant material properties can provide satisfactory results. However, it is still necessary to consider the material properties as functions of the state variables.

The value of  $\Theta$  is different for martensite and austenite as observed by Dye (1990). However, the thermoelastic tensor,  $\Theta$ , is much smaller than the other material constants; it affects the pre-transformation and post-transformation stage and is negligible during the phase transformation. A constant thermoelastic tensor is assumed here regardless of whether it is martensite or austenite.

The Young's modulus of a shape memory alloy varies significantly as shown in Fig. 1.5. Comparison between Fig. 1.5 and Fig. 2.1 leads to the following relation of the martensite fraction and the Young's modulus.

$$D = D_A + \xi(D_M - D_A) \quad (2.89)$$

where  $D_A$  is the Young's modulus of austenite and  $D_M$  is the Young's modulus of martensite. The martensite fraction is a function of stress and temperature as given by Eq. (2.30). This relation is substituted into the integrated constitutive relation, Eq. (2.50), in order to simplify the derivation. Most expressions for stress-strain

relations and the shape memory effect will remain the same excluding a very few relations. For example, the phase transformation tensor,  $\Omega$ , is derived in this case as

$$\Omega = -D_M \bar{\epsilon}_L \quad (2.90)$$

One of the most important results of considering a changing Young's modulus is the variation of the residual martensite fraction. Considering an SMA sample being loaded and unloaded in the temperature range of  $M_s$  to  $A_s$ , the stress-strain relation before unloading is

$$\bar{\sigma} = D(\bar{\epsilon}^e + \bar{\epsilon}^t) + \Omega \xi \quad (2.91)$$

where  $D$  is given by Eq. (2.89) and the phase transformation strain,  $\bar{\epsilon}^t$ , is given by Eq. (2.62). After an elastic unloading, the martensitic residual strain,  $\bar{\epsilon}_{res}$ , (it is now  $\bar{\epsilon}^t$ ) and the residual martensite fraction have the following relation.

$$\xi = \frac{D_A \bar{\epsilon}_{res}}{D_M \bar{\epsilon}_L + (D_A - D_M) \bar{\epsilon}_{res}} \quad (2.92)$$

More generally, the above equation can be expressed as

$$\xi = \frac{D_A \bar{\epsilon}^t}{D_M \bar{\epsilon}_L + (D_A - D_M) \bar{\epsilon}^t} \quad (2.93)$$

For most nitinol alloys,  $\frac{D_A}{D_M}$  is about four, this yields

$$\xi = \frac{4\bar{\epsilon}_t}{\bar{\epsilon}_L + 3\bar{\epsilon}_t} \quad (2.94)$$



## 2.5 Concluding Remarks

A mechanical constitutive model for shape memory alloys has been developed. This model has the following important features.

- This model is derived from thermomechanics; it reflects the essence of shape memory alloy behavior.
- An internal variable is introduced in this model to represent the extent of the phase transformations which makes this model more capable of dealing with phase transformation problems.
- The internal variable,  $\xi$ , can be derived from the transformation kinetics of shape memory alloys. Two empirical relations for the internal variable are proposed.
- This model has the capability to cope with the large deformation of shape memory alloys.
- This model is simple and easy to use in engineering design.
- The material properties required by this model are the Young's modulus, the thermoelastic tensor, the maximum recoverable strain, the stress influence coefficients, and four transition temperatures. They can be measured using standard material testing apparatus (DSC and tensile machine).

Based on the thermomechanical constitutive model, the stress-strain relations and relations between recovery stress, recovery strain, and temperature for shape memory effects have been developed. An experimental verification is presented in the next

chapter.

# Chapter 3

## Experimental Verifications

Any theoretical constitutive model requires experimental justification. A brief experimental verification of the thermomechanical constitutive model developed in this dissertation is presented in this chapter. A detailed description of experimental measurement techniques and procedures is presented in Dye's thesis (Dye, 1990).

### 3.1 Experimental Results

The SMA material used to verify this model is a nitinol alloy ( $\text{Ni}_{55}\text{Ti}$ ). An extensive experimental program has been conducted to measure the properties of this shape memory alloy (Dye, 1990). The experiments include the measurement of stress-strain relations at various temperatures, free recovery relations, recovery stress-temperature relations, and recovery stress-strain-temperature relations.

As discussed in Chapter 2, the material properties required to predict the mechanical behaviors of a shape memory alloy are the four transition temperatures ( $M_f$ ,  $M_s$ ,  $A_s$ , and  $A_f$ ), two stress influence coefficients ( $C_M$  and  $C_A$ ), the maximum recoverable strain ( $\epsilon_L$ ), the Young's modulus ( $D$ ), and the thermoelastic tensor ( $\Theta$ ).

The four transition temperatures can be accurately measured using differential scanning calorimeter (DSC) accurately. An alternative is to measure the electrical resistivity of shape memory alloys. They can also be estimated by examining the stress-strain relations and free recovery relations. The phase transformation start temperatures ( $M_s$  and  $A_s$ ) are defined at the temperature at which one-percent of the original phase has been transformed.  $M_f$  and  $A_f$  are defined to correspond to 99% transformed phase. Some error may not be avoided when experimentally determining the transformation temperatures and their related parameters, such as  $C_M$  and  $C_A$  by examining the mechanical behavior. However, in order to achieve correct theoretical prediction, the material properties should be measured strictly according to their definitions made in the formulation.

A manufacturer of shape memory alloys usually provides its customer with some transition temperatures. The only data provided by the manufacturer of the shape memory alloy used in our experiment is its austenite start temperature of 38 °C. There are two definitions of the transformation temperature of SMA. One is the strict metallurgical definition, which is used in this dissertation. Another is called the mechanical phase transformation temperature which is estimated from the mechanical behavior of a shape memory alloy. The transformation temperatures provided by manufacturers are usually from the second definition. The transformation temperatures used in this verification are obtained by DSC measurement (Abujudon et al., 1989) and are close to the mechanical experimental estimations.

The stress influence coefficients should also be measured from DSC or electrical re-

sistivity at different stress level. Unfortunately, no such data for the shape memory alloy is available; they can only be estimated from mechanical experiments. The stress influence coefficient of martensitic transformation,  $C_M$ , can be estimated indirectly by examining the relation of elastic stress limit,  $\sigma_e$ , and temperature, as shown in Fig. 3.1. The minimum point corresponds to the mechanical martensite start temperature and the slope provides the stress influence coefficient of martensitic transformation,  $C_M$ , according to Eq. (2.58). Theoretically, the stress-strain curve is linear in the elastic range and starts to be nonlinear at  $\sigma_e$ , which corresponds to one percent of martensitic transformation (one percent of austenite being transformed into martensite). It is difficult to determine the elastic stress limit from stress-strain curves. Figure 3.1 shows the elastic stress limit determined from the experimental stress-strain curves. The stress influence coefficient of martensitic transformation,  $C_M$ , is found to be 10.3 MPa/°C. The stress influence coefficients are assumed to be a constant; i.e., a linear relation of transformation temperature with applied stress, and  $C_A$  is assumed to be the same as  $C_M$ .  $C_A$  and  $C_M$  are listed in Table 3.1.

The maximum recoverable strain,  $\epsilon_L$ , is measured from stress-strain curves. In the experiment (Dye, 1990), a piece of SMA wire is elongated by eight percent at different temperatures below  $A_s$ . Unloading of the wire leaves about seven percent residual strain. Heating the wire results in an average of 6.7 percent recovery strain (measured with respect to the original length). Therefore, the maximum recoverable strain,  $\epsilon_L$ , for this shape memory alloy is determined to be 6.7 percent. Figure 3.2 shows the change of the  $\epsilon_L$  with respect to temperature.

Table 3.1: Material Properties Used for the Theoretical Verification

°C				GPa		MPa/°C				
$M_f$	$M_s$	$A_s$	$A_f$	$D_M$	$D_A$	$\Theta$	$C_M$	$C_A$	$\epsilon_L$ (%)	$n$
9.0	18.4	34.5	49.0	26.3	67.0	0.55	10.3	10.3	6.7	0.85

The maximum recoverable strain is almost constant for temperatures below  $A_s$ . Because of the pseudoelastic effect, the recovered portion of the residual strain when subjected to heating may not represent the total recoverable strain if the temperature is higher than  $A_s$ . The recoverable strain at a higher temperature ( $\geq A_s$ ) is measured from an assumed elastic unloading, as shown in Fig. 3.3.

The critical stress for martensitic transformation; i.e., the elastic limit,  $\sigma_e$ , increases with temperature. Plastic deformation may occur at higher stress. The dislocation corresponding to the plastic deformation creates an internal stress field which tends to increase the martensitic transformation and decrease the reverse transformation. In the experiment, an SMA wire was elongated by eight percent at 50 °C, and then unloaded as shown in Fig 3.3. The nonlinear unloading provides about 0.7 percent recovery strain due to the pseudoelastic effect. Heating to a much higher temperature after complete unloading results in another 4.3 percent recovery strain. Heating to a much higher temperature may release the internal stress caused by dislocations; therefore, the rest of the transformation strain may be restored. The total recovery strain attained at this temperature is about five percent, another two percent is the plastic strain.

The Young's modulus of the shape memory alloy is determined from experimental stress-strain curves. This is not a direct measurement of Young's modulus. Different results may be calculated even from the same stress-strain curve if different points are selected to fit a straight line. The stress and strain points up to the elastic stress limit are used to least-square-fit a linear function. The slope of the linear function provides the Young's modulus.

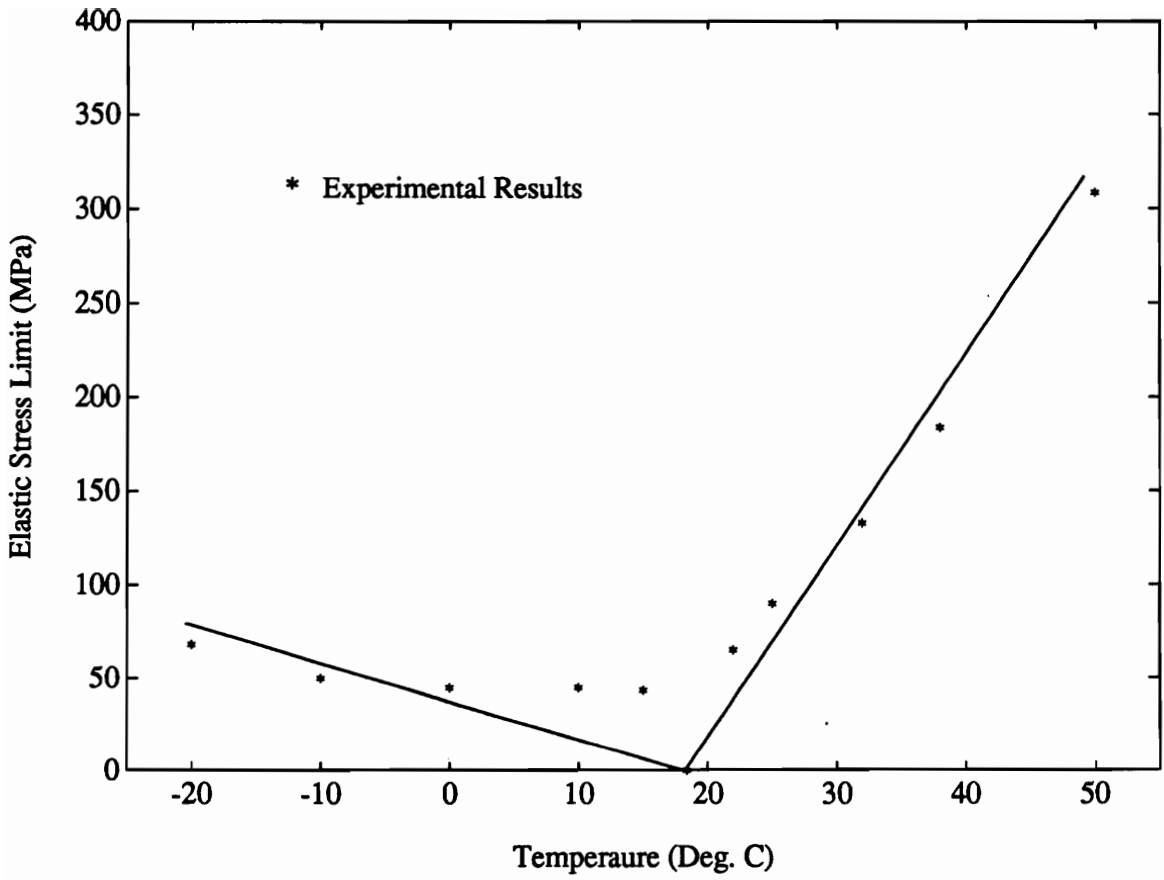


Figure 3.1: Elastic Stress Limit,  $\sigma_e$ , vs. Temperature



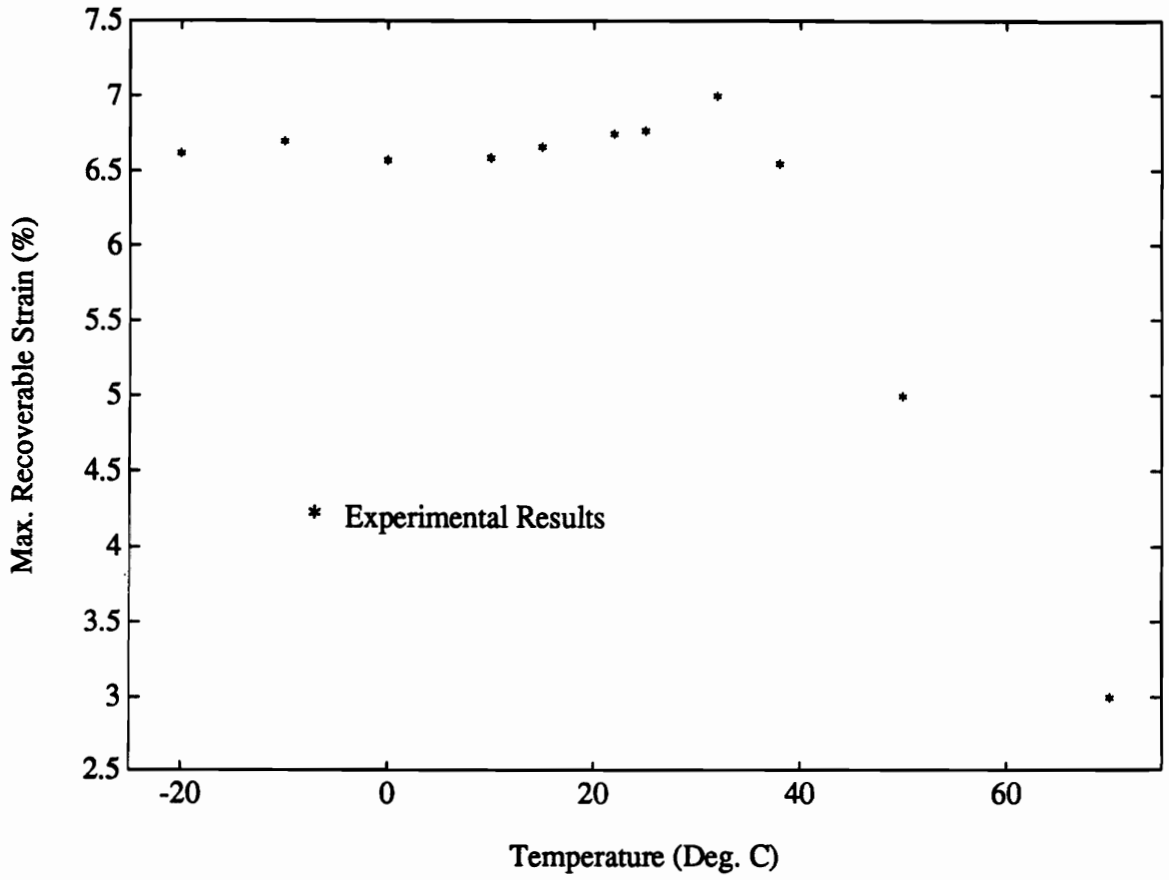


Figure 3.2: The Maximum Recoverable Strain,  $\epsilon_L$ , vs. Temperature

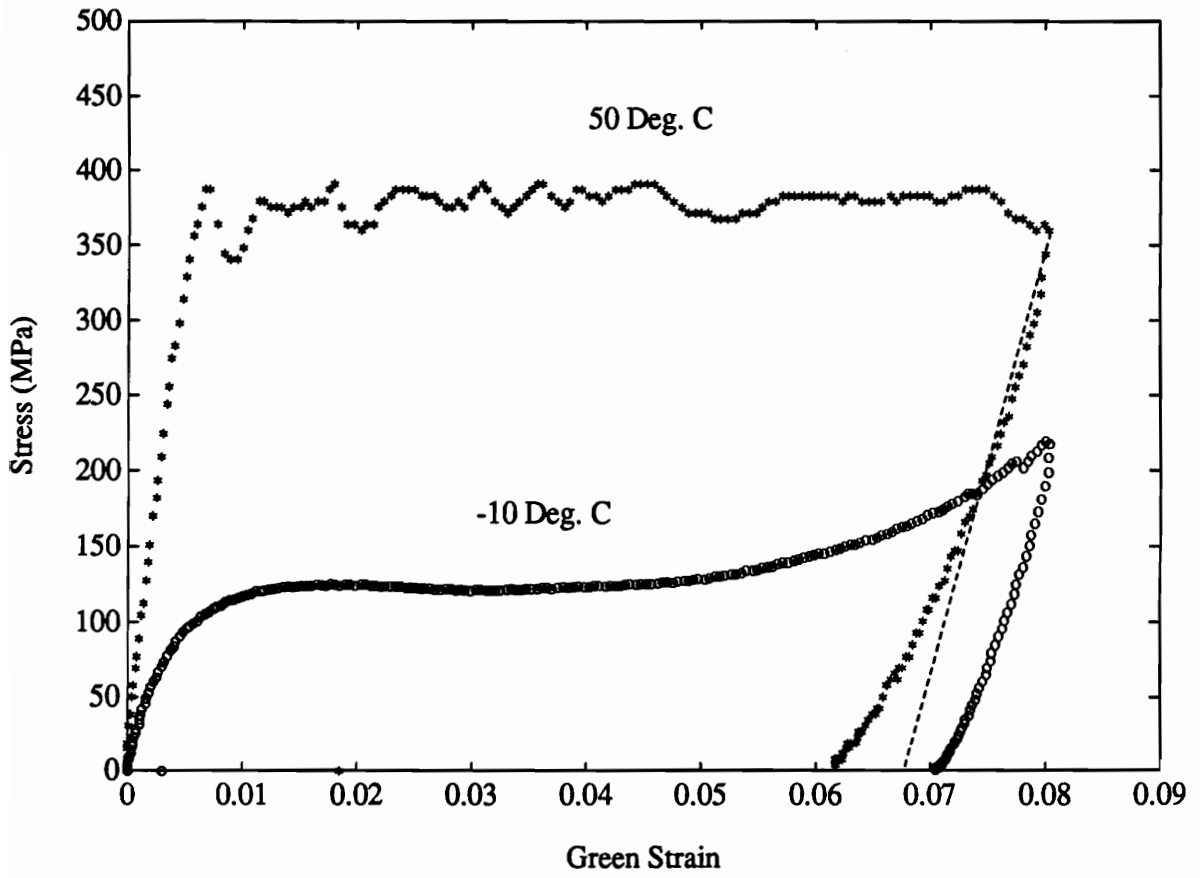


Figure 3.3: Stress-Strain Curves at 50 °C and -10 °C

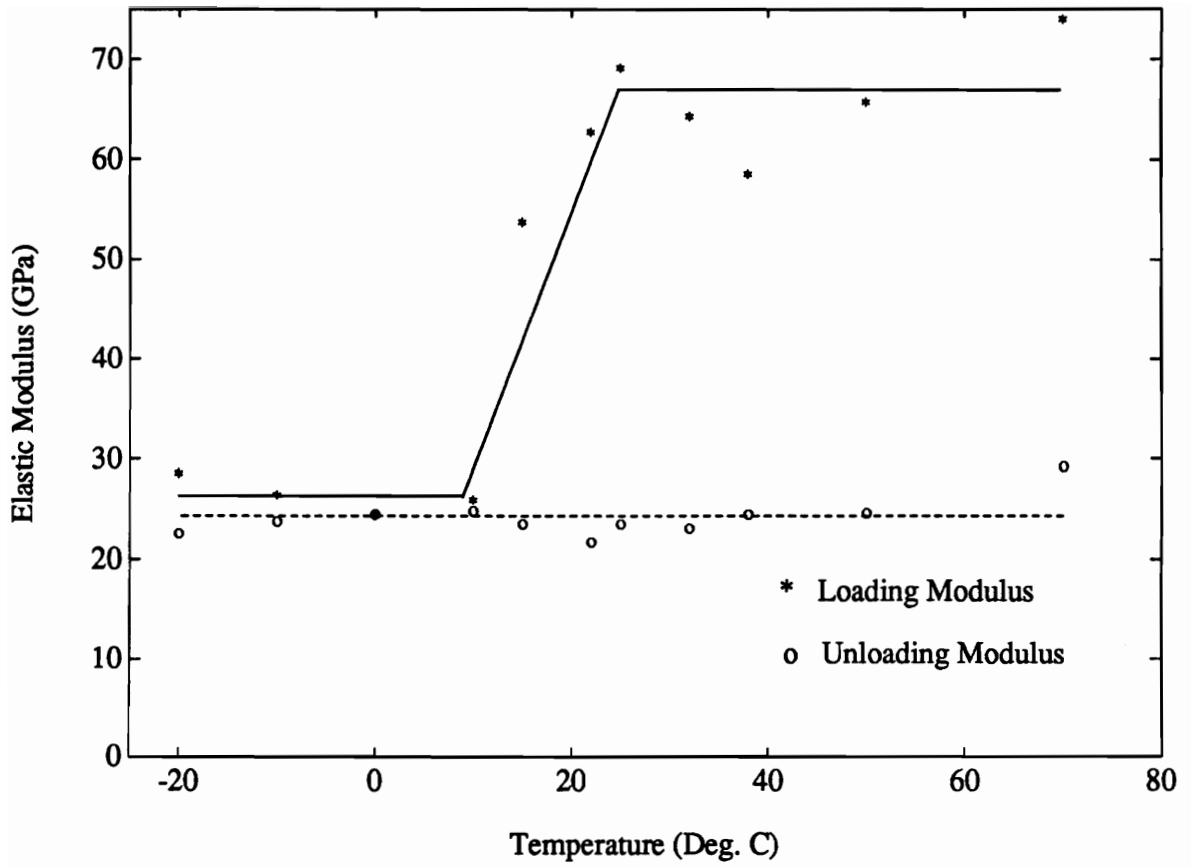


Figure 3.4: Loading and Unloading Young's Modulus vs. Temperature

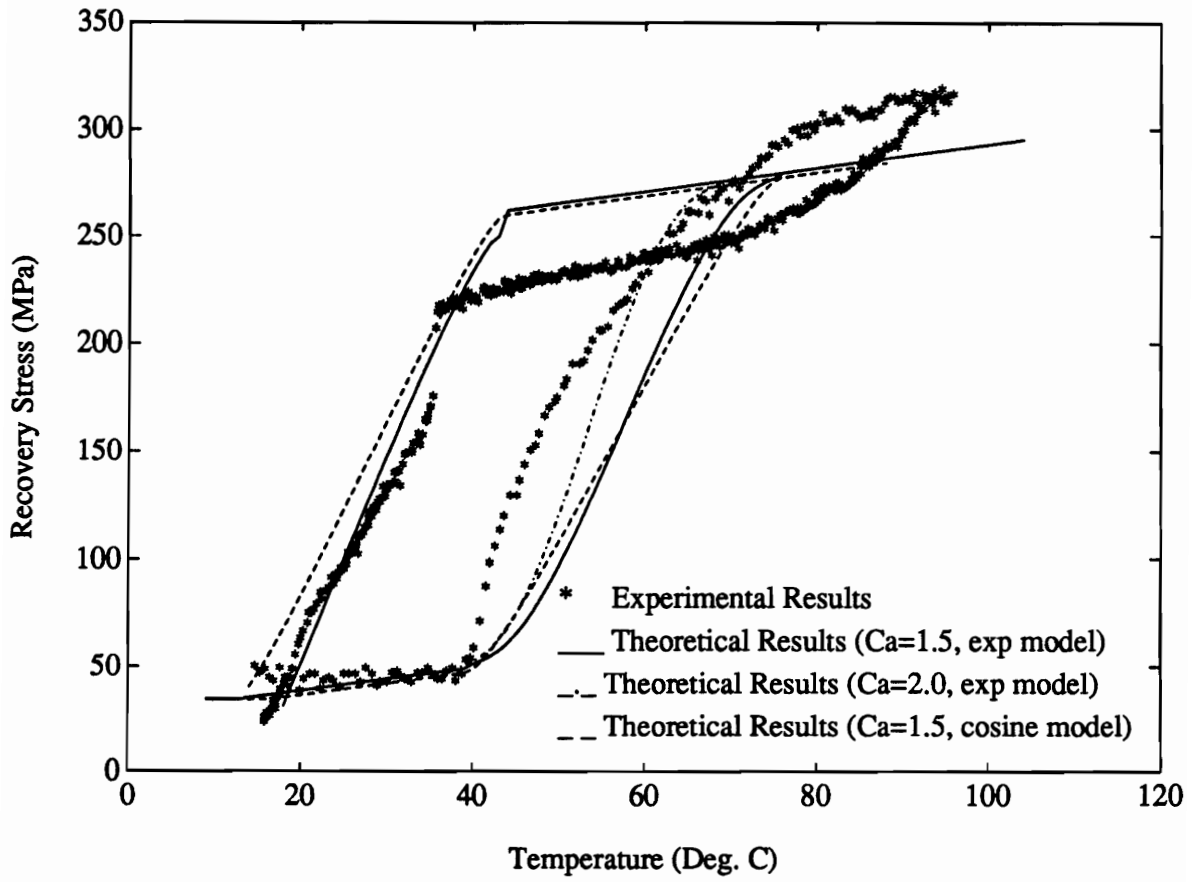


Figure 3.5: Recovery Stress vs. Temperature for One Percent Initial Strain

The Young's modulus is a function of temperature, as illustrated in Fig. 3.4. An SMA sample was first electrically heated to a high temperature in order to create 100 percent austenite. The tensile test after the electrical heating is a cooling processes (the maximum test temperature for elongation tests is 70°C, far less than the temperature reached during the electrical heating). The sharp change of Young's modulus in Fig. 3.4 occurs between about 10 °C ( $M_f = 9^\circ\text{C}$ ) and 22 °C ( $M_s = 18.4^\circ\text{C}$ ). The change of Young's modulus is synchronous with the phase transformation. This supports the assumption that the Young's modulus of SMA is a linear formulation of the martensite fraction. The average Young's modulus of low temperature martensite,  $D_M$ , is 26.3 GPa (3,810,000 Psi), and the average modulus of high temperature austenite,  $D_A$ , is 67.0 GPa (9,710,000 Psi). The ratio of  $D_A$  to  $D_M$  is about 2.6. Other experiments (Cross et al., 1970) have shown ratios of austenite to martensite Young's modulus for nitinol alloys in the range of about three to four. The difference of various Young's modulus ratio described on the literature (cross et al., 1970) and the experimental results shown in Fig. 3.4 may be due to the selection of different experimental points.

The Young's modulus of martensite is less than that of austenite due to different crystal structures. The stress-induced martensite has the same crystal structures as thermally induced martensite; therefore, they should have the same Young's modulus. The Young's modulus of stress-induced martensite may be measured from an unloading stress-strain relation. In order to have complete stress-induced martensite, the unloading must start from the yield strength,  $\sigma_y$ . The Young's modulus describing the unloading process (before  $\sigma_y$ ) corresponds to a mixed martensite and austenite

and is assumed to follow Eq. (2.89). The Young's modulus of stress-induced martensite is denoted by  $D_u$  and is shown in Fig. 3.4. The average value of  $D_u$  is 24.3 GPa (3,520,000 Psi) close to  $D_M$  (26.3 GPa).  $D_u$  is independent of temperature even during the pseudoelastic unloading (measured from the initial linear elastic unloading).

The thermoelastic tensor,  $\Theta$ , governs the pre-transformation and post-transformation recovery stress-temperature relations. The value of this material property varies in different phases. Nevertheless, since this value is much smaller (approximately four orders of magnitude) than other material constants such as  $D$  and  $\Omega$ , and therefore is assumed to be a constant. This value of  $\theta$  is determined as 0.55 MPa/°C (80 Psi/ °C) from the experimental result of restraint recovery, as shown in Fig. 3.5. The slope of the first linear section of the heating process is the thermoelastic tensor according to Eq. (2.70), as demonstrated in Fig. 2.5.

Table 3.1 lists the basic material properties of the shape memory alloy. The transformation tensor,  $\Omega$ , is determined from Eq. (2.90) as 1.76 GPa.

## 3.2 Numerical Studies

This constitutive model developed and presented in Chapter 2 is now used to predict and describe the mechanical behavior of shape memory alloys. Based on the material constant given in Table 3.1, the stress-strain curve, free recovery relation, and recovery stress relations are calculated and compared with experimental results. The 'exp model' is used unless otherwise specified.

### 3.2.1 Stress-Strain Relations

The stress-strain relations at three temperatures, 25 °C, 32 °C, and 50 °C are calculated. The theoretical and experimental results are compared in Fig. 3.6. The theoretical prediction does in fact provide a good approximation to the experimental results. The changing Young's modulus has been considered in the theoretical calculations. If Young's modulus is assumed to be constant, the result will have a relatively large error at the beginning and end of phase transformation, but a small difference during the phase transformation. As an example, the stress-strain relation at 32 °C is calculated based upon the constant material property assumption and is shown as the dash line in Fig. 3.6.

The experimental stress-strain curves are not as smooth as those obtained from theoretical analysis. The stress-strain curves at higher temperatures include both martensitic transformation and re-orientation of martensitic plates. Re-orientation of martensitic plate is a smooth process, while the martensitic transformation has a so-called snapping effect. The strain energy is stored and released at an energy threshold to induce the martensitic transformation resulting in a fluctuation of the stress-strain curves at higher temperatures. If the test temperature is below  $M_f$ , a SMA sample is composed of only one phase (martensite already), mechanical deformation results in the re-orientation of the existing martensitic plates, no phase transformation is involved. Therefore, the stress-strain relation curves will be smooth as shown in Fig. 3.3 (the stress-strain curve at -10 °C). The snapping effect is not considered in this constitutive model nor any other models in the current literature, therefore, the theoretical results cannot describe this physical phenomenon.

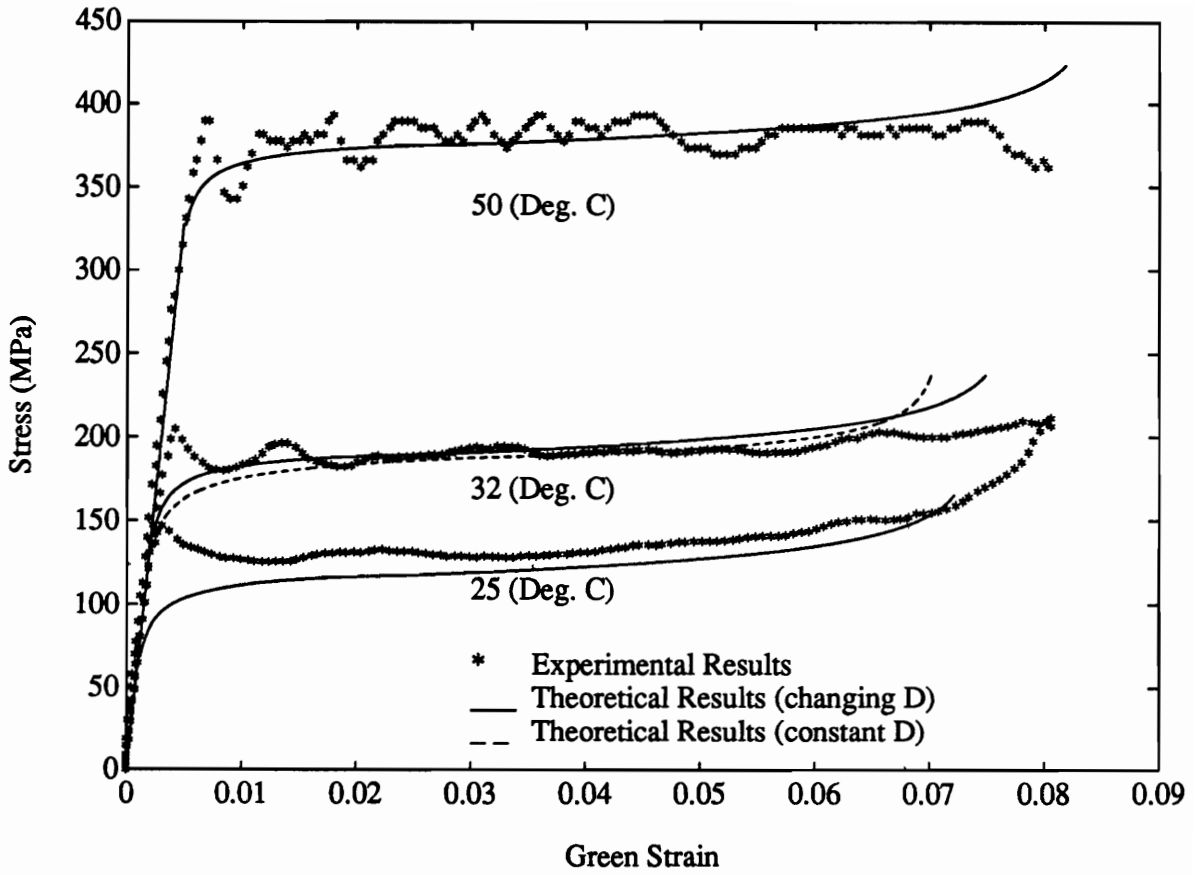


Figure 3.6: Comparison of Theoretical Prediction and Experimental Results of Stress-Strain Relations



### 3.2.2 Free Recovery Relation

Figure 3.7 shows the comparison of experimental free recovery and theoretical predictions. Different transformation coefficients,  $n$ , are used to predict the free recovery behavior. The dash line is obtained using a transformation coefficient,  $n$ , of 1.00; the solid line corresponds to  $n = 0.85$ . More trials have been done and it is found that  $n = 0.85$  provides the best theoretical prediction. Therefore, the transformation coefficient  $n$  is determined as 0.85. It is important to note that the constant material property assumption has been used. If the Young's modulus is considered as a linear function of martensite fraction, the predicted results show the same trend as the experimental results but with large error. The reason is not yet clear. It may be due to the assumption that the phase transformation tensor is a constant. The phase transformation tensor may have a similar relation to Eq. (2.89). Since this property cannot be measured directly from an experiment, it is very difficult at this moment to specify the reason. The dotted line is obtained using the cosine model.

### 3.2.3 Recovery Stress and Temperature Relations

Figure 3.5 shows both the experimental results and theoretical predictions of the recovery stress and temperature relations for an initial strain of one percent. The constitutive model developed in this dissertation reflects the fundamental characteristics, but it does not consider the secondary factors such as R-phase transformation, snapping effect, etc. The theoretical prediction provides a very good qualitative assessment to the experimental results and a satisfactory quantitative description. One of the important reasons for the discrepancy in the theory and experiment is the wires used in this recovery stress test. Virgin wires that do not have stable material prop-

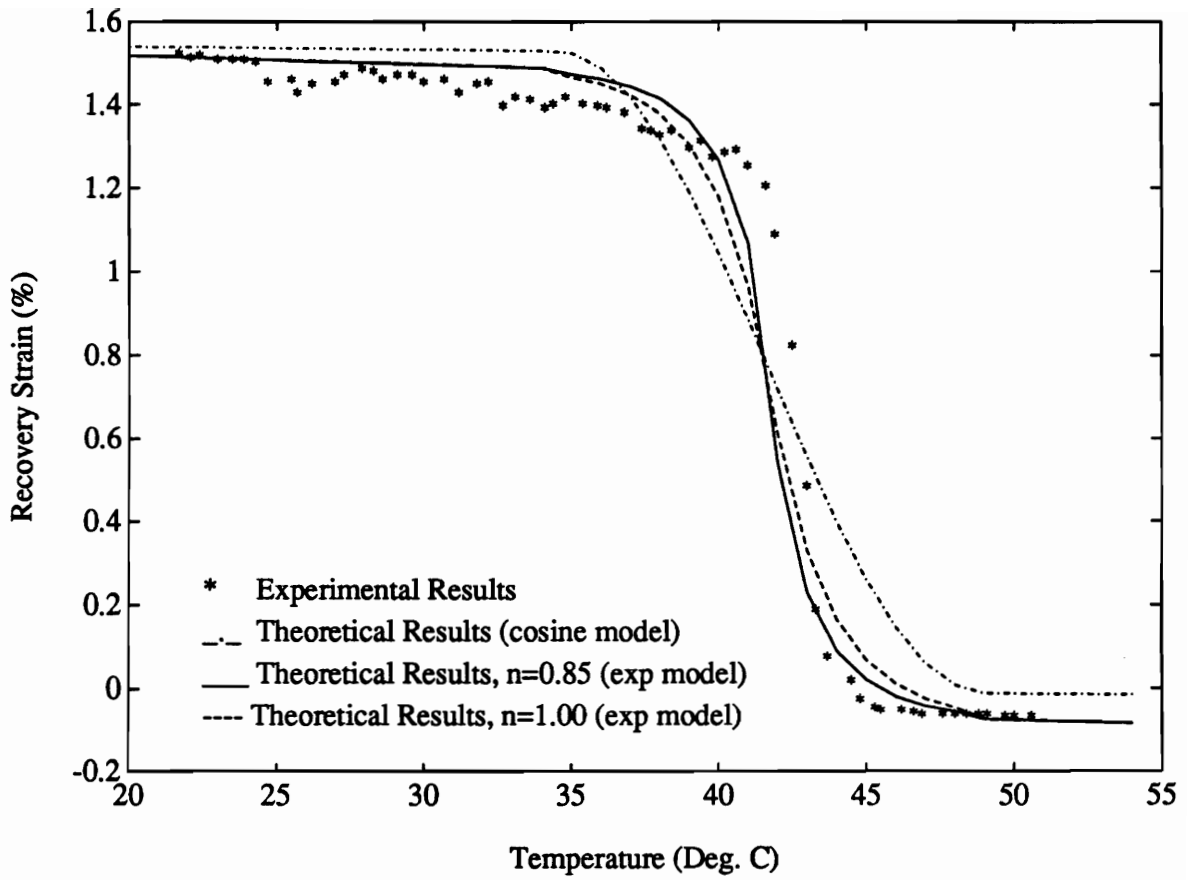


Figure 3.7: Comparison of Experimental Free Recovery Results with Theoretical Predictions

erties were used. The material properties may be stabilized by some heat treatment or pre-cycling. The reverse transformation stress influence coefficient,  $C_A$ , is assumed to be the same as  $C_M$ , and the slope of  $A_f$ -stress relation is also assumed to equal to  $C_A$ . The slope of  $A_f$ -stress is usually higher than  $C_M$ , which is believed to be another reason for the discrepancy between the theoretical prediction and experimental results. A higher  $C_A$  of 13.8 MPa/°C (2.0 Ksi/°C) is used to predict the recovery stress behavior, which provides better results as shown in the Fig. 3.5. Further efforts are still needed to get more accurate results for recovery stress-temperature relations.

### **3.2.4 Comparison of the Exp Model and the Cosine Model**

The relation of martensite fraction and other state variables derived from transformation kinetics is correct for steel or other materials having a wide transformation range. Since some variables are difficult to measure, empirical equations are used such as those relations used by Tanaka (1986). The exp model described in this dissertation is also an empirical relation. It describes the transformation kinetics more accurately because of the newly introduced transformation coefficient,  $n$ , and the piecewise description of the transformation relation.

The empirical cosine model is based on observation of experimental results such as free recovery. Its expression is much simpler than the exp model. It does not require the transformation coefficient,  $n$ , but is also less accurate than the exp model. However, it can still provide acceptable results, as demonstrated in Figs. 3.5 and 3.7. The exp model provides superior results at the beginning and the end of the phase transformation compared with the cosine model. There is not much difference

between these two models in the middle section of the phase transformation.

The exp model is accurate compared with the cosine model, but it requires more material properties, and its expressions are complex. The cosine model is less accurate at the beginning and the end of phase transformation but can still provide acceptable results; its expressions are simple and easy to use. The selection of these two models depends on the nature of a problem and the accuracy required.

### 3.3 Concluding Remarks

This section has presented some experimental results and comparisons between the theoretical prediction and experimental results. Some conclusions can be drawn from the above discussions.

- This thermomechanical constitutive model can provide quantitative predictions to the thermomechanical behavior of shape memory alloys. It describes successfully the basic features of shape memory alloys, including stress-strain-temperature relations, free recovery behavior, and recovery stress characteristics.
- Both the exp and cosine models can provide acceptable predictions. The exp model is more accurate but more complicated and requires new material properties. The cosine model is less accurate but simple and easy to use.
- The consideration of a changing Young's modulus may provide better prediction for stress-strain relations and recovery stress-temperature than that of a constant Young's modulus assumption.

- Further investigation is need in the following aspects: (1) pseudoelastic effect; (2) the influence of changing  $\epsilon_L$ ; (3) the influence of temperature on the phase transformation tensor,  $\Omega$ ; and (4) establishment of criteria of material property measurement.

## Chapter 4

# General Design of Shape Memory Alloy Actuators

This chapter describes the design of shape memory alloy force and displacement actuators based upon the thermomechanical constitutive relations developed in Chapter 2. Numerical simulations and design case studies are presented which show the utility and advantages of this method over design methods currently being used. The types of actuator described and analyzed include bias spring actuators, differential force actuators and their hybrid systems. The design approach includes coupling between the one-dimensional thermomechanical constitutive relations and a lumped capacitance transient thermal analysis. The design approach described herein will provide a practical and convenient method in the design of shape memory alloy actuators.

### 4.1 Transient Temperature Response of SMA Actuators

Consider a bias spring SMA actuator in which the SMA wire is resistively heated and cooled by natural convection, and assume the temperature distribution along the wire is uniform. If the initial temperature is  $T_0$ . The temperature response of the

wire can be expressed as

$$T - T_0 = T_f(1 - e^{-\frac{t}{\tau}}) \quad (4.1)$$

The final stable state temperature,  $T_f$ , and thermal time constant,  $\tau$ , are given as

$$\begin{aligned} T_f &= \frac{I^2 R}{\pi d h} \\ \tau &= \frac{d \rho c}{4 h} \end{aligned} \quad (4.2)$$

where 'I' is the electric current, 'R' is the resistance of the SMA wire, 'd' is the diameter of the wire,  $\rho$  is the density, 'c' is the specific heat, and 'h' the heat convection coefficient. It is assumed in this case that all material properties are constant.

After the wire has been heated for a period of time,  $\Delta t$ , cooling begins. The transient response for the cooling process can be derived as

$$T - T_0 = (T_i - T_0)e^{-\frac{t}{\tau}} \quad (4.3)$$

where  $T_i$  is the temperature at the beginning of cooling.

## 4.2 Bias Spring SMA Actuators

The stress-strain-temperature relations for a one-dimensional SMA actuator is governed by Eq. (2.48) and may be rewritten as Eq. (2.50) when only considering a quasi-static process. The general rate form of the stress-strain relation for the bias

spring of the actuator yields

$$\dot{\sigma} = -\frac{kL}{s}\dot{\epsilon} \quad (4.4)$$

where ‘k’, ‘L’, and ‘s’ are the spring constant, length and cross-section of the SMA actuator wire, respectively.

To completely model an SMA actuator, the working load represented by ‘W’ must be included. There are several ways to incorporate the influence of the working load such as modifying the bias spring constant or using a ‘dead weight’. It is relatively easy to modify the bias spring constant to account for the additional load, but in most cases, the external load is not linear. It is more appropriate in most cases to model the working load as a ‘dead weight’ as shown in Fig. 4.1. For a dynamic problem, the inertia of the “dead weight” should also be considered, however, for our purposes a quasi-static analysis will be assumed. This reduces the complexity of the problem and the resulting solution technique. Using the quasi-static assumption reduces the problem to a first order differential equation and modifying the initial conditions will be able to incorporate the influence of the working load. Substituting Eq. (4.4) into Eq. (2.48) results in

$$\left(1 + \frac{sD}{kL}\right)\dot{\sigma} = \Theta\dot{T} + \Omega\dot{\xi} \quad (4.5)$$

where

$$\dot{\xi} = \frac{\partial \xi}{\partial \sigma}\dot{\sigma} + \frac{\partial \xi}{\partial T}\dot{T} \quad (4.6)$$



From Eqs. (4.5), the stress rate is solved as

$$\dot{\bar{\sigma}} = \frac{\Theta + \Omega \frac{\partial \xi}{\partial T}}{1 + \frac{sD}{kL} - \Omega \frac{\partial \xi}{\partial \bar{\sigma}}} \dot{T} \quad (4.7)$$

The stress-temperature relation for the above equation which involves the time variable can be arranged to yield the stress-temperature relation as

$$\frac{d\bar{\sigma}}{dT} = \frac{\Theta + \Omega \frac{\partial \xi}{\partial T}}{1 + \frac{sD}{kL} - \Omega \frac{\partial \xi}{\partial \bar{\sigma}}} \quad (4.8)$$

or

$$\left(1 + \frac{sD}{kL} - \Omega \frac{\partial \xi}{\partial \bar{\sigma}}\right) d\bar{\sigma} + \left(-\Theta - \frac{\partial \xi}{\partial T}\right) dT = 0 \quad (4.9)$$

Since  $\frac{\partial^2 \xi}{\partial \bar{\sigma} \partial T} = \frac{\partial^2 \xi}{\partial T \partial \bar{\sigma}}$ , a close form solution of Eq. (4.9) can be found if the material properties (i.e.,  $D$ ,  $\Theta$ , and  $\Omega$ ) are assumed to be constant. Numerical solutions will be necessary if the material properties are allowed to vary as a function of  $\xi$ . The closed form solution of Eq. (4.9) is given by

$$\left(1 + \frac{Ds}{kL}\right) \bar{\sigma} - \Omega \xi - \Theta T = \text{constant} \quad (4.10)$$

It can be shown that Eq. (4.10) is of the same form as the general quasi-static relations given in Eq. (2.87) and (2.88). This means that the analysis method described in Chapter 2 for quasi-static analysis can also be used for the transient response of a SMA actuator by simply replacing ‘T’ with the transient temperature response as expressed by Eqs. (4.1) and (4.3).

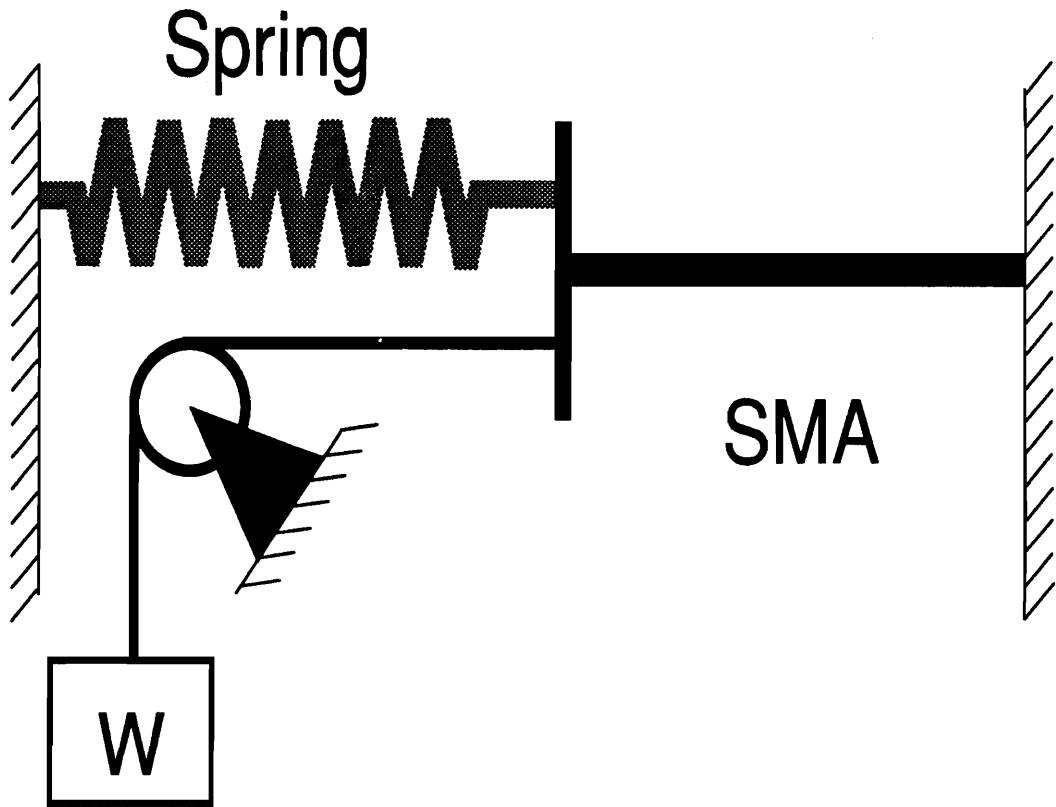


Figure 4.1: A Schematic of a Bias Spring Hybrid SMA Actuator System

The initial conditions and boundary conditions for a bias SMA actuator are modified to account for the external load ‘W’ as shown in Fig. 4.1. The initial equilibrium state of the actuator system is given by

$$\bar{\sigma}_0 s = F_s + W \quad (4.11)$$

where  $F_s$  is the spring force which can be expressed as

$$F_s = kL(\bar{\epsilon}_{res} - \bar{\epsilon}) \quad (4.12)$$

The reference position from which to measure the strain of the SMA wire is its undeformed configuration. The initial strain before activation of the SMA actuator is

$$\bar{\epsilon}_0 = \bar{\epsilon}_{res} + \Delta\bar{\epsilon}_0 \quad (4.13)$$

where  $\Delta\bar{\epsilon}_0 = \bar{\sigma}_0/D$  and  $\bar{\sigma}_0$  is given by

$$\bar{\sigma}_0 = \frac{DW}{kL + Ds} \quad (4.14)$$

The resulting stress of the bias spring is then expressed

$$\bar{\sigma} - \bar{\sigma}_0 = \frac{kL}{s}(\bar{\epsilon}_0 - \bar{\epsilon}) \quad (4.15)$$

Substituting Eq. (4.15) into Eq. (2.50) yields the general stress-temperature relation

$$\bar{\sigma} - \bar{\sigma}_0 = \Omega'(\xi - \xi_0) + \Theta'(T - T_0) \quad (4.16)$$

where

$$\begin{cases} \Theta' = \frac{\Theta}{1 + \frac{sD}{kL}} \\ \Omega' = \frac{\Omega}{1 + \frac{sD}{kL}} \end{cases} \quad (4.17)$$

If the actuator temperature is lower than the initial state temperature,  $T_M$ , of the shape memory alloy, then the stress of the SMA wire is  $\bar{\sigma}_0$ . When the temperature is higher than  $T_M$ , the stress-temperature relations are given by the following expressions.

$$\bar{\sigma} = \begin{cases} \Theta'(T - T_M) + \bar{\sigma}_0 & T_M \leq T \leq A_s^\sigma \\ \Theta'(T - A_s^\sigma) + \Omega'(\xi - \xi_0) + \bar{\sigma}_{A_s} & A_s^\sigma \leq T \leq A_f^\sigma \\ \Theta'(T - A_f^\sigma) + \bar{\sigma}_{A_f} & A_f^\sigma \leq T \end{cases} \quad (4.18)$$

The mechanical transition temperatures and their corresponding stresses can be found in Chapter 2. The influence of the initial stress  $\bar{\sigma}_0$  should be included. For example, the mechanical austenite start temperature and its corresponding stress are modified as

$$\begin{aligned} A_s^\sigma &= \frac{C_A A_s - \Theta' T_M + \bar{\sigma}_0}{C_A - \Theta'} \\ \bar{\sigma}_{A_s} &= \Theta'(A_s^\sigma - T_M) + \bar{\sigma}_0 \end{aligned} \quad (4.19)$$

The cooling process starts at  $(\bar{\sigma}_c, T_c, \xi_c)$  (which are the initial conditions for cooling),

the process can be described as

$$\bar{\sigma} = \begin{cases} \Theta'(T - T_c) + \bar{\sigma}_c & T_c \geq T \geq M_s^\sigma \\ \Theta'(T - M_s^\sigma) + \Omega'(\xi - \xi_c) + \bar{\sigma}_{M_s} & M_s^\sigma \geq T \geq M_f^\sigma \\ \Theta'(T - M_f^\sigma) + \bar{\sigma}_{M_f} & M_f^\sigma \geq T \end{cases} \quad (4.20)$$

where the mechanical transition temperatures and corresponding stresses can also be found exactly as described in Chapter 2.

The strain of the SMA wire,  $\bar{\epsilon}$ , can be determined from Eq. (4.15) and easily related to the travel distance 'S' of the 'dead weight' from Eq. (4.15). If the temperature-time response is known, the transient stress and travel distance as a function of time can also be determined.

In the design of a bias spring SMA actuator, the important design parameters are the properties of the SMA wire, i.e., the transition temperatures,  $D$ ,  $\Theta$ , and  $\Omega$ ; and the geometric parameters of the SMA spring (or wire) like the length and cross-section area. The spring constant is the basic design parameter for bias spring actuators. From Eqs. (4.16) and (4.17), all the undefined geometric variables are normalized as one term,  $\frac{kL}{sD}$ , which simplifies the design process. According to different working requirements such as the amount of stroke 'S', it is possible to choose the best  $\frac{kL}{sD}$  and then the individual  $k$ ,  $L$ , or  $s$  according to some other secondary design limitations such as space restrictions, etc.

The total cycle time of SMA actuators is generally governed by the cooling process as the heating process is done actively by resistive heating in many active control applications and the cooling process is typically passive. To reduce the cycle time,

it is necessary to use other method such as forced convection or conduction using thermoelectric devices. However, regardless of the active cooling method employed, the cycle time of bias spring actuators can be reduced further by incorporating an ‘active’ reformation force, i.e., SMA element, to replace the bias spring. This results in the actuator configuration known as the differential force actuator as illustrated in Fig. 4.2.

### 4.3 Differential SMA Force Actuators

A differential SMA force actuator contains two SMA springs (or wires), in which each SMA spring (or wire) functions as the others reformation or deformation source as shown in Fig. 4.2. The design parameters for this model are the geometrical variables of the SMA element ‘A’ and ‘B’ and material constants. Both elements are assumed to be made of the same SMA material here in order to simplify the analysis. All the variables with superscript (A) are related to SMA element ‘A’ and superscript (B) related to element ‘B’. The original length of ‘A’ and ‘B’ are  $L_A$  and  $L_B$ . It is also assumed that the material properties remain unchanged with temperature and martensite fraction. The initial temperature for both element ‘A’ and ‘B’ is the same as the surrounding temperature  $T_0$ . The other initial conditions for element ‘A’ are

$$\begin{cases} \xi_0^A = 0 \\ \bar{\sigma}_0^A = 0 \\ \bar{\epsilon}_0^A = 0 \end{cases} \quad (4.21)$$

while the initial conditions for element 'B' are

$$\begin{cases} \bar{\epsilon}_0^B = \bar{\epsilon}_{res} \\ \xi_0^B = \frac{\bar{\epsilon}_{res}}{s} \\ \bar{\sigma}_0^B = \frac{W}{s} \end{cases} \quad (4.22)$$

where  $\bar{\epsilon}_{res}$  is the residual martensitic strain (or the initial strain),  $\bar{\epsilon}_L$  the maximum recoverable strain, and  $W$  the load that models the working load. The governing rate form of the constitutive equations for this system are

$$\begin{cases} \dot{\bar{\sigma}}^A = D\dot{\bar{\epsilon}}^A + \Omega\dot{\xi}^A + \Theta\dot{T}^A \\ \dot{\bar{\sigma}}^B = D\dot{\bar{\epsilon}}^B + \Omega\dot{\xi}^B + \Theta\dot{T}^B \end{cases} \quad (4.23)$$

The geometric compatibility of elements 'A' and 'B' and the equilibrium condition of the system is assured by

$$\begin{cases} L_A\dot{\bar{\epsilon}}^A = -L_B\dot{\bar{\epsilon}}^B \\ s^A\bar{\sigma}^A = s^B(\bar{\sigma}^B - \bar{\sigma}_0^B) \end{cases} \quad (4.24)$$

The governing equation and compatibility equation together yields

$$[L_A(\dot{\bar{\sigma}}^A - \Omega\dot{\xi}^A - \Theta\dot{T}^A)] + [L_B(\dot{\bar{\sigma}}^B - \Omega\dot{\xi}^B - \Theta\dot{T}^B)] = 0 \quad (4.25)$$

From Eq. (4.6), the above equation can be written as

$$\begin{aligned} & L_A[(1 - \Omega\frac{\partial\xi^A}{\partial\bar{\sigma}^A})d\bar{\sigma}^A + (-\Theta - \Omega\frac{\partial\xi^A}{\partial T^A})dT^A] + \\ & L_B[(1 - \Omega\frac{\partial\xi^B}{\partial\bar{\sigma}^B})d\bar{\sigma}^B + (-\Theta - \Omega\frac{\partial\xi^B}{\partial T^B})dT^B] = 0 \end{aligned} \quad (4.26)$$

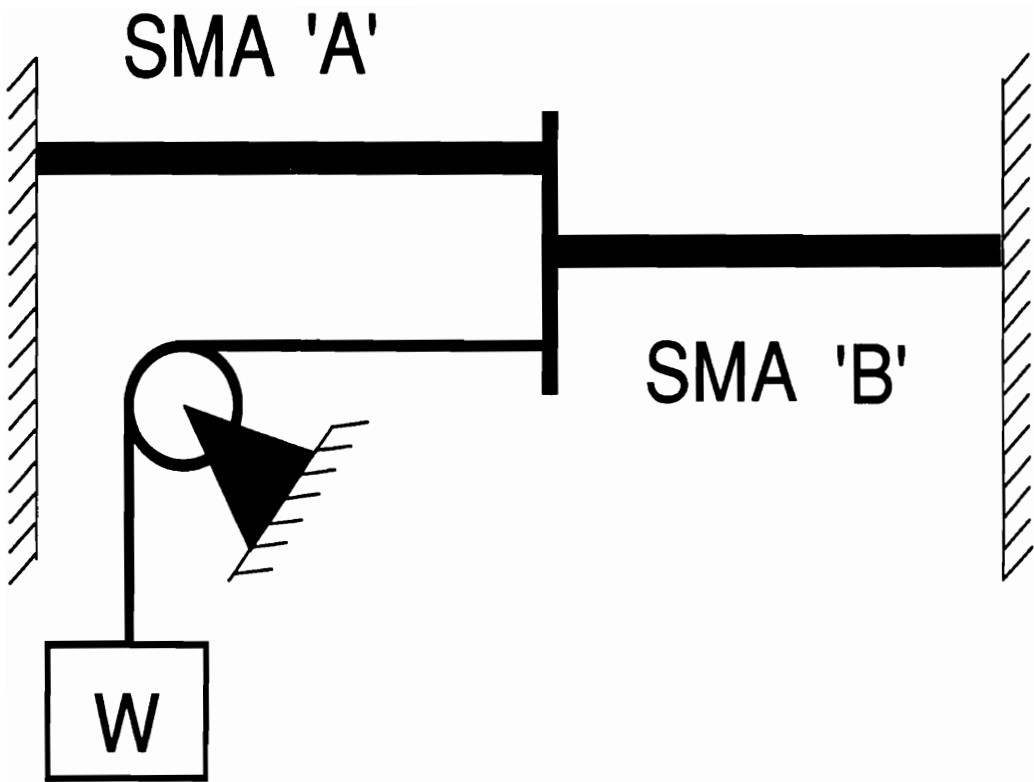


Figure 4.2: A Schematic of a Differential SMA Actuator



The coefficients of  $L_A$  and  $L_B$  are two exact differentials, which yields the closed form solution of Eq. (4.16) as

$$L_A(\bar{\sigma}^A - \Omega\xi^A - \Theta T^A) + L_B(\bar{\sigma}^B - \Omega\xi^B - \Theta T^B) = \text{constant} \quad (4.27)$$

The typical operation of a differential SMA actuator can be described as: first, element 'B' is heated while the temperature of element 'A' is constant. Element 'B' is prestrained and the deformed martensite will tend to restore to stable austenite, thus producing force against the constraining element 'A'. Element 'A' functions as a nonlinear spring with a high stiffness initially and very low stiffness later during the deformation process. If the maximum recovery force produced by 'B' cannot get 'A' over its elastic stress limit, element 'A' will simply be straining within its linear elastic strain range. Once the stress of 'A' is above its elastic stress limit, element 'A' will undergo the stress induced martensitic transformation thereby storing energy for the later recovery of element 'B'. During the reformation process of the system in which element 'A' is being heated and element 'B' is being cooled, element 'A' generates a much greater recovery force that pulls 'B' back to its initial position. The external stress on element 'B' will increase its mechanical martensitic start temperature resulting in an earlier martensitic transformation that causes a shorter cycle time for the differential SMA actuator. The actuator can be activated again by heating 'B' and starting a new cycle.

## 4.4 Numerical Simulation and Case Studies

In this section, a number of numerical simulations and case studies will be presented for SMA actuators made of a copper based shape memory alloy. Table 4.1 lists the material constants used in the simulations. The thermoelastic tensor,  $\Theta$ , is assumed to be  $0.1\text{MPa}/^\circ\text{C}$  and the maximum recoverable strain,  $\bar{\epsilon}_L$ , is calculated using Eq. (2.56) as 1% for the material data given in Table 4.1. The Cosine model is used here to simplify the numerical simulation and case studies.

### 4.4.1 Bias Spring SMA Actuator

The analysis of SMA force actuators must take into account the effect of the working load. The design relations shown in Figs. (1.13) and (1.14) cannot incorporate the effects of working load as a ‘dead weight’. However, the result can be very different if the working load is included in the analysis. This is clearly shown in Fig. 4.3 where the coupled analysis considers the working load a ‘dead weight’ and the decoupled analysis ignores the influence of the working load. These results lead to the following conclusions: first, the hysteresis of the coupled analysis is larger than that of the decoupled analysis; second, the superposition principle cannot be applied during the phase transformation range. If the material is composed of only one phase, the superposition principle may, however, be applied.

Table 4.1: Material Constants for a Copper Based SMA (after Tanaka, 1984)

MPa		° C				MPa/° C	
$D$	$\Omega$	$M_s$	$M_f$	$A_s$	$A_f$	$C_A$	$C_M$
7000	-70	-27	-34	-25	-14	1.5	1.5

The stress vs. temperature relations of a bias spring SMA actuator for different normalized spring constant,  $kL/s$ , are shown in Fig. 4.4. The normalized spring rate  $kL/s$  dominates the stress-temperature relation. The greater the value of  $kL/s$ , the higher the resulting recovery stress. The controlled recovery stress will approach the restrained recovery stress which corresponds to the infinite spring constant,  $k$ . Also, the larger the  $kL/s$ , the higher the temperature that will be required to finish the transformation due to the increase of stress.

The normalized travel distance,  $S/L$ , vs. temperature is shown in Fig. 4.5. Contrary to the conclusions drawn from Fig. 4.4, the lower the  $kL/s$  is, the longer the travel distance of the actuator, ' $S$ ', will be. It is also possible to determine the highest temperature required to complete the phase transition and provide the longest travel from Fig. 4.5. For example, if  $kL/s$  is 7000, it is only necessary to heat the wire to 5 °C. Heating beyond 5 °C would not increase the stroke of the actuator, but would increase the cooling time significantly.

The normalized spring rate,  $kL/s$ , is very important in determining the time response for a bias spring actuator. This is demonstrated in Fig. 4.6. The normalized travel distance,  $S/L$ , vs. time is very different for three normalized spring rates even though they have the same heating and cooling process. They are all heated to 12 °C in about 6.5 seconds. A lower  $kL/s$  bias spring actuator has a larger stroke but takes much more time to cool down to return back to its initial position, while a higher  $kL/s$  bias spring actuator has the opposite effect. The relatively flat region of each curve corresponds to the cooling process before the phase transition occurs. It is impossible to avoid this flat cooling stage completely but this section can be shortened. It is

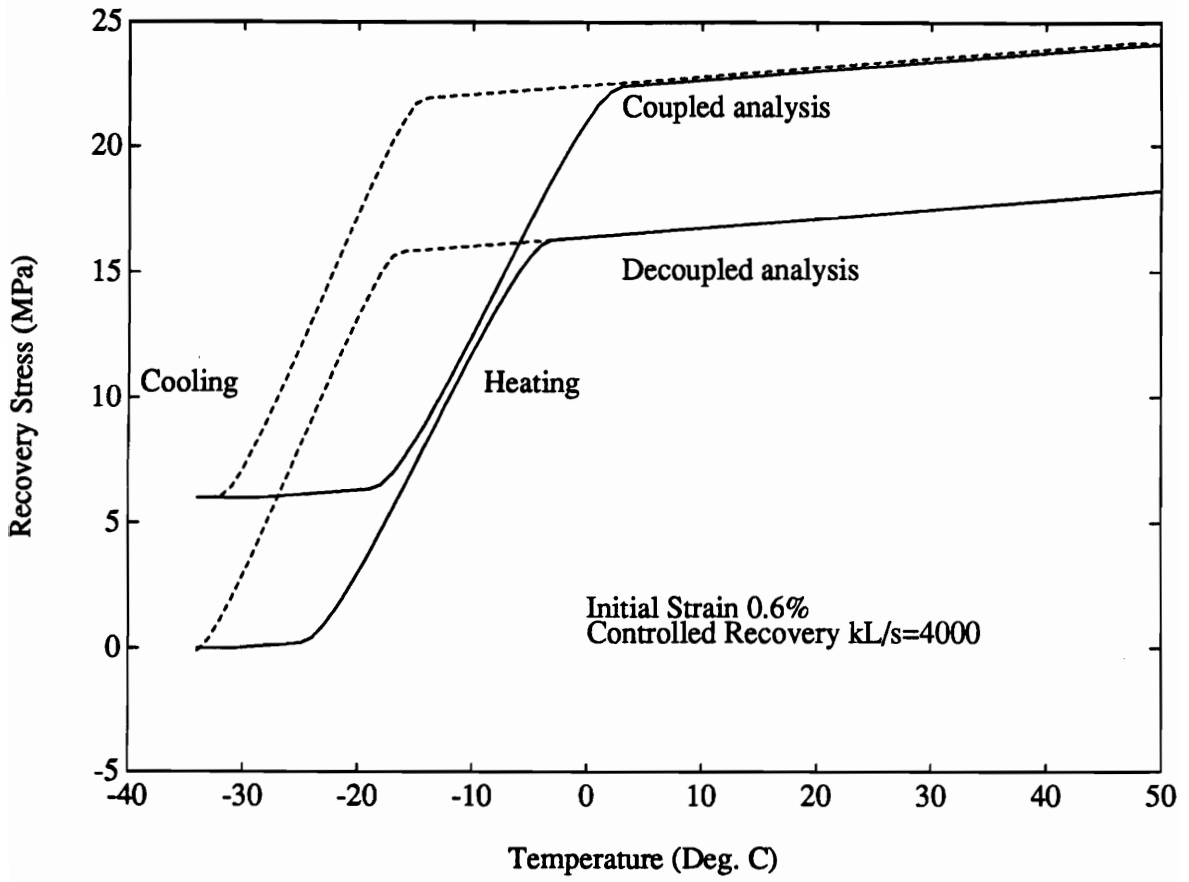


Figure 4.3: Comparison Between Coupled Analysis and Decoupled Analysis for a Bias Spring SMA Actuator

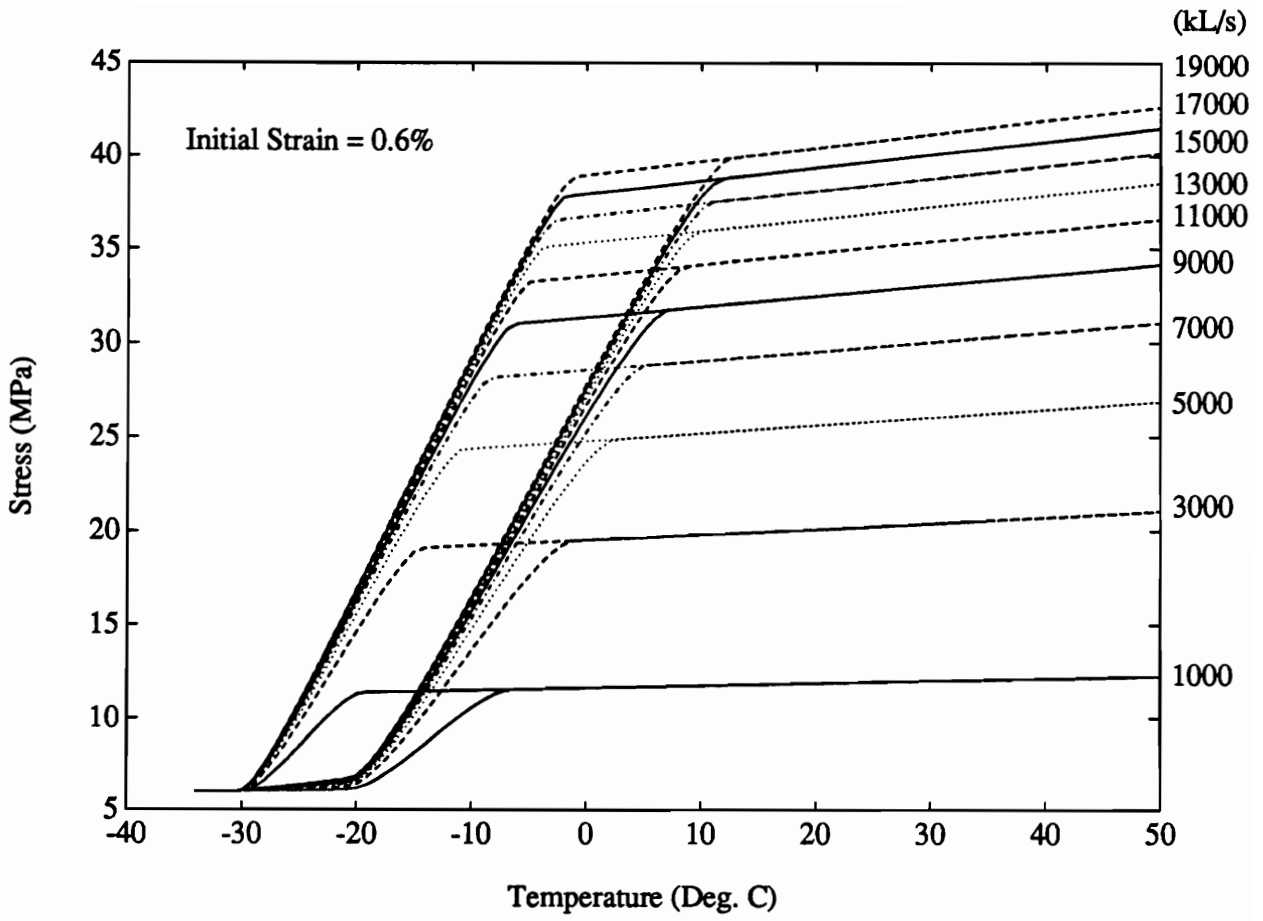


Figure 4.4: Stress vs. Temperature of a Bias Spring SMA Actuator for Different Normalized Spring Rate,  $kL/s$

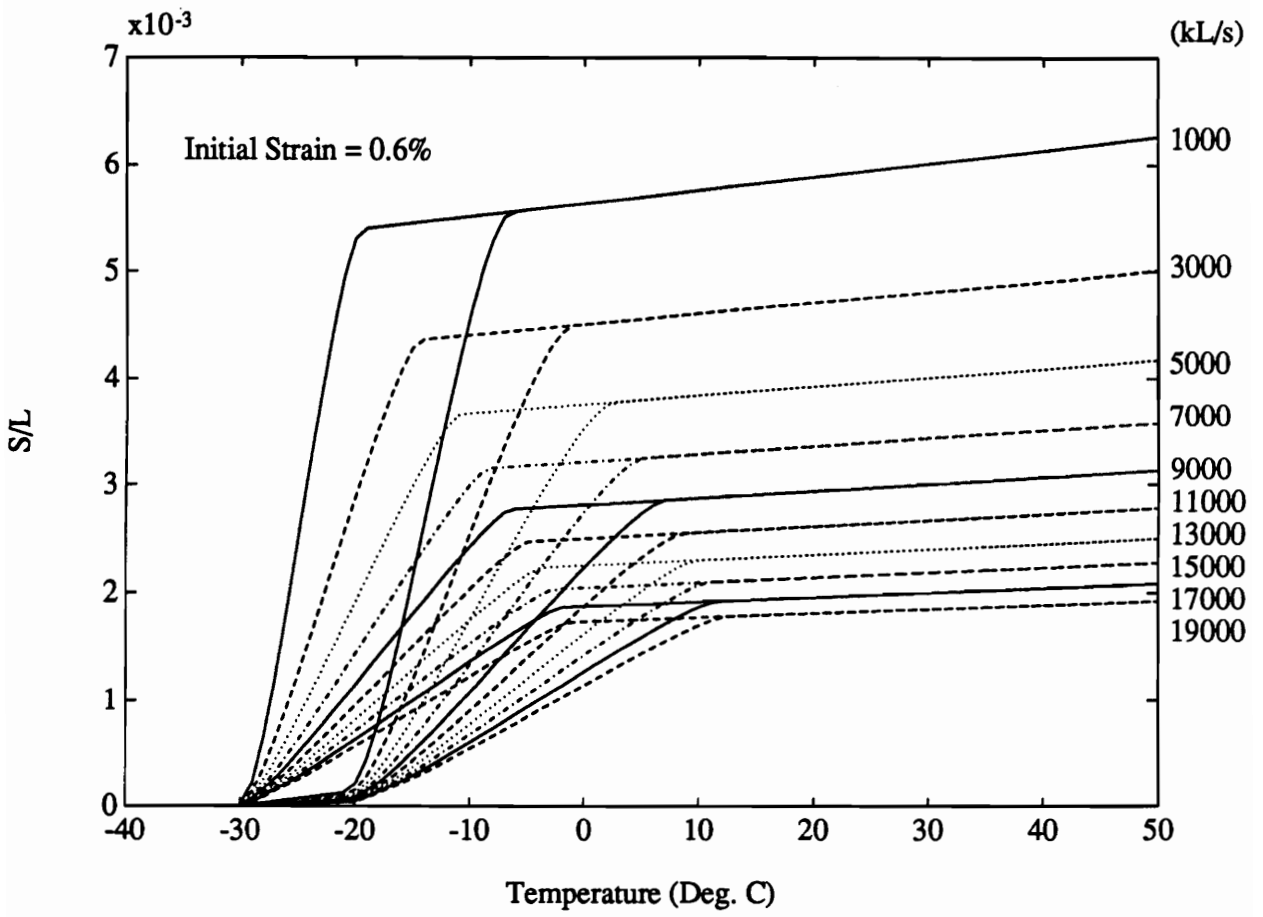


Figure 4.5: Normalized Travel Distance,  $S/L$ , vs. Temperature of a Bias Spring SMA Actuator

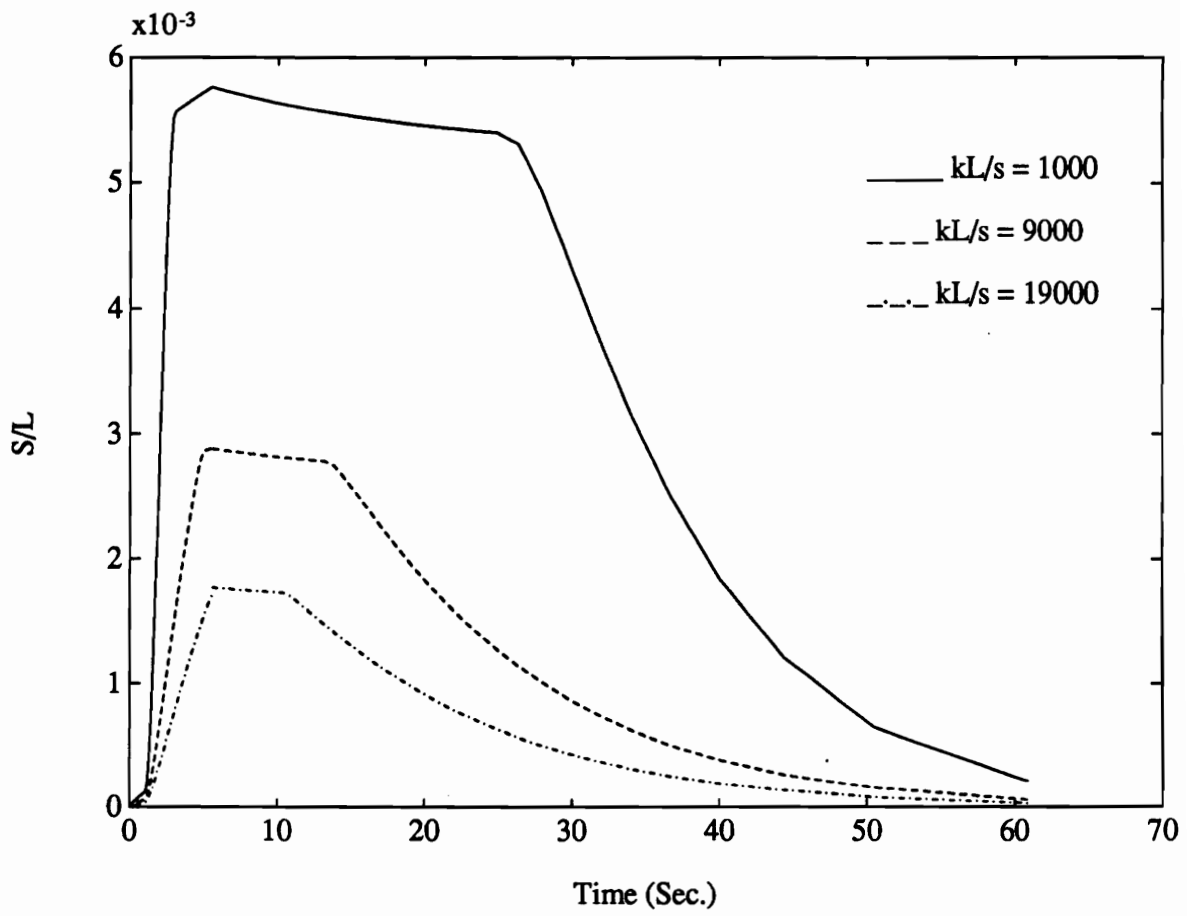


Figure 4.6: Normalized Travel Distance,  $S/L$ , vs. Time of a Bias Spring SMA Actuator



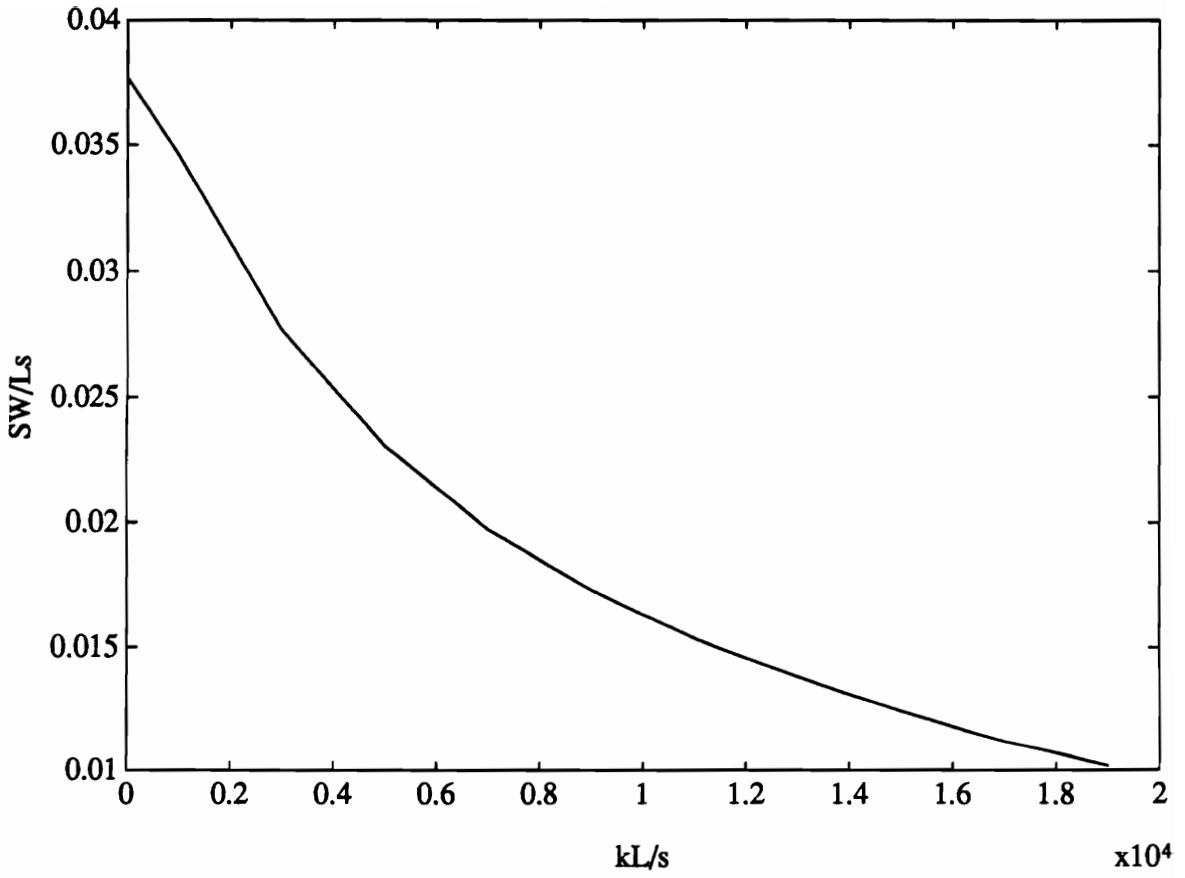


Figure 4.7: Maximum Work Output of a Bias Spring SMA Actuator

shown from Figs. 4.5 and 4.6 that for  $kL/s = 1000$ , the SMA wire only needs to heat to approximate  $-5\text{ }^\circ\text{C}$  which takes about 3.5 seconds in this case. The total cooling time will be decreased if the wire is only heated to  $-5\text{ }^\circ\text{C}$ , and the actuator can still provide about the same amount of travel distance. However, it is true that a higher  $kL/s$  can always reduce cooling time.

Another important technical requirement of a bias spring actuator is the maximum work output. The work output by the hybrid actuator system, shown in Fig. 4.1, is the work performed to raise the “dead weight”. The maximum work output is dependent on the stroke of the actuator. Therefore, the normalized spring rate is very important in determining the work output as shown in Fig. 4.7. The larger the  $kL/s$ , the less work that will be performed because higher  $kL/s$  provides less travel distance for the “dead weight”. Zero  $kL/s$  can do the most work, but this kind of device is no longer a force actuator. Infinite  $kL/s$  corresponds to the restrained recovery and obviously cannot provide any work.

#### **4.4.2 Differential SMA Actuator**

The design and analysis of a differential SMA force actuator is more complex than that of a bias spring SMA force actuators since differential actuator involves more phase transitions and more design variables. The analysis presented in this section will reveal some of the important characteristics and behavior of differential SMA force actuators. In order to simplify the analysis, both SMA elements of the actuator are assumed to have the same length and cross-section area and are made of the same SMA material. Before activation of the actuator, element ‘B’ has been

prestrained to 0.6% initial strain which corresponds to 60% of the initially deformed martensitic phase. Element 'A' has no prestrain. The working load (modeled by the 'dead weight') causes an initial stress of 6 MPa on element 'B' only. The temperature history of both SMA elements are shown in Fig. 4.8. The temperature of element 'A' is held constant as the ambient temperature for the first five seconds while element 'B' is heated. Element 'A' is then heated starting at  $t=6$  seconds, while element 'B' begins cooling. Both the heating and cooling processes follow Eqs. (4.1) and (4.2) with  $T_f = 10$  °C and  $\tau = 15s$ . There are two activation strategies. One is defined as shown in Fig. 4.8 and is referred to as 'continuous activation'. Another one has the same heating and cooling process for element 'B', but element 'A' is only heated for five seconds (from  $t=6$  seconds to  $t=10$  seconds) and then maintains that temperature. The second is referred to as 'discontinuous activation'.

Figure 4.9 illustrates the stress of element 'B' vs. time relation. Each element experiences a martensitic transformation and its reverse transformation during the entire cycle so the time response shown in Fig. 4.9 can be separated into four processes. The first sharp increase of stress corresponds to the reverse transformation of element 'B', the following slow increase of stress corresponds to the martensitic transformation of 'A', the second sharp increase of stress indicates the reverse transformation of 'A', and finally the decrease of stress indicates the martensitic phase transformation of element 'B'. The dash lines in Figs. 4.9 to 4.11 are for the discontinuous activation. The solid lines represent the continuous activation.

The normalized travel distance, ' $S/L$ ', vs. time is shown in Fig. 4.10. The continuous activation may reduce the cycle period for a single cycle. However, because this

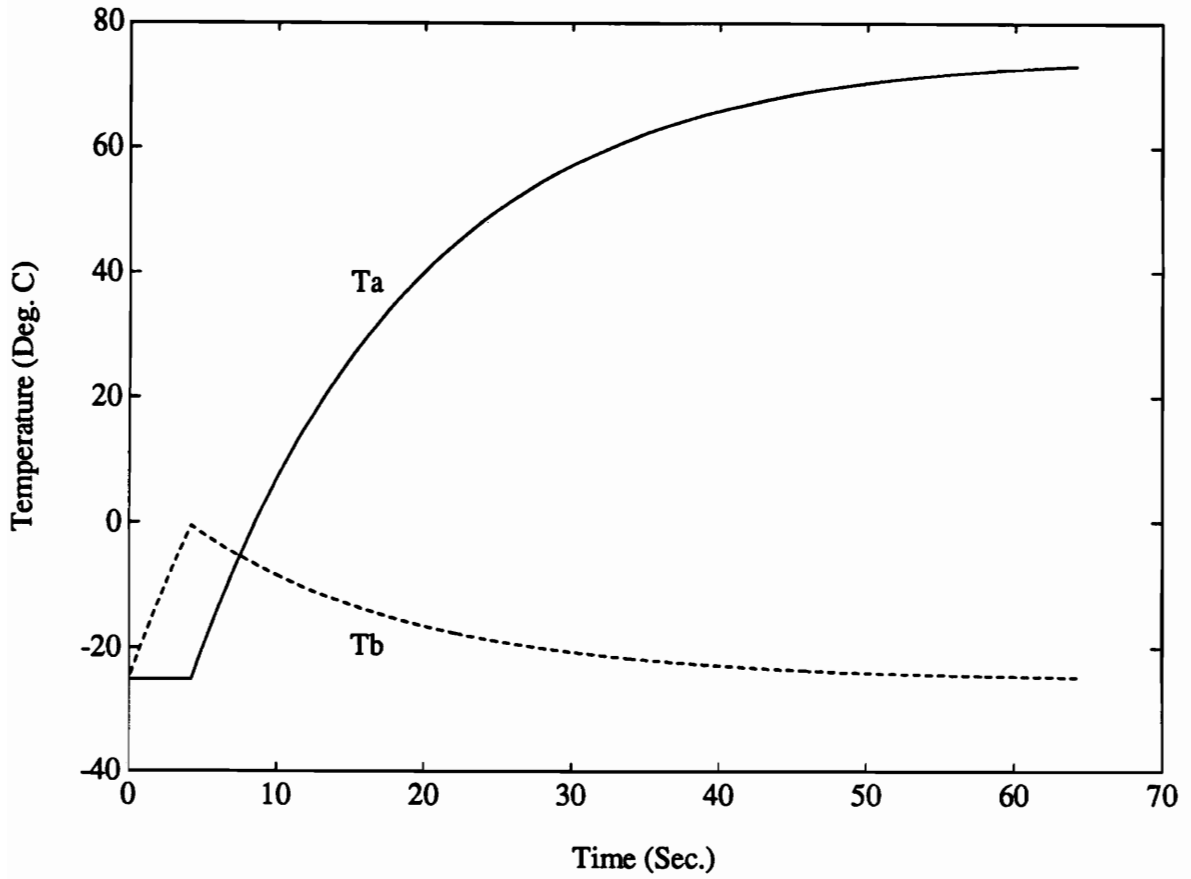


Figure 4.8: Temperature History of Element 'A' and 'B' of a Differential SMA Actuator with  $\tau = 15$  Seconds and  $T_f = 100$  °C

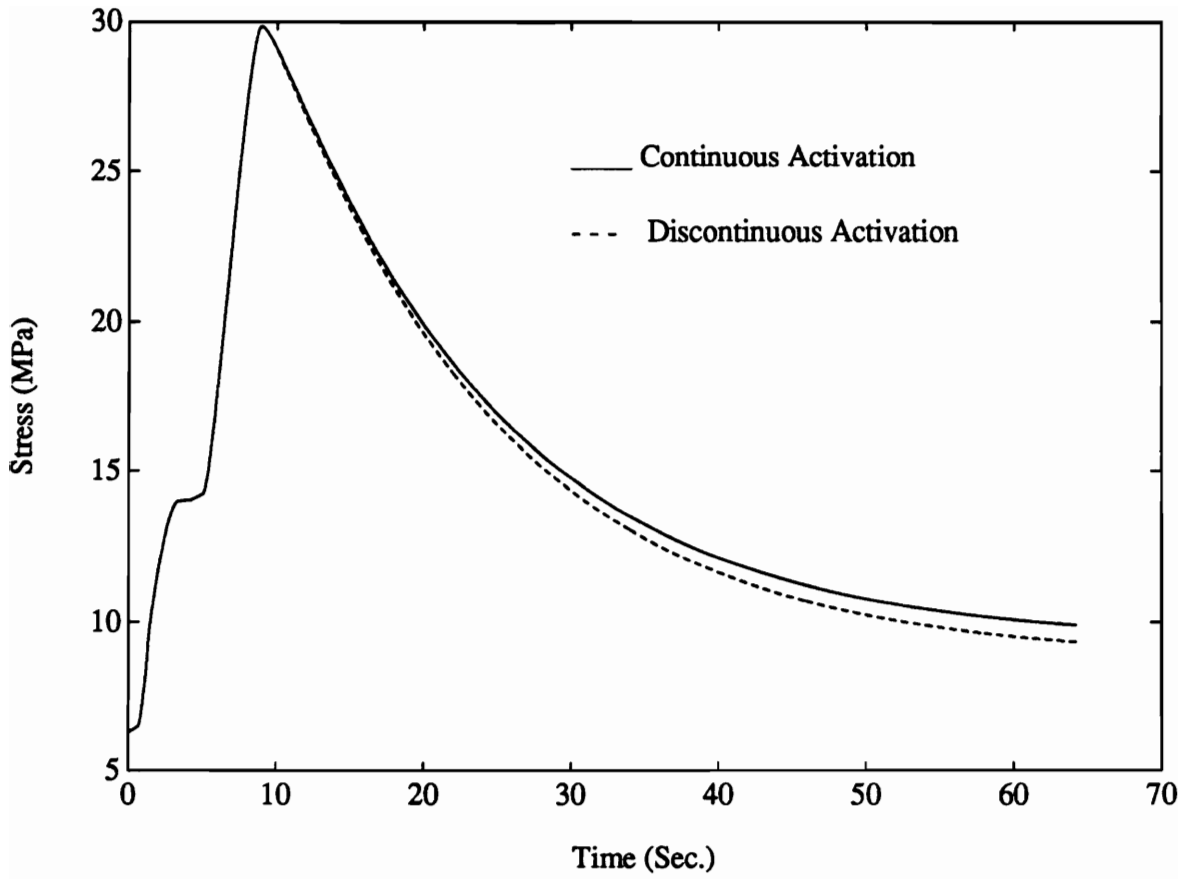


Figure 4.9: Stress of Element 'B' vs. Time of a Differential SMA Actuator

kind of activation results in a unnecessarily high temperature for element 'A', it will certainly delay the activation for the second cycle. Element 'A' must be cooled back to its initial temperature before the actuator can be re-activated or it will simply function as a linear spring under higher temperature.

Like a bias spring SMA actuator, the maximum work provided by a differential SMA actuator provides another index to be used to evaluate its performance. The maximum work performed by the differential actuator can be determined from Fig. 4.11 which shows the stress of element 'B' vs. normalized travel distance,  $S/L$ . The area of the triangle-like geometry represents the work output.

It has been shown from Eq. (4.27) that a differential SMA actuator has the advantage of separating temperature profiles (i.e. heating and cooling process) for the two SMA elements. This indicates that this type of actuator can generate a different path if different heating and cooling strategies are adopted. This is illustrated in Figs. 4.12 to 4.15. Figure 4.12 shows the 3-D plot of the stress of element 'B' vs.  $T^A$  and  $T^B$ . Figure 4.13 shows the normalized travel distance,  $S/L^A$ , vs.  $T^A$  and  $T^B$ . Figures 4.14 and 4.15 show the martensite fraction of element 'A' and 'B' vs.  $T^A$  and  $T^B$ , respectively. The four phase transitions are clearly seen from Figs. 4.14 and 4.15.

## 4.5 Concluding Remarks

This chapter presents a mathematical model of SMA force actuators based upon the constitutive relation of shape memory alloys.

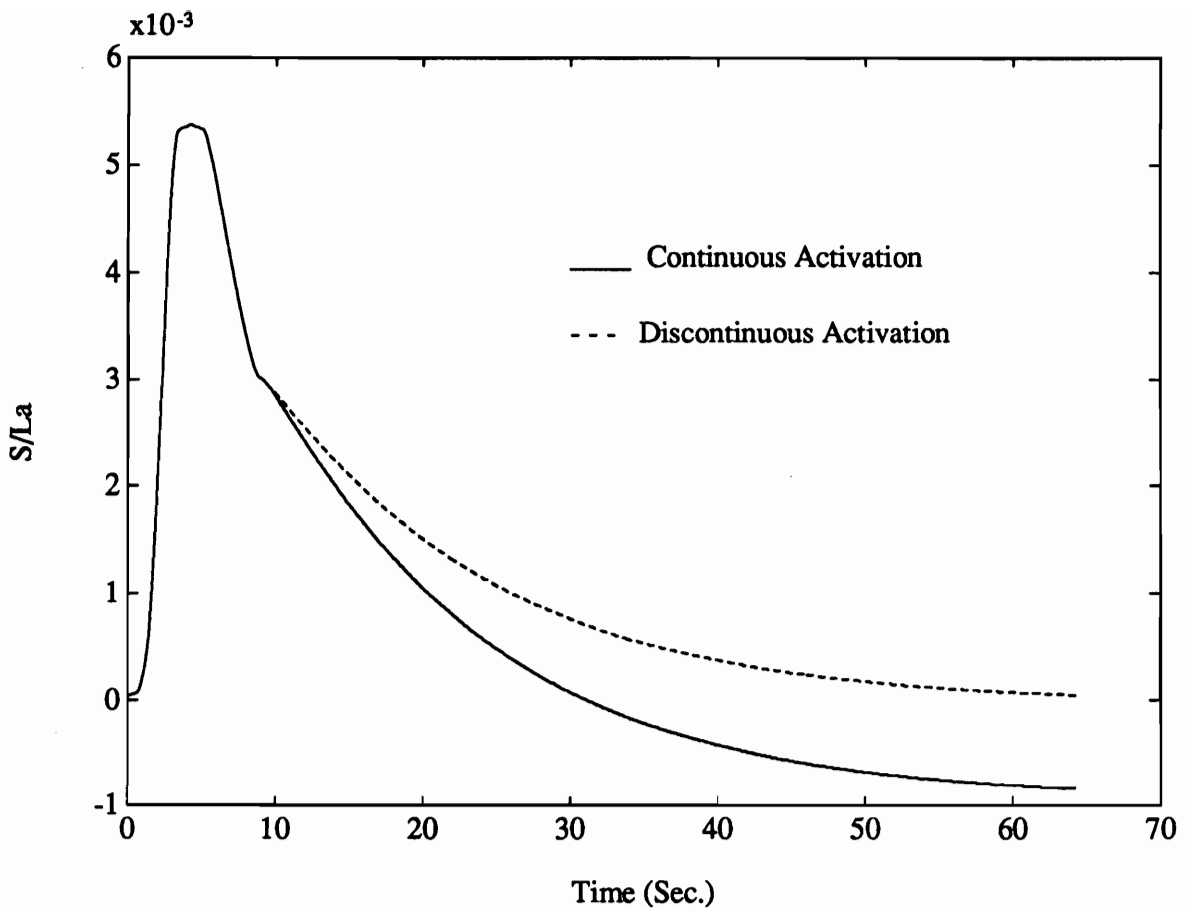


Figure 4.10: Normalized Travel Distance,  $S/L_A$ , vs. Time of a Differential SMA Actuator

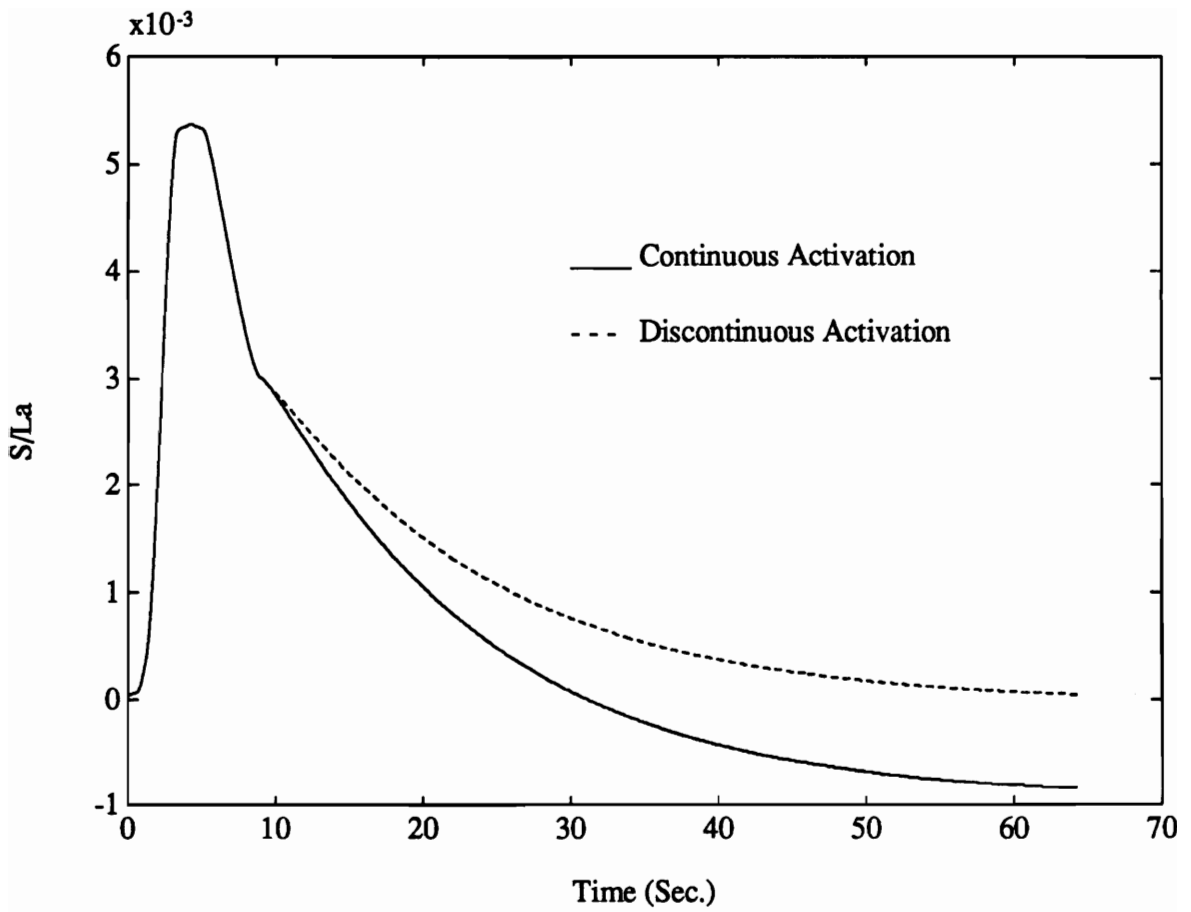


Figure 4.11: Stress of Element 'B' vs. Normalized Travel Distance of a Differential SMA Actuator



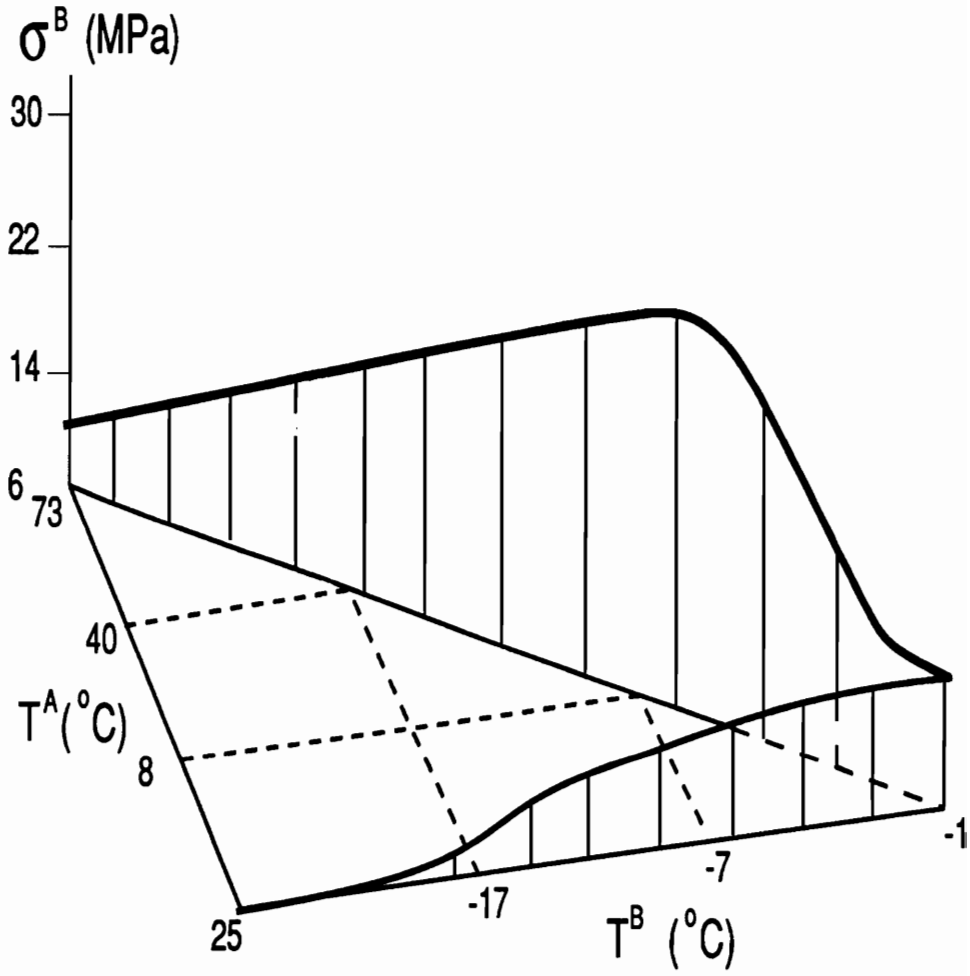


Figure 4.12: Stress of Element 'B' vs.  $T^A$  and  $T^B$

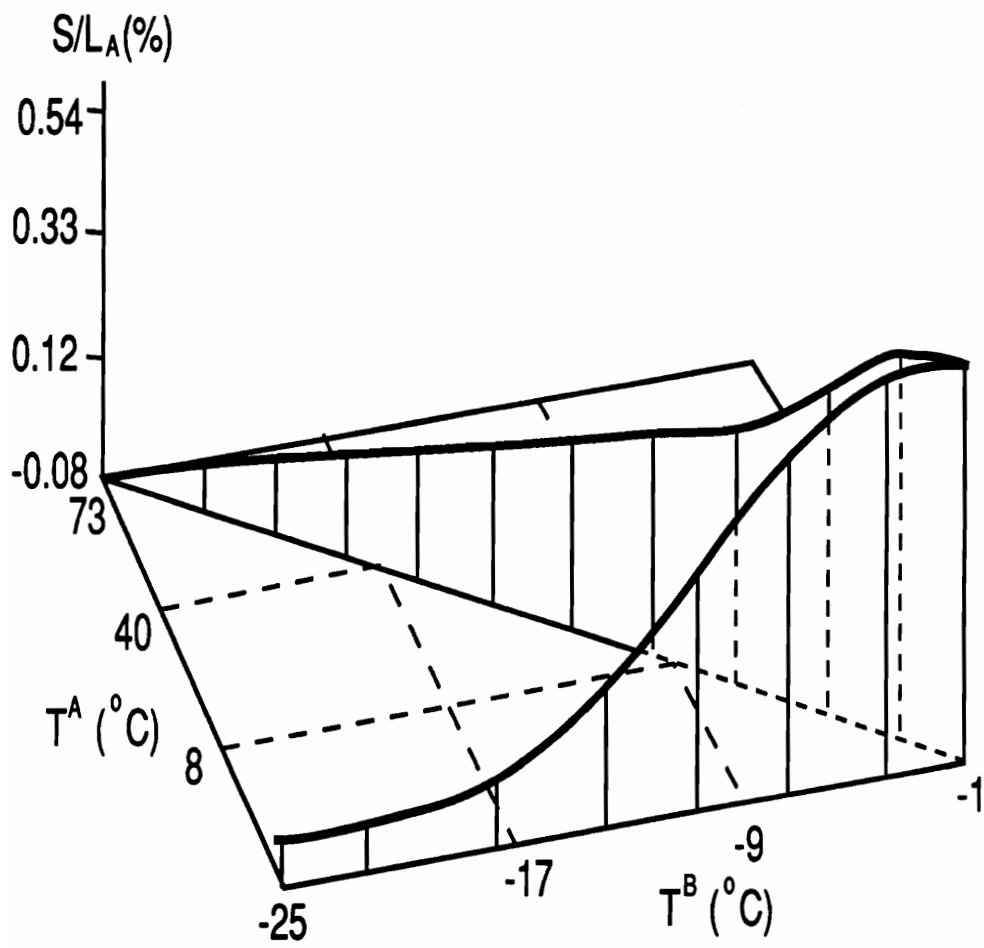


Figure 4.13: Normalized Travel Distance,  $S/L_A$ , vs.  $T^A$  and  $T^B$

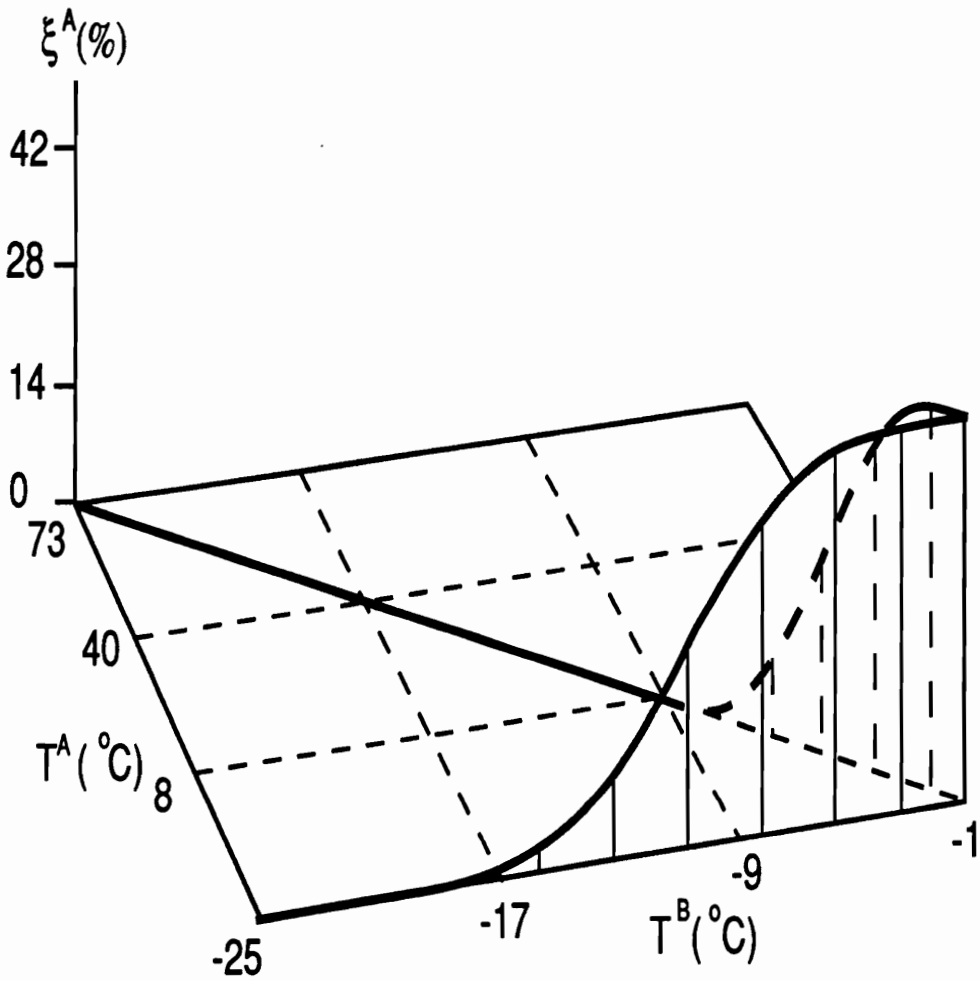


Figure 4.14: Martensite Fraction of Element 'A' vs.  $T^A$  and  $T^B$

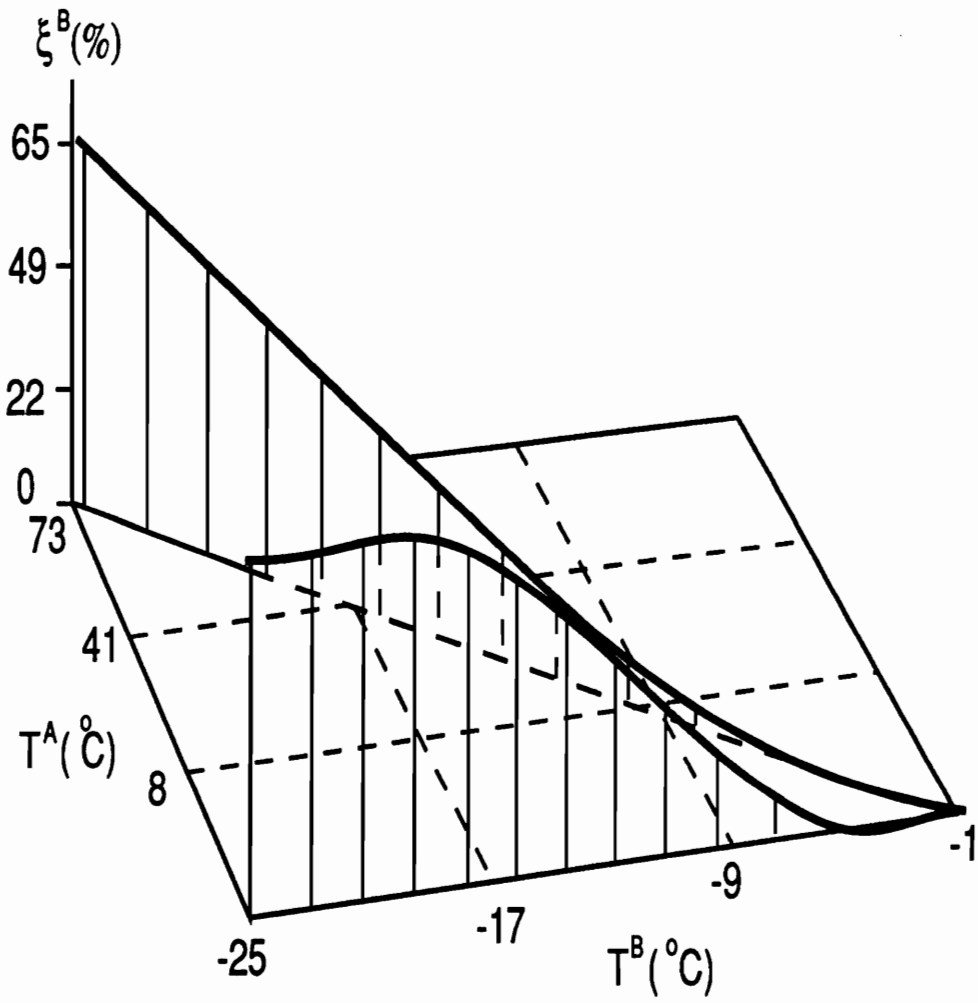


Figure 4.15: Martensite Fraction of Element 'B' vs.  $T^A$  and  $T^B$

- This model reflects the most important aspects of SMA force actuators, yielding convenient expressions to determine the basic design parameters for the two widely used SMA force actuators: bias spring SMA force actuators and differential SMA force actuators.
- The case studies of the bias spring SMA actuator provide fundamental information related to their design.
- The restriction of applying the superposition principle to SMA actuators is equally important to other applications of shape memory alloys and general stress analysis of martensitic phase transition materials.
- The numerical study of the differential SMA force actuator reveals its basic behavior and characteristics and provides further guidance to the design, heating, cooling, and operation of SMA actuator systems.

# Chapter 5

## Multi-Dimensional Constitutive Modeling of SMA

Based upon the one-dimensional thermomechanical constitutive relation developed in Chapter 2, a multi-dimensional thermomechanical constitutive model for shape memory alloys is further developed in this chapter. Unlike the constitutive model developed by Bondaryev and Wayman (1988), this multi-dimensional constitutive model begins with the newly introduced internal state variable, martensite fraction, instead of using the traditional plastic flow theory. This thermomechanical constitutive relation can reflect the most basic characteristics of shape memory alloys, i.e., the phase transformation involved in the characteristics of the shape memory effect. To begin describing the formulations it is necessary to provide some important experimental evidence that supports the model.

### 5.1 Experimental Background

Needless to say, the first concern when developing this multi-dimensional model is whether its one-dimensional version is correct. The verification and discussion in

Chapter 3 show that the one-dimensional constitutive model can provide a quantitative prediction and description of the mechanical behavior of shape memory alloys. However, more experiments besides the uniaxial tensile test are still needed to provide full array of data to substantiate and develop the full and correct multi-dimensional constitutive relations. These experiments include: (1) the influence of compressive load on SMA behavior; (2) the cyclic behavior of SMA; (3) the criterion governing the beginning of phase transformation in multi-dimensional stress state; and (4) the coupling effect of plastic deformation and the transformation deformation.

One of the important experiments in the development of a multi-dimensional constitutive relation for different materials is the hydrostatic pressure experiment. A multi-dimensional stress tensor may be decomposed into two parts, a hydrostatic stress and a deviatoric stress tensor. The hydrostatic stress affects the volume change while the deviatoric stress causes the distortion of the materials. The effect of hydrostatic pressure on the material behavior is mainly attributed to the influence of volume change of the material. The volume change of an elastic body is the summation of all principal strains, therefore, hydrostatic pressure can affect the elastic deformation. Plastic deformation, however, is characterized as zero-volume-change deformation, the Poisson's ratio of plastic strain is 0.5, which indicates a negligible influence of hydrostatic pressure on the plastic deformation. Therefore, the plastic deformation is basically of a shear nature.

Kakeshita et al. (1988) studied the effect of hydrostatic pressure on martensitic transformations in Cu-Al-Ni shape memory alloys. The purpose of their experiment was to investigate the influence of hydrostatic pressure on the phase transformation

mechanics. Previous work (Patel and Cohen, 1953; Gefen et al., 1973) shows the transformation temperatures decrease in Fe-Ni SMA while increase in Au-Cd SMA with increasing hydrostatic pressure. The difference is qualitatively explained to be due to the difference in sign of  $\Delta V = V^M - V^A$ , where  $V^M$  and  $V^A$  are the volumes of martensite and austenite respectively, being positive for Fe-Ni alloy and negative for Au-Cd alloy. Generally, the percentage volume change during martensitic transformation of SMA is around 0.002 (Hsu, 1982), which may be affected by hydrostatic pressure. Figure 5.1 shows the pressure dependence of the transformation temperatures for two type of Cu-Al-Ni alloys. The pressure is increased from zero to a relatively high 1.5 GPa (217Ksi). The transformation temperatures were obtained by measuring the electrical resistivity. The change of transformation temperature demonstrates a linear relation with pressure. The slope of the transformation temperature-pressure relation is determined to be 5 °C/GPa. The experiment also demonstrated that there is essentially no difference between the hydrostatic pressure-induced martensite and thermally induced martensite.

Two conclusions can be drawn from the above discussions. The first is that the volume change is almost negligible. The actual percentage volume change is so small (0.002) that a Poisson's ratio of 0.5 may be assumed for the transformation strain,  $\epsilon^t$ . The second is that the influence of hydrostatic pressure on phase transformation may also be neglected (5 °C/GPa). Therefore the deformation involved in the phase transformation may also be described as shear distortion. In fact, the orientated growth of martensitic plates is a result of martensitic twinning or de-twinning process (shear deformation). Therefore, it is possible to apply the approach used in plasticity to develop a multi-dimensional constitutive relation for SMA.



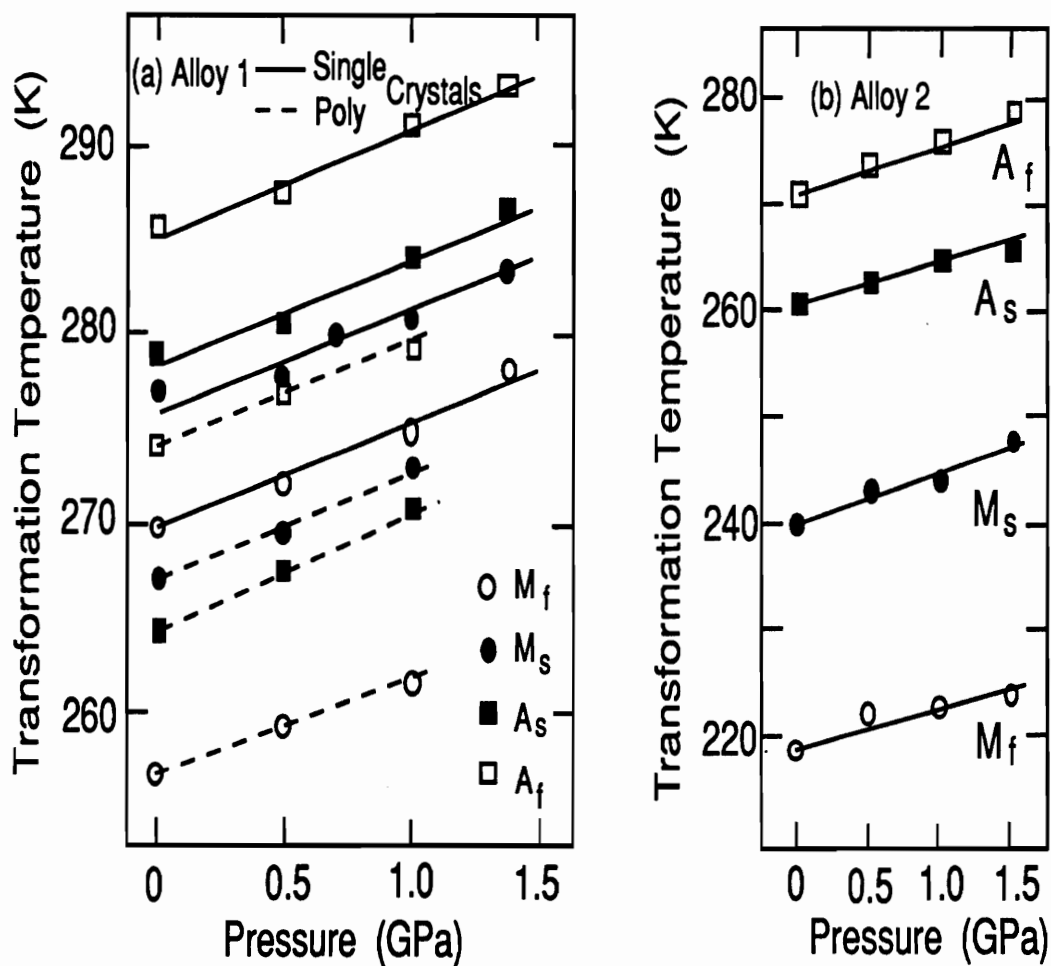


Figure 5.1: Pressure Dependence of Transformation Temperatures for Single-Crystals (solid line) and Poly-Crystals (dashed line) of two Cu-Al-Ni Shape Memory Alloys (after Kakeshita et al., 1988)

There have been very few experimental investigations which have studied the cyclic behavior and characteristics of SMA under compressive loads. Shape memory alloys have always been assumed to be homogeneous and isotropic. However, recent experiments show that the assumption that the SMA is an isotropic material can no longer be ensured, especially when subjected to a cyclic loading (Graesser, 1990).

Figure 5.2 shows the hysteretic response of a SMA rod sample subjected to a  $\pm 4.5\%$  strain cycles. The SMA sample is first elongated, and followed by a nonlinear unloading (pseudoelastic effect), leaving some residual strain. The compression starts with a nonlinear loading rather than a linear elastic loading as expected. The first smooth nonlinear compressive loading is believed to be accompanied by the reverse transformation. The reverse transformation finishes at the sharp transition point from which a linear elastic compressive loading starts. A compressive stress-induced martensitic transformation starts shortly after the elastic compressive loading. It is apparent that the stress-strain relation corresponding to the compressive loading is very different from the one of tensile loading.

The one-dimensional constitutive model presented in Chapter 2 cannot be applied to study the behavior of SMA under alternate tensile and compressive loading. The multi-dimensional constitutive model developed here has the same limitation.

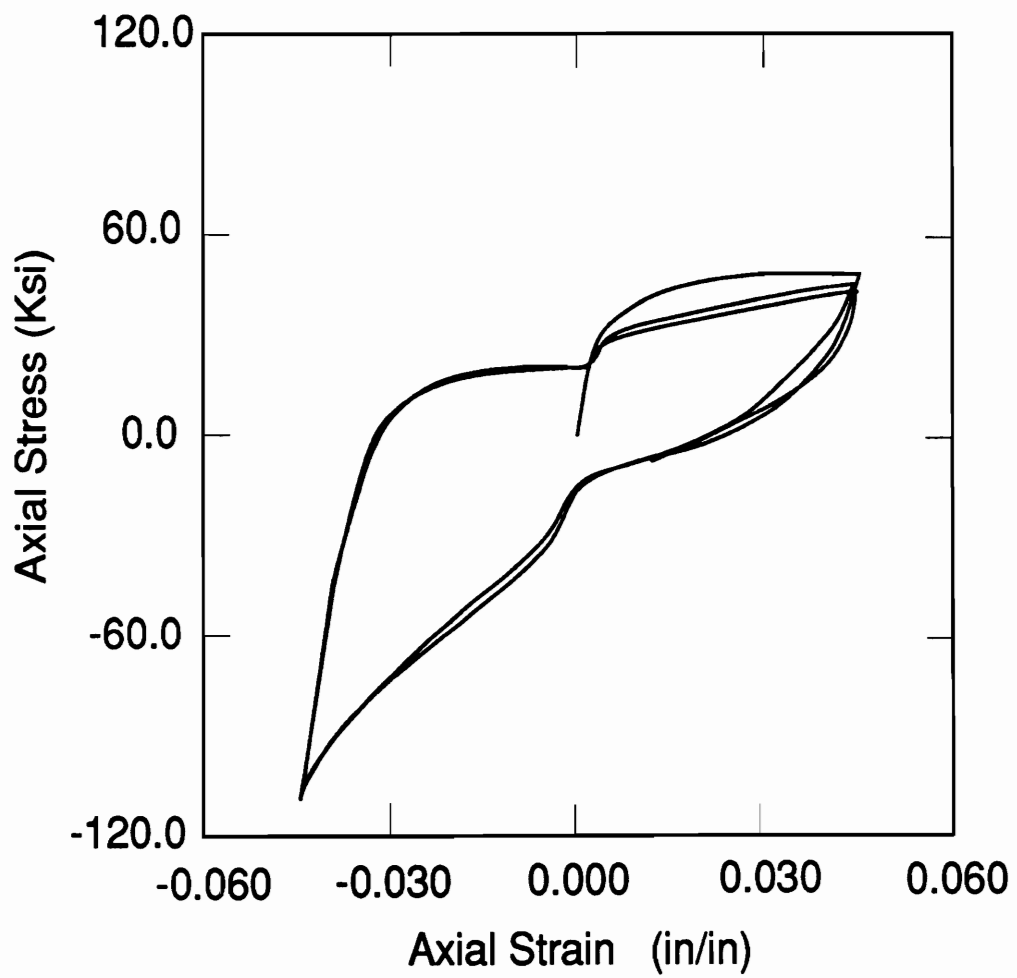


Figure 5.2: Hysteretic Response to  $\pm 4.5\%$  Strain of a Nitinol Alloy (After Graesser, 1990)

## 5.2 Generalized Multi-Dimensional Constitutive Relations of SMA

Considering a three-dimensional body, the original coordinate is denoted by  $\mathbf{X}$ , and the current deformed configuration is denoted by  $\mathbf{x}$ .  $\mathbf{X}$  stands for  $(X_1 X_2 X_3)^T$  where subscripts '1', '2', and '3' represent the X, Y, and Z coordinate axis and the superscript 'T' represents the transpose of a matrix.  $\mathbf{x}$  can also be written as  $(x_1 x_2 x_3)^T$ . The deformation gradient,  $\mathbf{f}$ , is given to be

$$\mathbf{f} = (\nabla \mathbf{x}^T)^T \quad (5.1)$$

where

$$\nabla = \begin{bmatrix} \frac{\partial}{\partial X_1} \\ \frac{\partial}{\partial X_2} \\ \frac{\partial}{\partial X_3} \end{bmatrix} \quad (5.2)$$

The deformation velocity tensor,  $\mathbf{v}$ , is defined as

$$\mathbf{v} = \dot{\mathbf{f}} \mathbf{f}^{-1} \quad (5.3)$$

The Green strain is defined as

$$\bar{\epsilon} = \frac{\mathbf{f}^T \mathbf{f} - \mathbf{I}}{2} \quad (5.4)$$

where  $\mathbf{I}$  is a unit tensor.

The Kirchhoff stress tensor can be derived as

$$\bar{\boldsymbol{\sigma}} = \frac{\rho_0}{\rho} \mathbf{f}^{-1} \boldsymbol{\sigma} (\mathbf{f}^{-1})^T \quad (5.5)$$

where  $\rho_0$  is the density in the original configuration and  $\rho$  is the density in the current configuration.  $\boldsymbol{\sigma}$  is the Cauchy stress tensor. The reason for using the Green strain and Kirchhoff stress are: (1) they are invariant under rigid body motion; (2) they are expressed in reference to the original configuration, therefore, it does not matter whether the deformation can significantly change the geometry of the 3-D body; and (3) they are energetical conjugates.

The first and the second laws of thermodynamics can be written in the current configuration as

$$\begin{cases} \rho \dot{U} - \text{tr}(\boldsymbol{\sigma} \mathbf{v}) + \text{div} \mathbf{q}_{sur} - \rho q = 0 \\ \rho \dot{S} + \rho \frac{q}{T} + \frac{1}{T} \text{div} \mathbf{q}_{sur} - \frac{1}{T^2} \mathbf{q}_{sur} \cdot \text{grad} T \geq 0 \end{cases} \quad (5.6)$$

where  $\text{tr}(\ )$  denotes the trace operator, ‘div’ and ‘grad’ the divergence and gradient operator in the current configuration. Rewriting the first and the second laws of thermodynamics in the original configuration yields

$$\begin{cases} \rho_0 \dot{U} - \text{tr}(\bar{\boldsymbol{\sigma}} \dot{\boldsymbol{\epsilon}}) + \text{Div} \mathbf{Q} + \rho_0 q = 0 \\ \rho_0 \dot{S} - \rho_0 \frac{q}{T} + \frac{1}{T} \text{Div} \mathbf{Q} - \frac{1}{T^2} \text{Div} \mathbf{Q} \cdot \text{Grad} T \geq 0 \end{cases} \quad (5.7)$$

where ‘Div’ and ‘Grad’ are the divergence and gradient operator in the original ref-

erence, respectively.  $\mathbf{Q}$  is defined as

$$\mathbf{Q} = \frac{\rho_0}{\rho} \mathbf{f}^{-1} \cdot \mathbf{q}_{sur} \quad (5.8)$$

Similar to Eq. (2.41), the general state variable,  $\Lambda$ , is defined as

$$\Lambda \equiv (\bar{\epsilon}_{ij}, T, \xi) \quad \begin{cases} i = 1, 2, 3 \\ j = 1, 2, 3 \end{cases} \quad (5.9)$$

Martensitic transformations are governed by the Helmholtz free energy. The free energy is the summation of the non-chemical energy such as strain energy and thermal energy and the chemical free energy. In other words, it is the overall strain energy that affects the phase transformation rather than individual strain and stress components. From the experimental study discussed in the last section, the hydrostatic pressure has a small influence on the phase transformations. The deformation along with phase transformation is mainly of a shear nature. The strain energy that affects the phase transformation should be the distortion energy. Therefore, the general state variable may be expressed as

$$\Lambda \equiv (\epsilon_{eq}, T, \xi) \quad (5.10)$$

where  $\epsilon_{eq}$  is the equivalent strain. The Helmholtz free energy is given by Eq. (2.42). Following the same approach discussed in Chapter 2, the Clausius-Duhem inequality in the original configuration can be derived as

$$tr\left[\left(\frac{1}{\rho_0} \bar{\boldsymbol{\sigma}} - \frac{\partial \Phi}{\partial \epsilon_{eq}} \frac{\partial \epsilon_{eq}}{\partial \bar{\boldsymbol{\epsilon}}}\right) \dot{\bar{\boldsymbol{\epsilon}}}\right] - \left(S - \frac{\partial \Phi}{\partial T}\right) \dot{T} - \frac{\partial \Phi}{\partial \xi} \dot{\xi} - \frac{1}{\rho_0 T} \mathbf{Q} \cdot \text{Grad} T \geq 0 \quad (5.11)$$

where  $\frac{\partial \epsilon_{eq}}{\partial \bar{\epsilon}}$  is a  $3 \times 3$  matrix. The general stress-strain relation based on continuum mechanics is given by

$$\bar{\sigma} = \rho_0 \frac{\partial \Phi}{\partial \epsilon_{eq}} \frac{\partial \epsilon_{eq}}{\partial \bar{\epsilon}} \quad (5.12)$$

The stress and strain vectors are

$$\{\bar{\sigma}\} = \begin{Bmatrix} \bar{\sigma}_{11} \\ \bar{\sigma}_{22} \\ \bar{\sigma}_{33} \\ \bar{\sigma}_{12} \\ \bar{\sigma}_{23} \\ \bar{\sigma}_{31} \end{Bmatrix} \quad (5.13)$$

and

$$\{\bar{\epsilon}\} = \begin{Bmatrix} \bar{\epsilon}_{11} \\ \bar{\epsilon}_{22} \\ \bar{\epsilon}_{33} \\ \bar{\epsilon}_{12} \\ \bar{\epsilon}_{23} \\ \bar{\epsilon}_{31} \end{Bmatrix} \quad (5.14)$$

The new form of the constitutive relation may now be written as

$$\begin{Bmatrix} \bar{\sigma}_{11} \\ \bar{\sigma}_{22} \\ \bar{\sigma}_{33} \\ \bar{\sigma}_{12} \\ \bar{\sigma}_{23} \\ \bar{\sigma}_{31} \end{Bmatrix} = \rho_0 \frac{\partial \Phi}{\partial \epsilon_{eq}} \begin{Bmatrix} \frac{\partial \epsilon_{eq}}{\partial \bar{\epsilon}_{11}} \\ \frac{\partial \epsilon_{eq}}{\partial \bar{\epsilon}_{22}} \\ \frac{\partial \epsilon_{eq}}{\partial \bar{\epsilon}_{33}} \\ \frac{\partial \epsilon_{eq}}{\partial \bar{\epsilon}_{12}} \\ \frac{\partial \epsilon_{eq}}{\partial \bar{\epsilon}_{23}} \\ \frac{\partial \epsilon_{eq}}{\partial \bar{\epsilon}_{31}} \end{Bmatrix} \quad (5.15)$$

or simply

$$\{\bar{\sigma}\} = \rho_0 \frac{\partial \Phi}{\partial \epsilon_{eq}} \left\{ \frac{\partial \epsilon_{eq}}{\partial \bar{\epsilon}} \right\} \quad (5.16)$$

The time derivative of stress may be written as

$$\{\dot{\bar{\sigma}}\} = \frac{\partial^2 \Phi}{\partial \epsilon_{eq}^2} \left\{ \frac{\partial \epsilon_{eq}}{\partial \bar{\epsilon}} \right\} \left\{ \frac{\partial \epsilon_{eq}}{\partial \bar{\epsilon}} \right\}^T \{\dot{\bar{\epsilon}}\} + \frac{\partial^2 \Phi}{\partial \epsilon_{eq} \partial \xi} \left\{ \frac{\partial \epsilon_{eq}}{\partial \bar{\epsilon}} \right\} \dot{\xi} + \frac{\partial^2 \Phi}{\partial \epsilon_{eq} \partial T} \left\{ \frac{\partial \epsilon_{eq}}{\partial \bar{\epsilon}} \right\} \dot{T} \quad (5.17)$$

The above relation may be written in incremental form.

$$\{d\bar{\sigma}\} = \frac{\partial^2 \Phi}{\partial \epsilon_{eq}^2} \left\{ \frac{\partial \epsilon_{eq}}{\partial \bar{\epsilon}} \right\} \left\{ \frac{\partial \epsilon_{eq}}{\partial \bar{\epsilon}} \right\}^T \{d\bar{\epsilon}\} + \frac{\partial^2 \Phi}{\partial \epsilon_{eq} \partial \xi} \left\{ \frac{\partial \epsilon_{eq}}{\partial \bar{\epsilon}} \right\} d\xi + \frac{\partial^2 \Phi}{\partial \epsilon_{eq} \partial T} \left\{ \frac{\partial \epsilon_{eq}}{\partial \bar{\epsilon}} \right\} dT \quad (5.18)$$

The strain increment is then decomposed into two components, the elastic strain and the transformation strain, as

$$\{d\bar{\epsilon}\} = \{d\bar{\epsilon}^e\} + \{d\bar{\epsilon}^t\} \quad (5.19)$$

where the elastic strain component can also be written as

$$\{d\bar{\epsilon}^e\} = \{\mathcal{E}\}^{-1} \{d\bar{\sigma}\} \quad (5.20)$$

where  $\{\mathcal{E}\}$  is the elastic material property matrix. After substituting Eqs. (5.19) and (5.20) into Eq. (5.18), Eq. (5.18) becomes

$$\left( \{I\} - D \left\{ \frac{\partial \epsilon_{eq}}{\partial \bar{\epsilon}} \right\} \left\{ \frac{\partial \epsilon_{eq}}{\partial \bar{\epsilon}} \right\}^T \{\mathcal{E}\}^{-1} \right) \{d\bar{\sigma}\} = D \left\{ \frac{\partial \epsilon_{eq}}{\partial \bar{\epsilon}} \right\} \left\{ \frac{\partial \epsilon_{eq}}{\partial \bar{\epsilon}} \right\}^T \{d\bar{\epsilon}^t\}$$



$$+ \Omega \left\{ \frac{\partial \epsilon_{eq}}{\partial \bar{\epsilon}} \right\} d\xi + \Theta \left\{ \frac{\partial \epsilon_{eq}}{\partial \bar{\epsilon}} \right\} dT \quad (5.21)$$

where ‘ $D$ ’, ‘ $\Omega$ ’, and ‘ $\Theta$ ’ are the Young’s Modulus, phase transformation tensor, and thermoelastic tensor used in the one-dimensional model, respectively. They are given by Eq. (2.49). Note, if the SMA material is in the elastic range and the temperature is constant, the right side of Eq. (5.21) vanishes. This gives the elastic material property matrix as

$$\{\mathcal{E}\} = D \left\{ \frac{\partial \epsilon_{eq}}{\partial \bar{\epsilon}} \right\} \left\{ \frac{\partial \epsilon_{eq}}{\partial \bar{\epsilon}} \right\}^T \quad (5.22)$$

As described in Chapter 2, the martensite fraction,  $\xi$ , is a function of stress and temperature, and can be generally expressed as follows for multi-dimensional problems.

$$\xi = \Xi(\sigma_{eq}, T) \quad (5.23)$$

where  $\sigma_{eq}$  stands for the equivalent stress.  $d\xi$ , therefore, can be written as

$$d\xi = \frac{\partial \Xi}{\partial \sigma_{eq}} d\sigma_{eq} + \frac{\partial \Xi}{\partial T} dT \quad (5.24)$$

and  $d\sigma_{eq}$  can be expressed as

$$d\sigma_{eq} = \left\{ \frac{\partial \sigma_{eq}}{\partial \bar{\sigma}_{11}} \quad \frac{\partial \sigma_{eq}}{\partial \bar{\sigma}_{22}} \quad \frac{\partial \sigma_{eq}}{\partial \bar{\sigma}_{33}} \quad \frac{\partial \sigma_{eq}}{\partial \bar{\sigma}_{12}} \quad \frac{\partial \sigma_{eq}}{\partial \bar{\sigma}_{23}} \quad \frac{\partial \sigma_{eq}}{\partial \bar{\sigma}_{31}} \right\} \begin{Bmatrix} d\bar{\sigma}_{11} \\ d\bar{\sigma}_{22} \\ d\bar{\sigma}_{33} \\ d\bar{\sigma}_{12} \\ d\bar{\sigma}_{23} \\ d\bar{\sigma}_{31} \end{Bmatrix} \quad (5.25)$$

or simply

$$d\sigma_{eq} = \left\{ \frac{\partial \sigma_{eq}}{\partial \bar{\sigma}} \right\}^T \{d\bar{\sigma}\} \quad (5.26)$$

Substituting Eqs. (5.24) and (5.26) into Eq. (5.21) and rearranging yields

$$\begin{aligned} \{d\bar{\sigma}\} &= \frac{D \left\{ \frac{\partial \epsilon_{eq}}{\partial \bar{\epsilon}} \right\} \left\{ \frac{\partial \epsilon_{eq}}{\partial \bar{\epsilon}} \right\}^T}{\{I\} - D \left\{ \frac{\partial \epsilon_{eq}}{\partial \bar{\epsilon}} \right\} \left\{ \frac{\partial \epsilon_{eq}}{\partial \bar{\epsilon}} \right\}^T \{\mathcal{E}\}^{-1} - \Omega \frac{\partial \Xi}{\partial \sigma_{eq}} \left\{ \frac{\partial \epsilon_{eq}}{\partial \bar{\epsilon}} \right\} \left\{ \frac{\partial \sigma_{eq}}{\partial \bar{\sigma}} \right\}^T} \{d\bar{\epsilon}^t\} \\ &+ \frac{\Theta \left\{ \frac{\partial \epsilon_{eq}}{\partial \bar{\epsilon}} \right\} + \Omega \frac{\partial \Xi}{\partial T} \left\{ \frac{\partial \epsilon_{eq}}{\partial \bar{\epsilon}} \right\}}{\{I\} - D \left\{ \frac{\partial \epsilon_{eq}}{\partial \bar{\epsilon}} \right\} \left\{ \frac{\partial \epsilon_{eq}}{\partial \bar{\epsilon}} \right\}^T \{\mathcal{E}\}^{-1} - \Omega \frac{\partial \Xi}{\partial \sigma_{eq}} \left\{ \frac{\partial \epsilon_{eq}}{\partial \bar{\epsilon}} \right\} \left\{ \frac{\partial \sigma_{eq}}{\partial \bar{\sigma}} \right\}^T} dT \end{aligned} \quad (5.27)$$

Equation (5.27) is a general expression of the constitutive relation of SMA. It can describe both the stress-strain-temperature relations of SMA and the shape memory effect. Although it is derived based on thermomechanics it is very much similar in form to the constitutive relations of thermo-plasticity (Liang, 1986). An internal state variable,  $\xi$ , is introduced in this thermomechanical model to represent the history dependence of the stress-strain behavior of SMA instead of the plastic strain for the constitutive model of plasticity. In fact, the internal state variable,  $\xi$ , has a direct relation with the transformation strain,  $\bar{\epsilon}^t$ , which is defined similarly to plastic strain. Equation (2.63) provides the relation between the phase transformation strain and the martensite fraction. To use this thermomechanical constitutive relation, the empirical relation of transformation kinetics must be used. Equation (5.27) can predict and describe the multi-dimensional stress without relying on the input of stress-strain data.

Equation (5.27) can be simplified as

$$\{d\bar{\sigma}\} = \{\mathcal{D}\}\{d\bar{\epsilon}^t\} + \{\kappa\}dT \quad (5.28)$$

where

$$\{\mathcal{D}\} = \frac{D\left\{\frac{\partial\epsilon_{eq}}{\partial\bar{\epsilon}}\right\}\left\{\frac{\partial\epsilon_{eq}}{\partial\bar{\epsilon}}\right\}^T}{\{I\} - D\left\{\frac{\partial\epsilon_{eq}}{\partial\bar{\epsilon}}\right\}\left\{\frac{\partial\epsilon_{eq}}{\partial\bar{\epsilon}}\right\}^T\{\mathcal{E}\}^{-1} - \Omega\frac{\partial\Xi}{\partial\sigma_{eq}}\left\{\frac{\partial\epsilon_{eq}}{\partial\bar{\epsilon}}\right\}\left\{\frac{\partial\sigma_{eq}}{\partial\bar{\sigma}}\right\}^T} \quad (5.29)$$

and

$$\{\kappa\} = \frac{\Theta\left\{\frac{\partial\epsilon_{eq}}{\partial\bar{\epsilon}}\right\} + \Omega\frac{\partial\Xi}{\partial T}\left\{\frac{\partial\epsilon_{eq}}{\partial\bar{\epsilon}}\right\}}{\{I\} - D\left\{\frac{\partial\epsilon_{eq}}{\partial\bar{\epsilon}}\right\}\left\{\frac{\partial\epsilon_{eq}}{\partial\bar{\epsilon}}\right\}^T\{\mathcal{E}\}^{-1} - \Omega\frac{\partial\Xi}{\partial\sigma_{eq}}\left\{\frac{\partial\epsilon_{eq}}{\partial\bar{\epsilon}}\right\}\left\{\frac{\partial\sigma_{eq}}{\partial\bar{\sigma}}\right\}^T} \quad (5.30)$$

Solving for the transformation strain yields

$$\{d\bar{\epsilon}^t\} = \{\mathcal{D}\}^{-1}\{d\bar{\sigma}\} - \{\mathcal{D}\}^{-1}\{\kappa\}dT \quad (5.31)$$

The elastic strain, plastic strain, and thermal expansion strain can be added to the above equation to generate a complete thermomechanical elasto-plastic constitutive relation for shape memory alloys. The Lèvy-Mises model provides a plastic strain increment as

$$\{d\bar{\epsilon}^p\} = \frac{3}{2} \frac{d\epsilon_{eq}^p}{\sigma_{eq}} \{\bar{s}\} \quad (5.32)$$

where  $\epsilon_{eq}^p$  is the equivalent plastic strain,  $\{s\}$  the deviatoric stress vector given by

$$\{\bar{s}\} = \begin{Bmatrix} \bar{\sigma}_{11} - \bar{\sigma}_m \\ \bar{\sigma}_{22} - \bar{\sigma}_m \\ \bar{\sigma}_{33} - \bar{\sigma}_m \\ \bar{\sigma}_{12} \\ \bar{\sigma}_{23} \\ \bar{\sigma}_{31} \end{Bmatrix} \quad (5.33)$$

where  $\bar{\sigma}_m$  is the hydrostatic stress given by

$$\bar{\sigma}_m = \frac{1}{3}(\bar{\sigma}_{11} + \bar{\sigma}_{22} + \bar{\sigma}_{33}) \quad (5.34)$$

The thermal expansion strain is given by

$$\{d\epsilon_T\} = \{\alpha\}dT = \{\alpha \ \alpha \ \alpha \ 0 \ 0 \ 0\}^T dT \quad (5.35)$$

where  $\alpha$  is the thermal expansion coefficient. A complete constitutive equation can be described by

$$\begin{aligned} \{d\bar{\epsilon}\} &= \{d\bar{\epsilon}^e\} + \{d\bar{\epsilon}^t\} + \{d\bar{\epsilon}^p\} + \{d\bar{\epsilon}_T\} \\ &= \{\mathcal{E}\}^{-1}\{d\bar{\sigma}\} + \{\mathcal{D}\}^{-1}\{d\bar{\sigma}\} + \{\mathcal{D}\}^{-1}\{\kappa\}dT \\ &\quad + \frac{3}{2} \frac{d\epsilon_{eq}^p}{\sigma_{eq}} \{\bar{s}\} + \{\alpha\}dT \end{aligned} \quad (5.36)$$

Most applications of SMA are in the transformation region. Very few applications utilize the plastic deformation range. The thermomechanical constitutive relation of SMA can be further simplified if the plastic strain is neglected here. The stress-strain

relation thus can be written as

$$\{d\bar{\sigma}\} = \frac{\{I\}}{\{\mathcal{E}\}^{-1} + \{\mathcal{D}\}^{-1}} \{d\bar{\epsilon}\} - \frac{\{\mathcal{D}\}^{-1}\{\kappa\} + \{\alpha\}}{\{\mathcal{E}\}^{-1} + \{\mathcal{D}\}^{-1}} dT \quad (5.37)$$

The  $\{\mathcal{D}\}^{-1}$  is zero in the elastic range as can be seen from Eq. (5.29). Therefore, the above constitutive equation is of the same form as Hook's law within elastic region. In case of proportional loading at a constant temperature, Eq. (5.37) may be integrated on both sides resulting in a total strain theory similar to Hencky's stress-strain relation of plastic materials (Chakrabarty, 1987) and given by

$$\{\bar{\sigma}\} = \frac{\{I\}}{\{\mathcal{E}\}^{-1} + \{\mathcal{D}\}^{-1}} \{\bar{\epsilon}\} \quad (5.38)$$

In a one-dimensional tensile test the martensitic transformation starts at a elastic stress limit,  $\sigma_e$ . It is assumed that the phase transformation in a multi-dimensional stress state occurs when the equivalent stress,  $\sigma_{eq}$ , reaches the elastic stress limit,  $\sigma_e$ .

From the study of distortion energy, the equivalent stress,  $\sigma_{eq}$ , and equivalent strain,  $\epsilon_{eq}$ , may be derived (Slater, 1977). The equivalent stress is expressed as

$$\sigma_{eq} = \sqrt{\frac{1}{2}[(\bar{\sigma}_{11} - \bar{\sigma}_{22})^2 + (\bar{\sigma}_{22} - \bar{\sigma}_{33})^2 + (\bar{\sigma}_{33} - \bar{\sigma}_{11})^2 + 6(\bar{\sigma}_{12}^2 + \bar{\sigma}_{23}^2 + \bar{\sigma}_{31}^2)]} \quad (5.39)$$

and the equivalent strain by

$$\epsilon_{eq} = \frac{\sqrt{2}}{3}[(\bar{\epsilon}_{11} - \bar{\epsilon}_{22})^2 + (\bar{\epsilon}_{22} - \bar{\epsilon}_{33})^2 + (\bar{\epsilon}_{33} - \bar{\epsilon}_{11})^2 + \frac{3}{2}(\bar{\epsilon}_{12}^2 + \bar{\epsilon}_{23}^2 + \bar{\epsilon}_{31}^2)]^{\frac{1}{2}} \quad (5.40)$$

The equivalent strain has the property that in a state of strain defined by  $\bar{\epsilon}_{22} = \bar{\epsilon}_{33} = -0.5\bar{\epsilon}_{11}$  and  $\bar{\epsilon}_{12} = \bar{\epsilon}_{23} = \bar{\epsilon}_{31} = 0$ , there is  $\epsilon_{eq} = \bar{\epsilon}_{11}$ . This implies that the Possion's ratio is 0.5. Some modifications are needed in order to describe the elastic strain. Assuming  $\bar{\epsilon}_{22} = \bar{\epsilon}_{33} = -\mu\bar{\epsilon}_{11}$  and  $\bar{\epsilon}_{12} = \bar{\epsilon}_{23} = \bar{\epsilon}_{31} = 0$ , where  $\mu$  is the Possion's ratio, the coefficient of Eq. (5.40) must be changed in order to keep  $\epsilon_{eq} = \bar{\epsilon}_{11}$ . The equivalent elastic strain is thus modified as

$$\epsilon_{eq} = \frac{\sqrt{2}}{2(1 + \mu)} [(\bar{\epsilon}_{11} - \bar{\epsilon}_{22})^2 + (\bar{\epsilon}_{22} - \bar{\epsilon}_{33})^2 + (\bar{\epsilon}_{33} - \bar{\epsilon}_{11})^2 + \frac{3}{2}(\bar{\epsilon}_{12}^2 + \bar{\epsilon}_{23}^2 + \bar{\epsilon}_{31}^2)]^{\frac{1}{2}} \quad (5.41)$$

It is apparent that when an SMA sample is loaded to have some non-elastic deformation such as phase transformation deformation or plastic deformation which both have a Possion's ratio of 0.5, the overall Possion's ratio can no longer be constant. The following assumption of a varying Possion's ratio,  $\nu$ , can be employed in the calculation.

$$\nu = 0.5 - (0.5 - \mu) \frac{\epsilon_{eq}^e}{\epsilon_{eq}^e + \epsilon_{eq}^t + \epsilon_{eq}^p} \quad (5.42)$$

The non-elastic strain of shape memory alloys is relatively larger than the elastic strain, therefore, a constant Possion's ratio of 0.5 may be assumed to simplify the calculations.

From the equivalent stress and strain expressions, Eqs. (5.39) and (5.40), the  $\left\{ \frac{\partial \sigma_{eq}}{\partial \bar{\epsilon}} \right\}$

and  $\left\{ \frac{\partial \epsilon_{eq}}{\partial \bar{\epsilon}} \right\}$  may be derived as

$$\left\{ \frac{\partial \epsilon_{eq}}{\partial \bar{\epsilon}} \right\} = \frac{2}{9\epsilon_{eq}} \begin{Bmatrix} \bar{\epsilon}_{11} \\ \bar{\epsilon}_{22} \\ \bar{\epsilon}_{33} \\ 1.5\bar{\epsilon}_{12} \\ 1.5\bar{\epsilon}_{23} \\ 1.5\bar{\epsilon}_{31} \end{Bmatrix} \quad (5.43)$$

and

$$\left\{ \frac{\partial \sigma_{eq}}{\partial \bar{\sigma}} \right\} = \frac{1}{2\sigma_{eq}} \begin{Bmatrix} \bar{\sigma}_{11} \\ \bar{\sigma}_{22} \\ \bar{\sigma}_{33} \\ 6\bar{\sigma}_{12} \\ 6\bar{\sigma}_{23} \\ 6\bar{\sigma}_{31} \end{Bmatrix} \quad (5.44)$$

### 5.3 Numerical Example

The constitutive relations developed in the previous section are nonlinear and they depend on the stress and strain state. Moreover, the behavior of SMA usually involves large deformation. Thus creating a material and geometric nonlinear problem. Solving even a simple problem requires a sophisticated finite element program. Here, in order to demonstrate the feasibility of using the multi-dimensional constitutive relation, a simple example is presented, a solid cylindrical SMA bar under torsion. It is basically a one-dimensional problem, but it is governed by shear stress and the stress is not constant throughout the cross section.

### 5.3.1 Stress-Strain Analysis

Consider a solid cylindrical bar with the outside radius of  $a$ , as the bar is elastic, the shear stress acting over any cross section is proportional to the radial distance  $r$  from the central axis. The applied torque is the resultant moment of the stress distribution about this axis. If the angle of twist per unit length of the bar is denoted by  $\theta$  and applied torque  $\mathcal{T}$ , the elastic shear stress may be written as

$$\bar{\tau} = G\bar{\gamma} = Gr\theta = \frac{2\mathcal{T}r}{\pi a^4} \quad (5.45)$$

where  $G$  is the shear modulus. The equivalent stress and strain from Eqs. (5.39) and (5.40) are

$$\sigma_{eq} = \sqrt{3}\bar{\tau} \quad (5.46)$$

and

$$\epsilon_{eq} = \frac{1}{\sqrt{3}}\bar{\gamma} \quad (5.47)$$

Since the shear stress has its greatest value at  $r = a$ , the bar begins to have stress-induced phase transformation at this radius. It is assumed that the SMA bar is austenite before applying a moment. When the equivalent stress,  $\sigma_{eq}$ , at the radius  $a$  reaches  $\sigma_e$ , the corresponding critical torque and twist are

$$\mathcal{T}_e = \frac{\sqrt{3}}{6}\pi\sigma_e a^3 \quad (5.48)$$



and

$$\theta_e = \frac{\sigma_e}{\sqrt{3}Ga} \quad (5.49)$$

If the torque is increased further, a transformation annulus forms near the boundary, leaving a central zone of elastic material within a radius  $c$ , the stress distribution in the elastic region is linear with the equivalent stress reaching  $\sigma_e$  at  $r = c$ . The shear stress in the central elastic region is given by

$$\bar{\tau} = \frac{\sigma_e r}{\sqrt{3} c} \quad 0 \leq r \leq c \quad (5.50)$$

The stress distribution in the transformation annulus obeys Eq. (5.37). Note, the shear strain  $\gamma$  is always  $r\theta$  no matter whether it is in the elastic region or not.

From Eqs. (5.43) and (5.44) the terms  $\left\{\frac{\partial \epsilon_{eq}}{\partial \bar{\gamma}}\right\}$  and  $\left\{\frac{\partial \sigma_{eq}}{\partial \bar{\tau}}\right\}$  may be determined to be

$$\left\{\frac{\partial \epsilon_{eq}}{\partial \bar{\gamma}}\right\} = \frac{1}{\sqrt{3}} \quad (5.51)$$

and

$$\left\{\frac{\partial \sigma_{eq}}{\partial \bar{\tau}}\right\} = \sqrt{3} \quad (5.52)$$

The inverse of the elastic material property matrix is simply  $1/G$  in this case. The Poisson's ratio,  $\mu$ , is assumed to be 0.5. The shear modulus,  $G$ , is thus  $D/3$ . All material properties are assumed to be constant herein. Based on the above discussion,

$\{\mathcal{D}\}^{-1}$  and  $\{\kappa\}$  are given as

$$\{\mathcal{D}\}^{-1} = 3\epsilon_L \frac{\partial \Xi}{\partial \sigma_{eq}} \quad (5.53)$$

and

$$\{\kappa\} = -\frac{\Theta + \Omega \frac{\partial \Xi}{\partial T}}{\sqrt{3} \Omega \frac{\partial \Xi}{\partial \sigma_{eq}}} \quad (5.54)$$

The stress-strain relation in the transformation annulus is given by

$$d\bar{\tau} = \frac{G}{1 - \Omega \frac{\partial \Xi}{\partial \sigma_{eq}}} d\bar{\gamma} \quad (5.55)$$

or

$$\left(1 - \Omega \frac{\partial \Xi}{\partial \sigma_{eq}}\right) d\bar{\tau} = G d\bar{\gamma} \quad (5.56)$$

Integrating on both sides yields

$$(\bar{\tau} - \bar{\tau}_0) = G(\bar{\gamma} - \bar{\gamma}_0) + \frac{\Omega}{\sqrt{3}}(\xi - \xi_0) \quad (5.57)$$

where the variables with subscript '0' are the initial conditions. Assuming the initial phase of the bar is austenite and it is free of any residual stress and deformation, and the ambient temperature is between  $M_s$  and  $A_s$ , The stress-strain relation can

be simplified to

$$\bar{\tau} = G\bar{\gamma} + \frac{\Omega}{\sqrt{3}}\xi \quad (5.58)$$

The martensite fraction,  $\xi$ , using the cosine model, is derived from Eq. (2.31) as

$$\xi = \frac{1}{2}\{\cos[a_M(T - M_f) + b_M\sqrt{3}\bar{\tau}] + 1\} \quad (5.59)$$

The shear stress distribution in the transformation annulus  $\bar{\tau}(r)$  is given by

$$\bar{\tau} = G\theta r + \frac{\Omega}{2\sqrt{3}}\{\cos[a_M(T - M_f) + b_M\sqrt{3}\bar{\tau}] + 1\} \quad c \leq r \leq a \quad (5.60)$$

A numerical iteration scheme is required to determine the shear stress. The equivalent stress at the elastic interface is the elastic stress limit,  $\sigma_e$ . The radius of the central elastic zone,  $c$ , can be determined from the following equation.

$$c = \frac{\sigma_e}{\sqrt{3}G\theta} \quad (5.61)$$

The resultant moment from the distributed shear stress is expressed as

$$\mathcal{T} = \int_0^c \frac{\sigma_e r^2}{\sqrt{3}c} dr + \int_c^a \bar{\tau}(r)r^2 dr \quad (5.62)$$

The above equation provides the relation between the applied torque and the corresponding twist. Solving  $\theta(\mathcal{T})$  ( $\theta$  as a function of the applied torque,  $\mathcal{T}$ ) from Eq. (5.62) and substituting  $\theta(\mathcal{T})$  into Eq. (5.60) yields the stress-torque relation. With

increasing torque, the equivalent stress at  $r = a$  reaches the yield strength,  $\sigma_y$ , which corresponds to a critical torque,  $T_y$ . A torque higher than  $T_y$  will result in plastic deformation requiring plastic constitutive relations. The applied torque is restricted to be below  $T_y$  in this study. The critical torque,  $T_y$ , can thus be determined from

$$\frac{\sigma_y}{\sqrt{3}} = Ga\theta(T_y) + \frac{\Omega}{\sqrt{3}} \quad (5.63)$$

The martensite fraction distribution,  $\xi(r)$ , can be determined by substituting  $\bar{\tau}(r)$  into to Eq. (5.59).

The residual stress-strain distribution may be obtained by superimposing an elastic stress distribution caused by a torque of  $-T$ . It is assumed that the maximum equivalent stress of the residual stress field is less than  $\sigma_e$ , so the martensite fraction distribution may not be altered. The residual stress distribution may then be given by

$$\bar{\tau}_{res} = \bar{\tau}(r) - \frac{2Tr}{\pi a^4} \quad (5.64)$$

The residual twist,  $\theta_{res}$ , is determined by the same superposition approach.

$$\theta_{res} = \theta(T) - \frac{2T}{\pi Ga^4} \quad (5.65)$$

and the residual strain is obtained from the expression:

$$\bar{\gamma}_{res} = r\theta_{res} \quad (5.66)$$

### 5.3.2 Analysis of the Shape Memory Effect

Some of the residual twist of the SMA bar will be recovered upon heating due to the shape memory effect. If the boundary condition of the SMA bar is free, heating of the SMA bar results in a controlled recovery. This is different from the uniaxial free recovery in which the residual transformation strain is fully recovered and stress is zero. In the case of the ‘free recovery’ of an SMA bar, the central elastic zone may generate an internal reactionary force to the transformation of the outside transformation annulus. Heating the bar results in a certain amount of twist recovery while storing energy in the central elastic zone. The stored energy will be released upon cooling the SMA bar resulting in deformation of the outside transformation annulus (generating new martensite). It is similar to a bias spring SMA actuator or an SMA bar with two-way effect.

This unique characteristic of an SMA bar (or other similar geometries) may be very useful. This 3-D SME characteristic is actually a two-way effect by structure rather than a two way effect by material. A SMA bar itself functions as both a SMA actuator and a bias spring. Proper design of the size of the central elastic region may achieve an overall two-way effect. A “smart” blade of turbine compressors which can adjust its attacking angle according to in-coming flux may be designed based on this concept.

The theoretical analysis of this “free recovery” of an SMA bar is very difficult. A numerical technique such as finite element method must be used. On the contrary, it is relatively easy to analyze the behavior of restrained recovery in this case.

In the restrained recovery case, the residual deformation is restrained and no deformation is allowed during the heating and cooling process. It is assumed that heating starts from  $A_s$  (ignoring the thermoelastic effect) and the temperature is uniform throughout the SMA bar. Equation (5.37) becomes

$$\{d\bar{\sigma}^r\} = -\frac{\{\mathcal{D}\}^{-1}\{\kappa\}}{\{\mathcal{E}\}^{-1} + \{\mathcal{D}\}^{-1}}dT \quad (5.67)$$

where superscript 'r' denotes 'recovery'. In the case of restrained recovery of SMA bars, the above equation may be simplified to

$$(1 - \Omega \frac{\partial \Xi}{\partial \sigma_{eq}})d\bar{\tau}^r = \frac{\Theta + \Omega \frac{\partial \Xi}{\partial T}}{\sqrt{3}}dT \quad (5.68)$$

Integrating on both sides yields

$$\bar{\tau} - \bar{\tau}_0 = \frac{\Theta}{\sqrt{3}}(T - T_0) + \frac{\Omega}{\sqrt{3}}(\xi - \xi_0) \quad (5.69)$$

where  $\bar{\tau}_0$  is the residual stress obtained from Eq. (5.64),  $T_0$  is  $A_s$ , and  $\xi_0$  is the martensite fraction obtained from the stress-strain analysis (Eq. (5.59)).  $\xi$  is given by

$$\xi = \frac{\xi_0}{2} \{ \cos[a_A(T - A_s) + b_A\sqrt{3}\bar{\tau}^r] + 1 \} \quad (5.70)$$

Substituting Eq. (5.70) into Eq. (5.69) yields the shear stress distribution in the transformation annulus. Note that the residual stress in the central elastic zone is not altered due to the restrained boundary condition. The resultant torque from the

recovery shear stress thus may be calculated using Eq. (5.62).

## 5.4 Concluding Remarks

A multi-dimensional constitutive model of SMAs based on the newly developed one-dimensional model is developed in this chapter. The multi-dimensional constitutive model is based on the thermomechanical aspects of the shape memory alloys and can be used to study the mechanical behavior of complex structures made of SMA. As an example of utilizing the constitutive relations, an analysis of a SMA bar has also presented, which indicates some possible new applications of shape memory alloys as 3-D actuators.

# Chapter 6

## Conclusions

A one-dimensional thermomechanical constitutive relation of shape memory alloys based on Tanaka's early work is developed in this dissertation.

- This thermomechanical constitutive relation is derived from fundamental aspects of materials, i.e., the thermodynamic behaviors. It reflects the physical essence of the characteristics of shape memory alloys. The final expression of this constitutive relation is simple, therefore, it is easy to use in engineering design.
- A new internal variable is introduced to describe the behavior of shape memory alloys. A relation between the new internal variable, defined as martensite fraction, with transformation strain is established. This relation links the macro-mechanics and micro-mechanics.
- No matter how shape memory alloys behave macroscopically, they are governed microscopically by basic phase transformation kinetics. Shape memory alloys may be described by the same transformation kinetics regardless of different mechanical conditions. Two empirical relations are suggested in this dissertation to describe the transformation kinetics, i.e., the relation of martensite fraction



with temperature of shape memory alloys. One is called the exp model, another is named the cosine model. Both of these models can be used to study shape memory alloys quantitatively. The exp model can provide more accurate results compared with the cosine model but is more complex and requires more material constants.

- The thermomechanical constitutive relation uses practical and experimentally measurable material properties. The material properties required by the thermomechanical constitutive relation are four characteristic transition temperature defined metallurgically, two stress influence coefficient which reflect the influence of stress on phase transformations, a transformation coefficient (required by the exp model only), material Young's modulus, thermoelastic tensor, and the maximum recoverable strain. These metallurgical and mechanical material constants may be easily measured from standard experimental equipment such as differential scanning calorimeter (DSC) and MTS tensile machine. This is very convenient in engineering design.
- An experimental verification of this constitutive model is also presented. Although more experimental verification and theoretical modification are needed, this constitutive relation is proved to be capable of predicting and describing the important characteristics of SMA quantitatively.
- The multi-dimensional constitutive relation developed based on the one-dimensional constitutive model has similar features to plastic theory. It is based on thermodynamic relations rather than the flow rule assumption. This multi-dimensional constitutive relation can be used to analyze shape memory alloy structures such as SMA pipe fitting devices. By studying the new features of

SMA structures, more knowledge of SMA behavior may be attained and more new applications of SMA may be inspired.

- A general design method based on the constitutive relation is developed for SMA force actuators, including bias spring SMA force actuators and differential SMA force actuators. The method can determine effectively the basic design parameters of an SMA actuator according to the performance requirement of the SMA actuator.

This dissertation focuses on the development of the constitutive relation of SMA which can be used easily in engineering design. As an example of utilizing this constitutive relation, a design method of SMA force actuators has been developed. In order to consummate this thermomechanical constitutive relation, more work are still needed in following aspects: pseudoelastic effect, the influence of initial mixed phase on stress-strain relations, and cyclic behavior of SMA.

# References

Abujudon, D. N., Thoma, P. E., and Fariabi, S., 1989, "The Effect of Cold Work and Heat Treatment on the Phase Transformations of Near Equiatomic NiTi Shape Memory Alloy," Private communication.

Achenbach, M., Atanackovic, T., and Müller, I., 1986, "A Model for Memory Alloys in Plane Strain", *Int. J. of Solid Structures*, Vol. 22, No. 2, p. 171-193.

American Society for Metals, 1970, **Phase Transformation**, (Papers presented at a seminar of the American Society for Metals, Oct. 12-13, 1968), Chapman & Hall Ltd., London.

Andreasen, G. F. and Morrow, R. E., 1978, *Am. J. Orthod*, Vol. 73, No. 2, pp. 142-151.

Bank, R., 1975, **Shape Memory Effects in Alloys**, p. 537, Plenum.

Barker, D., 1989, **Active Dynamic Response Tuning of Adaptive Composites Utilizing Embedded Nitinol Actuators**, Master Thesis, Department of Mechanical Engineering, Virginia Polytechnic Institute and State University, Blacksburg,

Virginia, July.

Baz, A., Iman, K. and McCoy, J., 1990, "The Dynamics of Helical Shape Memory Actuators," *Journal of Intelligent Materials Systems and Structures*, Vol. 1, No. 1, January.

Biometal Company, 1987, **Biometal**, Biometal Company, Tokyo, Japan.

Bondaryev, E. N. and Wayman, C. M., 1988, "Some Stress-Strain-Temperature Relationships for Shape Memory Alloys," *Metallurgical Transactions*, Vol. 19A, October.

Buehler, W. J. and Wiley, R. C., 1965, **Nickle-Based Alloys**, US Patent 3,174,851, 1965.

Buehler, W. J. and Cross, W. R., 1969, *Wire Journal*, Vol. 2, p. 41.

Castleman, L. S., Motzkin, S. M., Alicandri, F. P. and Bonawit, V. L., 1976, *Journal of Biomed. Materials*, No. 10, pp. 695-731.

Clark, H. M. and Wayman, C. M., 1970, "Surface Relief Effects in Solid-State Phase Transformation," **Phase Transformation**, ed. American Society for Metals, (Papers presented at a seminar of the American Society for Metals, Oct. 12-13, 1968), pp. 59-114, Chapman & Hall Ltd., London.

Cory, J. S., 1978, "Nitinol Thermodynamic State Surfaces", *Journal of Energy*, Vol.

2, No. 5, September-October.

Cory, J. S. and McNichols, J. L., Jr., 1985, "Nonequilibrium Thermostatistics", *Journal of Applied Physics*, Vol. 58, No. 9, November.

Cross, W. B., Kariotis, A. H. and Stimler, F. J., 1970, "Nitinol Characterization Study," Goodyear Aerospace Corporation Report No. Ger 14188, (NASA CR-1433), Akron, Ohio.

Delaey, L., Krishnan, R. V., Tas, H. and Warlimont, H., 1974, "Review of Thermoelasticity, Pseudoelasticity and the Memory Effects Associated with Martensitic Transformations: Part 1. Structural and Microstructural Changes Associated with the Transformations," *Journal of Materials Science*, Vol. 9, pp. 1521-1535.

Duerig, T. W., Albrecht, J., and Gessinger, G. H., 1982, "A Shape Memory Alloy for High-Temperature Applications," *Journal of Metals*, December.

Duerig, T. W. and Melton, K. N., 1988, "Design with the Shape Memory Effect," Proceedings of MRS International Meeting on Advanced Materials, Japan, June.

Dye, T., 1990, **An Experimental Verification of a One-dimensional Constitutive Model of Shape Memory Alloys**, Master Thesis, Department of Mechanical Engineering, Virginia Polytechnic Institute and State University, Blacksburg, Virginia, August.

Escher, K. Exner, A., Honnbogen, E. and Schmidt, H., 1990, "The Two Way Shape Memory Effect for Mechanical Hands," Proceedings of 31st AIAA Conference, AIAA 90-1027, Long Beach, CA, April.

Falk, F., 1980, "Model Free Energy, Mechanics, and Thermodynamics of Shape Memory Alloys," *Acta Metallurgical*, Vol. 28, pp. 1773-1780.

Furuya, Y., Shimada, H., Goto, Y. and Honda, R., 1988, "An Extreme Operation Submarine Robot Actuator by Shape Memory Alloy," Proceedings of MRS International Meeting on Advanced Materials, Japan, June.

Filonenko-Borodich, M., **Theory of Elasticity**, Stechert-Hafner Service Agency, Inc. New York.

Funakubo, H., 1987, **Shape Memory Alloys**, Gordon and Breach Science Publishers, New York.

Gefen, Y., Halwany, A., and Rosen, M., 1973, "Influence of Hydrostatic Pressure on Martensitic Transformations in Au-Cd Shape Memory Alloys," *Phil. Mag.*, Vol. 28, No. 1.

Genell, W. S., McNichols, Jr. J. L., and Cory, J. S., 1979, *Mechanical Engineering*, Vol. 101, No. 5, p. 28.

Goldstein, D., Kabacoff, L., and Tydings, J., 1987, "Stress Effects on Nitinol Phase

Transformations,” *Journal of Metals*, March.

Graesser, E. J., 1990, **Multi-dimensional Modeling of Hysteretic Materials Including Shape Memory Alloys: Theory and Experiment**, PhD Dissertation, Dept. of Mech. and Aero. Eng., State Uni. of New York at Buffalo, January.

Harrison, J. D. and Hodgson, D. E., 1975, **Shape Memory Effects in Alloys**, p. 517, Plenum.

Hillert M., 1970, “Calculation of Phase equilibrium,” **Phase Transformation**, ed. American Society for Metals, (Papers presented at a seminar of the American Society for Metals, Oct. 12-13, 1968), pp. 181-218, Chapman & Hall Ltd., London.

Hodgson, D. E., 1988, **Using Shape Memory Alloys**, Shape Memory Applications, Inc.

Hoffmann, K., H. and Sprekels, J., 1987, “Phase Transformation in Shape Memory Alloys I: Stability and Optimal Control”, Preprint No. 136, Inst. fur Mathe, Uni. Augsburg.

Hoffmann, K. H. and Zheng, S. M., 1986, “Uniqueness for Nonlinear Coupled Equations Arising From Alloy Mechanism”, Preprint No. 118, Inst. fur Mathe, Uni. Augsburg.

Honma, D., Miwa, Y., and Iguchi, N., 1981, Proceedings of the Japan Society of

Mechanical Engineers, No. 813-5, p. 82.

Hsu, C. H., 1982, **The Effect of Stress on the Transformation in Nickel-Titanium**, Ph.D dissertation, Iowa State University.

Jackson, C. M., Wagner, H. J. and Wasilewski, R. J., 1972, "55-Nitinol—The Alloy with a Memory: Its physical Metallurgy, Properties, and Applications," NASA Report, SP 5110.

Johnson, A. D., 1975, *Record of the Tenth Intersociety Energy Conversion Engineering Conference*, Newark, DE, p. 530.

Kakeshita, T., Yoshimura, Y., and Shimizu, K., 1988, "Effect of Hydrostatic Pressure on Martensitic Transformations in Cu-Al-Ni Shape Memory alloys," *Transactions of Japan Institute of Metals*, Vol. 29, No. 10, pp. 781-789.

Krishnan, R. V., Delaey, L., Tas, H. and Warlimont, H., 1974, "Review of Thermoelasticity, Pseudoelasticity and the Memory Effects Associated with Martensitic Transformations: Part 2. The Macroscopic Mechanical Behavior," *Journal of Materials Science*, Vol. 9, pp. 1536-1544.

Koistinen, D. P. and Marsburger, R. E., 1959, *Acta Met*, Vol. 7, No. 59.

Levinsohn, R. and Jervis, J. E., **US Patent 3,759,552**.



Liang, C., 1986., **Transient Thermoelasto-Plastic Constitutive Relations of Materials**, Master Thesis, Department of Jet Propulsion, Beijing Institute of Aeronautics and Astronautics.

Liang, C. and Rogers, C. A., 1990a, "A One-Dimensional Thermomechanical Constitutive Relation of Shape Memory Materials," *Journal of Intelligent Material Systems and Structures*, Vol. 1, No. 2, pp. 207-234.

Liang, C. and Rogers, C. A. 1990b, "Design of Shape Memory Alloy actuator," submitted to *Journal of Mechanical Design*.

Liang, C. and Rogers, C. A., 1989, "Behavior of Shape Memory Actuators Embedded in Composites," *Proceedings of the 7th International Composites Conference*, Beijing, PRC, August.

Liang, C., Jia, J., and Rogers, C. A., 1989, "Behavior of Shape Memory Alloy Reinforced plates - Part II: Results," *Proceedings of the 30th Structures, Structural Dynamics and Materials Conference*, AIAA 89-AL, April.

Liang, C., Rogers, C. A., and Fuller, C. R., 1989, "Acoustic Transmission/Radiation Analysis of Shape Memory Alloy Reinforced Laminated Plates," accepted by *Journal of Sound and Vibration*.

Lin, Z. C., Liang, K. F., Zhang, J. X., and Zhang, W. G., 1988, "Resistance of Phase Interface Motion in the Process of Pre-Martensitic Transformation of Ti<sub>50</sub>Ni<sub>39</sub>Fe<sub>1</sub>

and Ti<sub>47.9</sub>Ni<sub>50.3</sub> Alloys,” *Proceedings of MRS Int’l Mtg. on Adv. Mats.*, Japan, June.

Lockett, F. J., 1972, **Nonlinear Viscoelastic Solids**, Academic Press, London.

Magee, C. L., 1979 “The Nucleation of Martensite,” **Phase Transformation**, ed. American Society for Metals, (Papers presented at a seminar of the American Society for Metals, Oct. 12-13, 1968), pp. 115-156, Chapman & Hall Ltd., London.

McLellan, A. G., 1980, **The Classical Thermodynamics of Deformable Materials**, Cambridge University Press, Cambridge.

McNichols, J. L. Jr. and Cory, J. S., 1987, “Thermodynamics of Nitinol”, *Journal of Applied Physics*, 61 (3), 1 February.

Müller, I., 1979, “A Model for a Body with Shape Memory”, *Arch. Rat. Mech. Anal.*, Vol. 70, p. 61-77.

Müller, I. and Wilmanski, K., 1980, “A Model for Phase Transformation in Pseudoelastic Bodies”, *Il Nuovo Cimento*, Vol. 57B, p. 238-318.

Müller, I., 1985, “Pseudoelasticity in Shape Memory Alloys - an Extreme Case of Thermoelasticity”, IMA Preprint No. 169, July.

Müller, I., “Shape Memory Alloys Phenomenology and Simulation”, *Shape Memory*

*Alloys, Preprints.*

Nadai, A. and Wahl, A. M., 1931, **Plasticity**, McGraw-Hill Book Company, New York.

Niezgodka, M. and Sprekels, J., 1986, "On the Dynamics of Structural Phase Transformation in Shape Memory Alloys," Preprint No. 114, Inst. fur Mathe, Uni. Augsburg.

Niezgodka, M. and Sprekels, J., 1985, "Existence of Solutions for a Mathematical Model of Structural Phase Transitions in Shape Memory Alloys", Preprint No. 89, Inst. fur Mathe, Uni. Augsburg.

Niezgodka, M., Zheng, S. M. and Sprekels, J., 1986, "Global Solutions to Structural Phase Transitions in Shape Memory Alloys", Preprint No. 105, Inst. fur Mathe, Uni. Augsburg.

Ohnishi, Hamaguchi, Nabeshima, Miyagi, Hamada, Suzuki, and Shikida, 1982, Proceedings of the 3rd Conference of the Japanese Society for Biomaterials, p. 121.

Patel, J. R. and Cohen, M., 1953, *Acta. Met.*, Vol. 1, p. 531.

Pearson, W. B., 1958, **A Handbook of Lattice Spacing and Structural of Metals and Alloys**, Pergamon Press, New York.

Perkins, J. (Edited), 1975, **Shape Memory Effects in Alloys**, Plenum.

Reed-Hill, R. E., 1973, **Physical Metallurgy Principles**, 2nd Edition, D. Van Nostrand Company, New York.

Rogers, C. A. and Barker, D., 1990, "Experimental Studies of Active Strain Energy Tuning of Adaptive Composites with Embedded Nitinol Actuators," *Proceedings of 31st Structures, Structural Dynamics and Materials Conference*, AIAA90-1086, April.

Rogers, C. A., 1988, "Novel Design Concepts Utilizing Shape Memory Alloy Reinforced Composites," *Proceedings of the American Society for Composites 3rd Technical Conference on Composite Materials*, Technomic Publishing Co., Seattle, September.

Rogers, C. A. and Robertshaw, H. H., 1988, "Shape Memory Alloy Reinforced Composites", *Eng. Sci. Preprints*, ESP25.88027, June.

Sanders, K., 1981, "Miracle Metal," *Science Digest*, October.

Saunders, W. R., Robertshaw, H. H., and Rogers, C. A., 1990, "Experimental Studies of Structural Control for a Shape Memory Alloy Composite Beam," *Proceedings of 31st Structures, Structural Dynamics and Materials Conference*, AIAA90-1090, April.

Sato, Y., Tanaka, K., and Kobayashi, S., 1986, "Pseudoelasticity and Shape Memory Effect Associated with Stress-induced Martensitic Transformation: A Thermomechanical Approach", *Trans. of Japan Soc. of Aero. & Space Science*, Vol. 28.

Sato, Y. and Tanaka, K., 1988, "Estimation of Energy Dissipation in Alloys due to Stress-induced Martensitic Transformation", *Res. Mechanica*, 23 (1988) 381-393, *Elsevier Applied Science Publishers Ltd, England*.

Slater, R. A. C., 1977, **Engineering Plasticity: Theory and Application to Metal Forming Processes**, John Wiley & Sons, New York.

Suh, N. P. and Turner, A. P. L., 1975, **Elements of the Mechanical behavior of Solids**, Scripta Book Company, Washington, D. C.

Tadaki, T., Nakata, Y. and Shimizu, K., 1987, "Thermo-Cycling Effects in an Aged Ni-rich TiNi Shape Memory Alloy," *Transaction of the Japan Institute of Metals*, Vol. 28, No. 11, pp. 883-890.

Tanaka, K. and Nagaki, S., 1982, "A Thermomechanical Description of Materials with Internal Variables in the Process of Phase Transformation", *Ingenieur-Archiv*, 51, pp. 287-299.

Tanaka, K. and Iwasaki R., 1985, "A Phenomenological Theory of Transformation Superplasticity", *Engineering Fracture Mechanics*, Vol. 21, No. 4, pp. 709-720.

Tanaka, K., 1986, "A Thermomechanical Sketch of Shape Memory Effect: One-dimensional Tensile Behavior", *Res. Mechanica*, 18, pp. 251-263.

Tiihonen, T., 1988, "A Numerical Approach to a Shape Memory Model," Report No. 98, Inst. Für Mathe., Universität Augsburg.

Todorodi, T. and Tamura, H., 1987, "Effect of Heat Treatment after Cold Working on the Phase Transformation in TiNi Alloy," *Transaction of the Japan Institute of Metals*, Vol. 28, No. 2, pp. 83-94.

Toki Corporation, 1987, **BioMetal Guidebook**, Toki Corporation, Japan.

Warlimont, H., Deleay, L. K., Krishnan, R. V., and Tas, H., 1974, "Review of Thermoelasticity, Pseudoelasticity and the Memory Effects Associated with Martensitic Transformations, Part 3: Thermodynamics and Kinetics," *Journal of Materials Science*, pp. 1545-1555.

Wayman, C. M., 1980, "Some Applications of Shape-Memory Alloys", *Journal of Metals*, June.

Wayman, C. M. and Shimizu, K., 1972, "The Shape Memory Effect in Alloys," *Metal Science Journal*, Vol. 6, No. 175.

Zhou, G. Q., Li, Y. C. and Chen, J. Y., 1988, "A Constitutive Representation Developed from Thermo-Activated Mechanism," *Journanl de Physique*, Colloque C3, Tome 49, September.

# Vita

Chen Liang was born in Kunming, Yunnan Province, People's Republic of China on June 6, 1964. He grew up in Kunming, where he graduated from The Third High School of Kunming in 1980. He attended Beijing Institute of Aeronautics and Astronautics (BIAA), and majored in structures and strength of jet engines. He received a bachelor's degree from the Jet Propulsion Department in 1984 and a master's degree in 1986. After working for a year at BIAA he came to Virginia Polytechnic University & State University to pursue his PhD in August 1987. He started working in the area of intelligent structures and material systems in August 1988. In August 1990 he graduated with a PhD in Mechanical Engineering.

A handwritten signature in black ink, appearing to read 'Liang Chen', written in a cursive style.

Chen Liang